**UNIVERSIDADE FEDERAL DO CEARÁ**
**CENTRO DE TECNOLOGIA**
**DEPARTAMENTO DE ENGENHARIA DE TRANSPORTES**
**PROGRAMA DE PÓS-GRADUAÇÃO EM ENGENHARIA DE TRANSPORTES**

**LUCAS SASSAKI VIEIRA DA SILVA**

# INFLUENCE OF MOISTURE DAMAGE ON FATIGUE CRACKING OF ASPHALT BINDERS, AGGREGATE-BINDER INTERFACE, AND MIXTURES

**FORTALEZA**
**2023**

LUCAS SASSAKI VIEIRA DA SILVA

# INFLUENCE OF MOISTURE DAMAGE ON FATIGUE CRACKING OF ASPHALT BINDERS, AGGREGATE-BINDER INTERFACE, AND MIXTURES

Thesis submitted as a partial fulfillment of the requirements for the Master's degree in Transportation Engineering at *Universidade Federal do Ceará*.
Area within the graduate program: Transportation Infrastructure.

Advisor: Jorge Barbosa Soares, Ph.D.
Co-advisor: Juceline Batista dos Santos Bastos, Dr.

FORTALEZA

2023

Dados Internacionais de Catalogação na Publicação
Universidade Federal do Ceará
Sistema de Bibliotecas
Gerada automaticamente pelo módulo Catalog, mediante os dados fornecidos pelo(a) autor(a)

---

D11i da Silva, Lucas Sassaki Vieira.
Influence of moisture damage on fatigue cracking of asphalt binders, aggregate-binder interface, and mixtures / Lucas Sassaki Vieira da Silva. – 2023.
113 f. : il. color.

Dissertação (mestrado) – Universidade Federal do Ceará, Centro de Tecnologia, Programa de Pós-Graduação em Engenharia de Transportes, Fortaleza, 2023.
Orientação: Prof. Dr. Jorge Barbosa Soares.
Coorientação: Profa. Dra. Juceline Batista dos Santos Bastos.

1. trincamento por fadiga. 2. dano por umidade induzida. 3. melhorador de adesividade. 4. interface agregado-ligante. 5. misturas asfálticas. I. Título.

CDD 388

LUCAS SASSAKI VIEIRA DA SILVA

# INFLUENCE OF MOISTURE DAMAGE ON FATIGUE CRACKING OF ASPHALT BINDERS, AGGREGATE-BINDER INTERFACE, AND MIXTURES

Thesis submitted as a partial fulfillment of the requirements for the Master's degree in Transportation Engineering at *Universidade Federal do Ceará*.

Area within the graduate program: Transportation Infrastructure.

Approved in: 09/05/2023.

COMITEE

_____

Prof. Dr. Jorge Barbosa Soares (Advisor)
Universidade Federal do Ceará (UFC)

_____

Profa. Dra. Juceline Batista dos Santos Bastos (Co-Advisor)
Instituto Federal de Educação, Ciência e Tecnologia do Ceará (IFCE)

_____

Profa. Dra. Suelly Helena de Araújo Barroso (Internal evaluator)
Universidade Federal do Ceará (UFC)

_____

Profa. Dr. Jorge Luiz Oliveira Lucas Júnior (External evaluator)
Universidade Federal do Ceará (UFC)

_____

Prof. Dr. Luciano Pivoto Specht (External evaluator)
Universidade Federal de Santa Maria (UFSM)

## AGRADECIMENTOS

A seção de agradecimentos do trabalho é uma das mais complexas. Sempre existe o medo de esquecer de alguém ou de não expressar o quanto cada pessoa foi importante. Bom, as pessoas citadas me conhecem e sabem que tentei fazer o melhor. O texto aqui não seria suficiente para agradecer como deveria.

Inicialmente expresso minha gratidão aos meus pais, Afonso Vieira da Silva e Nadir Mitico Sassaki, em especial ao meu pai pelo apoio em todas as minhas decisões e por ser o meu amigo em todas as horas e situações.

Agradeço aos professores Jorge Soares e Juceline Bastos pela orientação, confiança, paciência e compreensão desde a oportunidade na Iniciação Científica até a conclusão deste Mestrado. Muito mais do que professor e professora "orientadores", vocês foram amigos e estiveram ao meu lado. Sem a chance de desenvolver pesquisa em uma área que me interessou desde o primeiro momento (Pavimentação Asfáltica), não sei se teria seguido na área acadêmica ou mesmo permanecido na Engenharia. Em tempo, agradeço demais o apoio nesta reta final mais corrida do que o desejado para a conclusão do trabalho e futura ida para o doutorado.

Obrigado aos professores membros da banca Suelly Barroso, Jorge Lucas e Luciano Specht pela disponibilidade e contribuições à dissertação. A participação de todos foi fundamental para o resultado aqui presente.

Agradeço separadamente três amigos que me ajudaram a revisar o trabalho pré-qualificação durante a madrugada: Aline Vale, Carlos Augusto e Isabella Quaranta. Sou grato aos amigos que o CT-Asfalto me deu, afinal vocês foram essenciais para a execução do trabalho: Rômulo, Annie, Iolanda, Hermano, Weslley, Lucas Babadopulos, Jácio, Karol, Andressa, Lucas Lira. Obrigado aos amigos que me acompanham há mais tempo pelos momentos fora da UFC: Alina, Kennedy, Luiz, Matheus Martins, Mateus Aguiar, Mateus Nobre, Letícia e Mariane.

Por último, um agradecimento mais do que especial ao Guilherme Teixeira pela paciência, compreensão, companheirismo e apoio durante o Mestrado.

O presente trabalho foi realizado com apoio da Coordenação de Aperfeiçoamento de Pessoal de Nível Superior - Brasil (CAPES) - Código de financiamento 001 e da Agência Nacional do Petróleo, Gás Natural e Biocombustíveis (ANP), Financiadora de Estudos e Projetos (FINEP) e Ministério da Ciência, Tecnologia e Inovação (MCTI) por meio do Programa de Recursos Humanos da ANP para o Setor de Petróleo e Gás – PRH-ANP/MCTI. Também agradeço à empresa Insttale Engenharia por parte dos materiais usados neste trabalho.

Obrigado!

"A vida é como andar de bicicleta. Para manter seu equilíbrio, você deve continuar se movendo."
(Albert Einstein, 1930 adaptado por Isaacson, 2008, p.11)

## RESUMO

O revestimento asfáltico é suscetível a diversos defeitos, dentre eles o trincamento por fadiga. O tráfego e as condições climáticas durante a vida útil impactam seu comportamento e podem potencializar o referido defeito. A investigação em diferentes escalas da evolução da fadiga sob efeito da umidade é uma das lacunas verificadas na literatura. Portanto, o objetivo desta pesquisa é contribuir para a avaliação dos efeitos do dano por umidade induzida no trincamento por fadiga de materiais asfálticos em diferentes escalas: ligante, interface agregado-ligante e mistura asfáltica. Os materiais utilizados no estudo são agregado gnáissico, ligante asfáltico caracterizado por penetração como 50/70 e dois melhoradores de adesividade: o aditivo orgânico a base de amina (DOPE) e a Cal Hidratada. A metodologia é composta de ensaios secos e condicionados à umidade e da simulação computacional para previsão de trincamento com duas ferramentas computacionais: CAP3D-D e FlexPAVE$^{TM}$. Foram realizados os seguintes ensaios laboratoriais: de reologia (*Frequency Sweep - FS* e *Linear Amplitude Sweep - LAS*) para o ligante; de arrancamento por meio do *Asphalt Bond Strength* (ABS) para a interface agregado-ligante; e uniaxiais em misturas asfálticas (Módulo Dinâmico – |E*| e Fadiga à Tração-Compressão), além da Resistência à Tração (RT) e do Dano por Umidade Induzida (DUI) com o uso da Relação de Resistência à Tração Retida (RRT). As principais conclusões são de que: (i) para a escala do ligante, não foram observadas variações significativas sobretudo para o ensaio LAS; (ii) para a interface agregado-ligante, foi possível verificar a influência da taxa e da temperatura de arrancamento com a construção de uma curva de falha sendo recomendado realizar este ensaio em condições próximas as de campo; (iii) para a mistura asfáltica, o aditivo orgânico e a Cal Hidratada melhoram o comportamento quanto ao DUI, sendo os valores de RRT bons indicativos para a classificação do |E*| e da fadiga condicionados; (iv) a simulação computacional demonstra explicitamente a redução da vida útil em relação ao trincamento por fadiga quando os danos por umidade são considerados; e (v) a realização de ensaios de Fadiga sem condicionamento pode superestimar a resistência ao trincamento dos materiais devido às condições ambientais.



**Palavras-chave**: trincamento por fadiga; dano por umidade induzida; melhorador de adesividade; interface agregado-ligante; misturas asfálticas.

## ABSTRACT

The asphalt surface course in pavements is susceptible to several distresses, among of which there is fatigue cracking. Traffic and climate conditions during the pavement's lifetime impact its behavior and might enhance the referred distress. The investigation in different scales of fatigue evolution under moisture effect is one of the verified gaps in the literature. Therefore, the objective of this research is to contribute to evaluate the effects of moisture induced damage on fatigue cracking on asphaltic materials in multiscale: binder, aggregate-binder interface, and asphalt mixtures. The used materials are gneiss aggregate, asphalt binder characterized by penetration as 50/70 and two adhesiveness promoters: an organic additive and Hydrated Lime. The methodology consists of dry and moisture-conditioned tests and computational simulation to predict cracking using two computational tools: CAP3D-D and FlexPAVE$^{TM}$. The following laboratory tests were performed: rheology (Frequency Sweep - FS and Linear Amplitude Sweep - LAS) for the binder; Asphalt Bond Strength (ABS) for the aggregate-binder interface; and uniaxial on asphalt mixtures (Dynamic Modulus - |E*| and Tensile-Compression Fatigue), in addition to Tensile Strength (TS) and Moisture-Induced Damage (MID) with the use of the Tensile Strength Ratio (TSR). The main conclusions are as follows: (i) no significant variations were observed for the binder scale, especially in the LAS test; (ii) the influence of pull-off rate and temperature on the aggregate-binder interface was confirmed by constructing a failure envelope. It is recommended to perform this test under conditions that closely resemble the actual field conditions; (iii) the asphalt mixture exhibited improved behavior in terms of MID when an organic additive and hydrated lime were used. The TSR values were found to be good indicators for the classification of |E*| and conditioned fatigue; (iv) computational simulation explicitly demonstrates the reduction of service life regarding fatigue cracking when moisture damage is taken into account; (v) fatigue tests performed without conditioning may overestimate the material's cracking resistance due to environmental conditions.



**Keywords:** fatigue cracking; moisture induced damage; anti-stripping agent; aggregate-binder interface; asphalt mixtures.

## FIGURES LIST

## TABLES LIST

# TABLE OF CONTENTS

# 1 INTRODUCTION

Traffic loads associated with weather conditions might lead to fatigue cracking on the asphalt mixture used on the pavement surface layer. This layer as well as the whole pavement system must resist traffic loading, climatic conditions, and distresses evolution to maintain user safety (HUANG, 2004; BERNUCCI *et al.*, 2022). Despite great advance in pavement mechanics and materials testing, it is not uncommon that current project's predictions do not properly match actual pavement service life. In some locations, especially after rainy seasons, distresses emerge greatly affecting the pavement serviceability as perceived by road users.

Moisture damage resistance is one of the key factors for asphalt mixture performance reduction (LOTTMAN, 1978; HICKS, 1991). Distresses such as raveling, fatigue and potholes evolution might be worsened due to moisture effects (KIM *et al.*, 2008; ALKOFAHI and KHEDAYWI, 2021). Fatigue cracking is one of the most affected by moisture due to the effects of water and the origins of cracks at the aggregate-binder interface, air voids, or mastic (CARO *et al.*, 2008; LAMOTHE *et al.*, 2019; LUCAS JÚNIOR *et al.*, 2020).

Asphalt mixtures are constituted of mineral aggregates (elastic response particles) and asphalt binder (viscoelastic response material) (HUANG, 2004; KIM, 2009). The overall composite presents a thermoviscoelastic behavior. Additives and other constituents such as hydrated lime, amine-based anti-stripping liquid agents, and polymers, among others, might also be incorporated for a specific purpose such as improvement of fatigue and moisture resistances, which would change materials ranking as more or less susceptible to such distress.

Some authors address moisture damage to the aggregate-binder interface properties (SUDARSANAN *et al.*, 2020; CALA and CARO, 2021; LUCAS JÚNIOR *et al.*, 2021; MAIA *et al.*, 2021), but others suggest that its occurrence is at the isolated binder (VASCONCELOS *et al.*, 2011). Either way, asphalt materials are susceptible to moisture damage and such distress may be affected by constituent materials and interfacial properties. The effects of water on both material and structure scales are illustrated in Figure 1.

Figure 1 – Water effects on (a) aggregate-binder and (b) complete pavement.

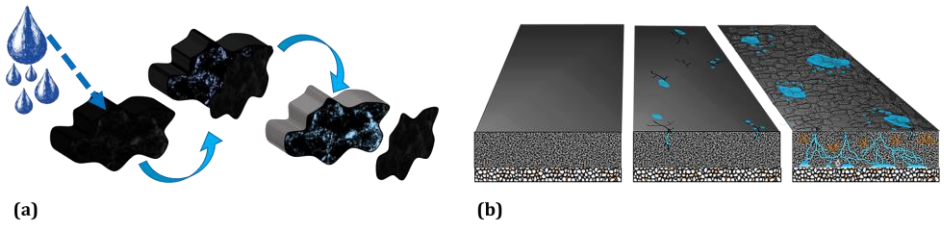


(Source: Author).

When it comes to test methods to investigate moisture susceptibility, a variety of analysis are possible. Some authors focus on asphalt mixtures behavior as it relates to Indirect Tensile Strength (RIBEIRO, 2011; ANITELLI, 2013; BARBOZA JÚNIOR, 2018; LUCAS JÚNIOR, 2020), Dynamic Modulus (ALMEIDA *et al.*, 2018; BRONDANI *et al.*, 2022), Fatigue (BARRA *et al.*, 2012; ALMEIDA *et al.*, 2018; LAMOTHE *et al.*, 2019; CARDONA *et al.*, 2021); while others use different techniques to comprehend the interface itself (OROZCO *et al.*, 2019; NAZZAL *et al.*, 2021; CALA and CARO, 2021), or to study binders and aggregates individually, or still as interfaces to try to assess the overall mixture's behavior (LUCAS JÚNIOR *et al.*, 2019a, 2019b and 2021).

Based on the context presented, the effect of moisture on fatigue resistance of asphalt mixtures is an important topic when it comes to roadway pavement projects. A given material is expected to follow a certain pattern, but such pattern might change considerably upon conditioning, thus the pavement's design should consider the possibilities related to conditioning.

## 1.1 Research problem

The comprehension of fatigue cracking evolution on the asphalt surface layer still has knowledge gaps due to laboratory testing considerations and complexities in the field. Some gaps are related to field-laboratory transfer-functions calibration, whereas there are also gaps related to material-characterization methods. Characterization methods might consider effects such as rest periods, thermal variation, and moisture presence. Thus, a deeper comprehension of isolated effects on material characterization is important. Among them, one of the most relevant to the mixture fatigue-life is adhesiveness, which relates to water impacts on different scales of the composite.

The hypothesis of the investigation herein derives from previous research works on

water effect, material characterization, and adhesiveness, indicating the need of this kind of analysis. Understanding the effect of water on fatigue modeling parameters becomes of relevance when considering both the technical aspects of material selection and the financial efforts for promoting an increase in pavement lifetime. Therefore, the research problem of this work remains in the following question: what happens to asphaltic materials' performance when in contact with water?

## 1.2 Objectives

The main objective of this research is an evaluation of moisture effects on fatigue cracking of asphaltic materials at different scales (asphalt binder, aggregate-binder interface, and complete asphalt mixture). The specific objectives are as follows:

At the binder scale:

- Compare Stiffness and Fatigue on dry and conditioned binders using Frequency Sweep and Linear Amplitude Sweep tests.

At the interface scale:

- Investigate the influence of different additives on the interface between aggregate and binder on the Pull-Off test with the construction of a Curve considering: loading rate, temperature, and pull-off strength.

At the mixture scale:

- Evaluate the Damage Characteristic Curve sensibility due to moisture conditioning considering the results obtained by the other objectives and scales.
- Compare real structures expected mechanical behavior without damage and with moisture induced damage.

Analysis between scales:

- Establish relations between binders, interface, and complete asphalt mixtures' behavior in dry and conditioned states.

## 1.3 Thesis structure

This thesis is divided into 5 main chapters although the work consists of 3 separate experimental campaigns that lead to a single objective of contributing to an evaluation of moisture effects on fatigue cracking of asphaltic materials on multiscale.

- Chapter 1: presents a brief introduction to the investigated theme, the research problem, the objective of the work, and the overall document structure.
- Chapter 2: contains a literature review on (i) how water comes into contact with the pavements' surface layer; (ii) determination of fatigue life of asphalt mixtures, considering laboratorial testing and analysis approaches; (iii) moisture damage in asphalt mixtures and tests performed after the damage protocol; (iv) the influence of water in adhesion of binder-aggregate; (v) the effects of water conditioning solely on asphalt binders.
- Chapter 3: describes the used materials in the research, the asphalt mixtures design specifications, and the testing methods and analysis used on all data.
- Chapter 4: presents the obtained results from the 3 main experimental campaigns and the simulation: (i) rheological testing of binders; (ii) aggregate-binder interface tests; (iii) asphalt mixtures testing; (iv) simulation of real structures.
- Chapter 5: the final chapter is a summary containing all conclusions from the thesis and a section suggesting future works.

# 2 LITERATURE REVIEW

The literature review presented herein is organized into topics related with the sections of the thesis: how water comes in contact with the pavement, the state-of-the-art on fatigue behavior of asphalt mixtures, recent discussions about moisture-induced damage testing regarding different damage protocols, moisture-induced damage on aggregate-binder interfaces and asphalt binders.

## 2.1 Linear Viscoelasticity (LVE) and Complex Modulus (E*)

The mechanical behavior of different asphalt mixtures components defines the material response (HUANG, 2004; KIM, 2009). Therefore, it can be divided into the main components:

- Elastic solids-behavior: aggregates;
- Viscoelastic-behavior: binders.

Due to this combination, asphalt mixtures do not behave simply as purely elastic nor as purely viscous material, but as a viscoelastic material. The relationship between applied stress ($\sigma$) and resulting strain ($\varepsilon$) determines the mechanical response, as observed in Figure 2.

Figure 2 – Strain response to a given stress.

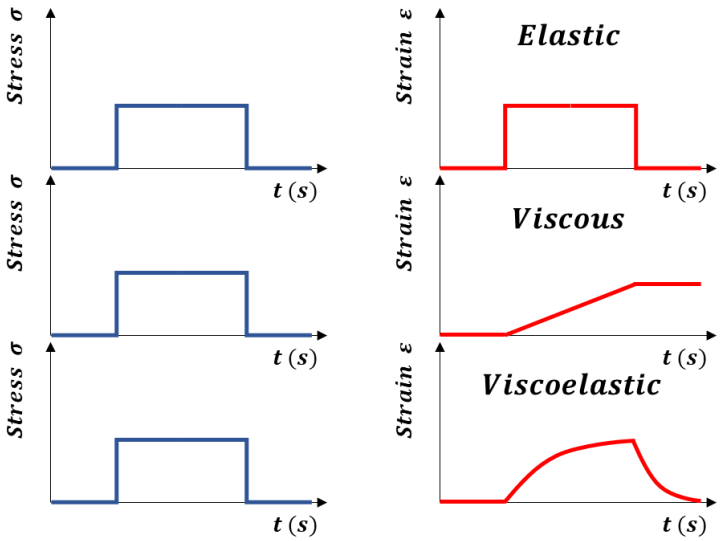


(Source: Author).

During loading for elastic materials, the applied stress results in immediate strain; contrary to that, for viscous materials, the same stress results in a time-dependent strain response. This delay is described as the phase-angle ($\varphi$) between stress and strain signals (Figure **3**), and its range is $0° \leq \varphi \leq 90°$. For viscoelastic materials, a superposition of the effects is observed.

Figure 3 – Stress, strain, and phase-angle on sinusoidal loading.

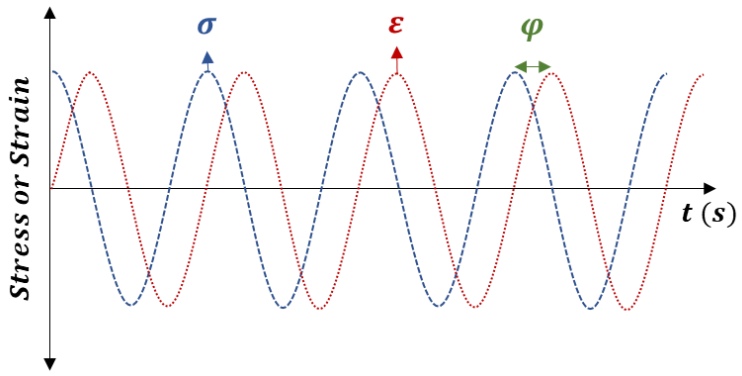


(Source: Adapted from DNIT 416, 2019).

The stiffness parameter, which is the axial Complex Modulus (E*) for asphalt mixtures and the Complex Shear Modulus (G*) for asphalt binder, is determined as the ratio between stress and strain. The Complex Modulus can be obtained from the relations in Equations 1 and 2. The norm of E* (Equation 3) is usually called the Dynamic Modulus (|E*|) when referred to the testing protocol (PAPAZIAN, 1962).

$$E^* = \frac{\sigma^*}{\varepsilon^*} = \frac{\sigma_0 e^{i\omega t}}{\varepsilon_0 e^{i(\omega t - \varphi)}} \quad (1)$$

$$\frac{\sigma_0 e^{i\omega t}}{\varepsilon_0 e^{i(\omega t - \varphi)}} = \frac{\sigma_0}{\varepsilon_0} \cos\varphi + i \frac{\sigma_0}{\varepsilon_0} \sin\varphi \quad (2)$$

$$|E^*| = \frac{\sigma_0}{\varepsilon_0} \quad (3)$$

Where:

$\sigma_0$, $\sigma^*$ = stress amplitude;

$\varepsilon_0$, $\varepsilon^*$ = strain amplitude;

$\omega$ = angular frequency;

$t$ = time.

Despite that, the domain in which the response of the material fits is determined depending on strain amplitudes and the number of loading cycles that the material is evaluated. In Figures 4 and 5, respectively, the binder's and mixture's behavior due to loading and strain are presented.

Figure 4 – Mechanical behavior of the binder due to loading and strain.

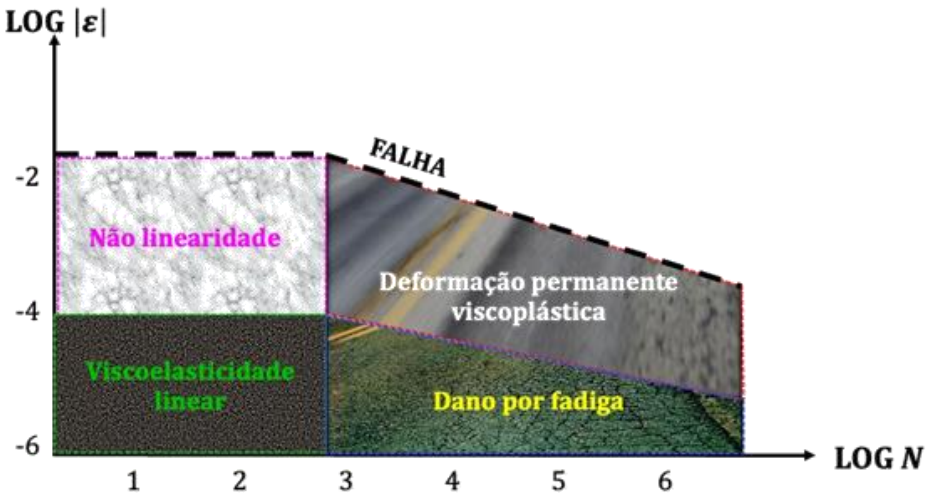


(Source: Adapted by LUCAS JÚNIOR (2018) from MANGIAFICO, 2014).

Figure 5 – Mechanical behavior of the mixture due to loading and strain.

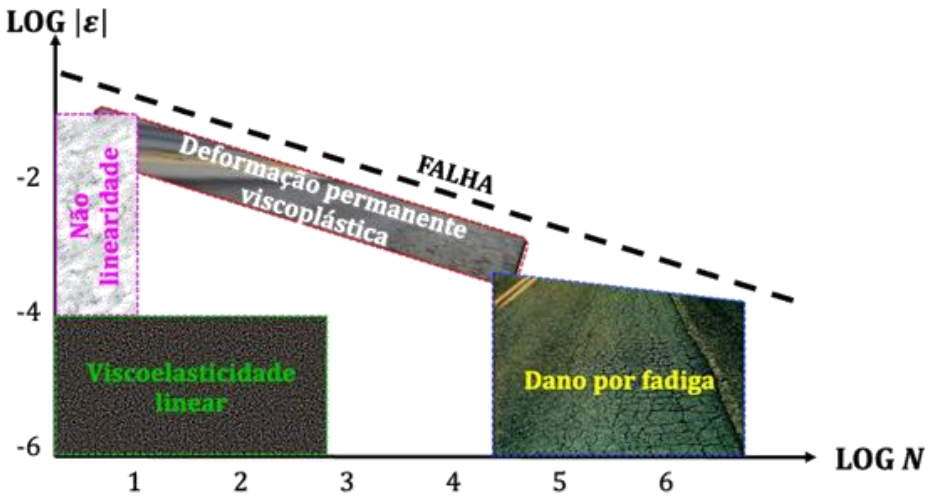


(Source: Adapted by LUCAS JÚNIOR (2018) from DI BENEDETTO *et al.*, 2013).

As observed in Figures 4 and 5, for small strain amplitudes and lower loading cycles, the material behaves in the linear viscoelastic domain. However, as strain levels increase non-linear effects might take place, and excessive loading leads to damage such as Fatigue or Permanent deformation.

### *2.1.1 Time-Temperature Superposition Principle (TTSP)*

Temperature change the behavior of both asphalt binders, and asphalt mixtures due to binder. Therefore, loading, frequency, and temperature are key factors to the mechanical characterization of asphaltic materials. Due to this property, a wide range of combinations can be observed as possible material responses. This could represent an issue since an extensive spectrum requires multiple logarithm decades of data that both in time or frequency domains would be prohibitive to determine for extremely low frequencies or longer times of stress/strain analysis (FERRY, 1980; CHRISTENSEN, 1982; KIM, 2009).

As temperature, loading, and frequency determine the material response, some E* results are likely to overlap in different frequencies and frequencies combinations. This means that in plotting with all data, isotherms can be determined, and similar results are observed.

According to the Time-Temperature Superposition Principle (TTSP), a single curve can be determined to describe the viscoelastic spectra using a time-temperature shift factors ($a_T$). These $a_T$ are responsible for horizontally shift curves to the equivalent points over other data into a given reference temperature ($T_r$), for E* or $\varphi$ values, these are the Master Curves in both time and frequency domains (FERRY, 1980; CHRISTENSEN, 1982; KIM, 2009; NGUYEN *et al.*, 2009). TTSP describes that a temperature increase is equivalent to frequency reduction, and temperature decrease is related to a frequency rise. Therefore, the prohibitive testing time problem no longer exists. If the viscoelastic material obeys this relation, it is considered a thermorheological-simple material (FERRY, 1980).

In addition to a single E* or $\varphi$ Master Curve in time or frequency domain, other characterization plots are determined as a function of real or imaginary parts of |E*| and unshifted curves, as illustrated in Figure 6.

Figure 6 – Characterization Curves.

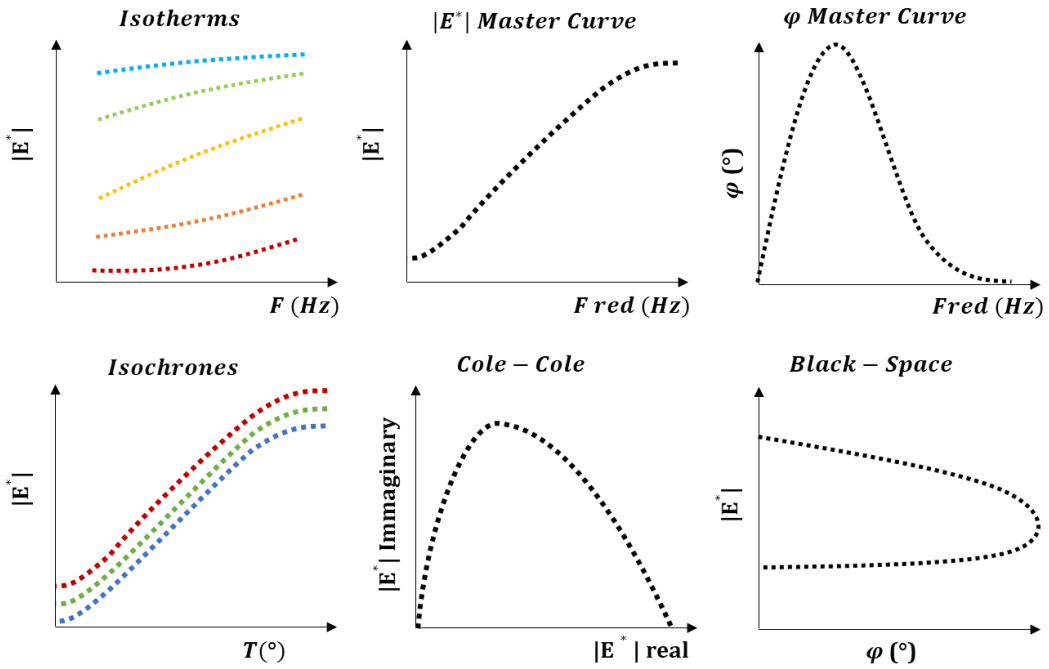


(Source: adapted from CORTÉ and DI BENEDETTO, 2005).

### *2.1.2 Mechanical analogs and 2S2P1D rheological model*

Material behavior can be estimated by different methods, such as mathematical expressions adjusted by curve fitting or mechanical analogs that represent a physical description of the observed phenomena.

As described in the literature (FLÜGGE, 1975; CHRISTENSEN, 1982), a purely elastic element, or Hooke analog, is depicted as a Spring with "*E*" Young's modulus. Opposite to that, a viscous element, or Newton analog, is represented as a Dashpot with "$\eta$" viscosity. These elements are illustrated in Figure 7.

Figure 7 – Elastic and viscous analogs graphical representation.


(Source: Adapted from LUCAS JÚNIOR, 2018).

Although these elements might mirror a part of the materials behavior, as previous shown in Figure **2**, they do not completely behave as a viscoelastic material. Therefore, different combinations are necessary to represent viscoelastic materials behavior. The Maxwell-fluid

coupling uses a series coupling of a Hooke and a Newton element to represent the material, while Kelvin-solid coupling associates these individual elements in a parallel distribution (Figure **8**). The distinct types of coupling imply different constitutive equations and, therefore, stress-strain behavior.

Figure 8 – Maxwell-fluid and Kelvin-solid couplings.

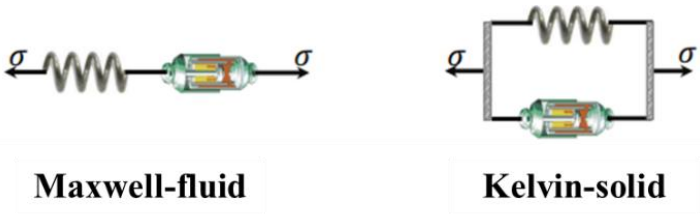


(Source: Adapted from LUCAS JÚNIOR, 2018).

Multiple associations are also possible, as indicated in Figure **9**, by using combinations of Maxwell-fluid elements in parallel, resulting in the Maxwell-Wiechert-Generalized Model (MWG), and Kelvin-solid in series as the Kelvin-Voigt-Generalized model (KVG).

Figure 9 – MWG and KVG models.

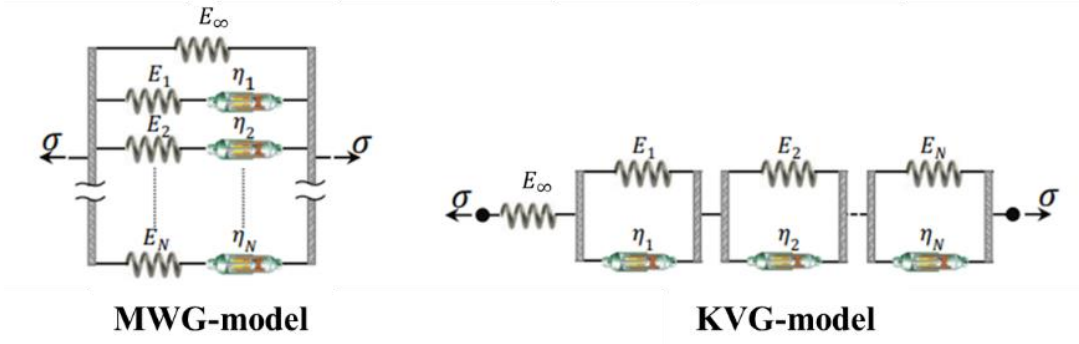


(Source: Adapted from LUCAS JÚNIOR, 2018).

These couplings are discrete spectrum representations known as Prony Series, but do not describe asphalt materials behavior properly, and each of them carries characteristic times: the former is defined as relaxation time ($\rho$), and the latter as retardation time ($\tau$). Their ruling equations are for the Relaxation Modulus ($E(t)$) in Equation 4 and Creep Compliance ($D(t)$) in Equation 5. As observed, each "$i$" or "$j$" element has its own characteristic time and relaxation or retardation modulus as well as the isolated spring $E_\infty$.

$$E(t) = \frac{\sigma(t)}{\varepsilon} = E_\infty + \sum_{i=1}^{n} E_i e^{-\frac{t}{\rho_i}} \quad (4)$$

$$D(t) = \frac{\varepsilon(t)}{\sigma} = \frac{1}{E_\infty} + \sum_{j=1}^{n} \frac{1}{E_j} (1 - e^{-\frac{t}{\tau_i}}) \quad (5)$$

The use of a Parabolic-dashpot (Figure **10**) element is responsible to approximate the time-dependent behavior of asphalt binder. These elements have been associated to Hooke elements in a linear parallel coupling to derive the so-called Huet and Huet-Sayegh continuum spectra models (YUSOFF *et al.*, 2011).

Figure 10 – Parabolic-dashpot element, Huet and Huet-Sayegh models.

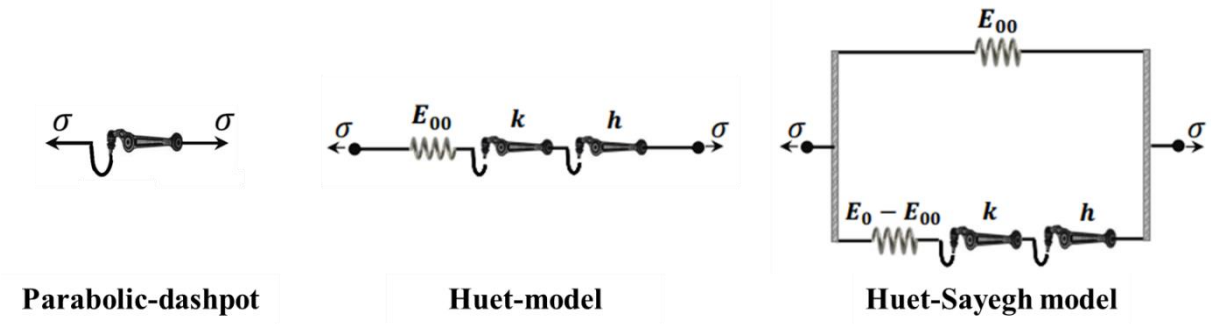


(Source: Adapted from LUCAS JÚNIOR, 2018).

Despite the elements associations modifications over time, both Huet and Huet-Sayegh models still present deviations on asymptotic portions of the master curves. Thus, another continuous spectrum rheological model was developed by Olard and Di Benedetto (2003) and is a good approximation of complex materials such as asphalt mixtures.

This model (Figure 11) is based on mechanical analogs associated with a combination of 4 elements in series and 1 parallel to the other group 2 Springs, 2 Parabolic-dashpots, and 1 linear Dashpot.

Figure 11 – 2S2P1D graphic model.

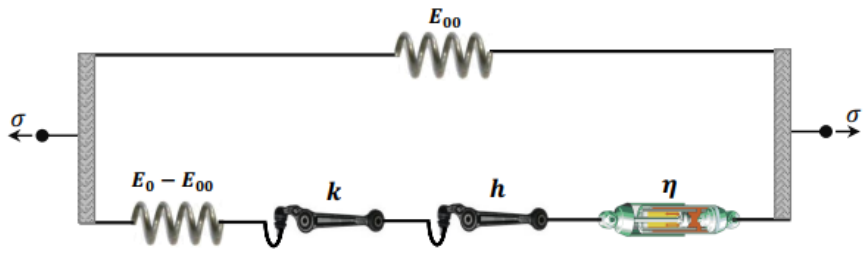


(Source: Adapted from LUCAS JÚNIOR, 2018).

This model is valid ranging from binders to complete asphalt mixtures, and Equation 6 describes its behavior on sinusoidal loading.

$$E^*(i\omega\tau) = E_\infty + \frac{E_0 - E_\infty}{1+\delta(i\omega\tau)^{-k}+(i\omega\tau)^{-h}+(i\omega\beta\tau)^{-1}} \quad (6)$$

Where:

$E_\infty$ = asymptotic modulus when frequency tends to zero;

$E_0$ = asymptotic modulus when frequency tends to infinite;

$\delta$, $\beta$ = dimensionless constants;

$k$, $h$ = exponents associated to the parabolic dashpots;

$\eta$ = linear dashpot behavior obtained by $\eta = (E_0 - E_\infty)\beta\tau$;

$\omega$ = angular frequency;

$\tau$ = characteristic time determined using time-temperature shift factors at a given temperature, calibrated using $\tau_0$ as the reference characteristic-time.

For further details on the development of 2S2P1D model, the reader is referred to Olard and Di Benedetto (2003). As for the influence of calibration of the parameters, Dias (2016) describes how they affect each of the LVE characterization curves (Cole-Cole, Black-Diagram, and Master Curve).

## 2.2 Fatigue damage

Fatigue in each material is described as the loss of material resistance or material properties due to repetitive loading which leads to cracking. The referred loss continues until a complete rupture, or a pre-defined stiffness reduction is observed. This way, fatigue life can be defined as the number of necessary solicitations to rupture a given material or until it reaches an arbitrary stiffness reduction based on modulus values or other pre-defined failure criteria (KACHANOV, 1986; LEMAÎTRE and CHABOCHE, 1990; HUANG, 2004).

Despite the concept based on cyclic loading, in the laboratory, this loading cycles reproduction might reproduce effects not directly related to the expected damage. These parasite effects can be permanent strain accumulation, creeping, self-heating, and thixotropy which difficult the analysis based on parameters variation (MANGIAFICO *et al.*, 2015;

BABADOPULOS, 2017; BABADOPULOS *et al.,* 2017 and 2019).

Along with these effects, the type of loading, sample geometry, temperature, frequency, and the use of rest periods can alter damage evolution. Different types of loading generate homogenous and non-homogenous stress states, whether they are stress or strain-controlled. The controlling scheme used in cyclic tests results in different responses, as observed in Figure **12**. If a test is strain-controlled, it is observed that induced stress reduces, while in stress-controlled tests, strains increase due to the constant applied load. Therefore, the cracking growth rate depends also on the controlling scheme (MANGIAFICO, 2014).

Figure 12 – Representation of different types of stress-strain combinations.

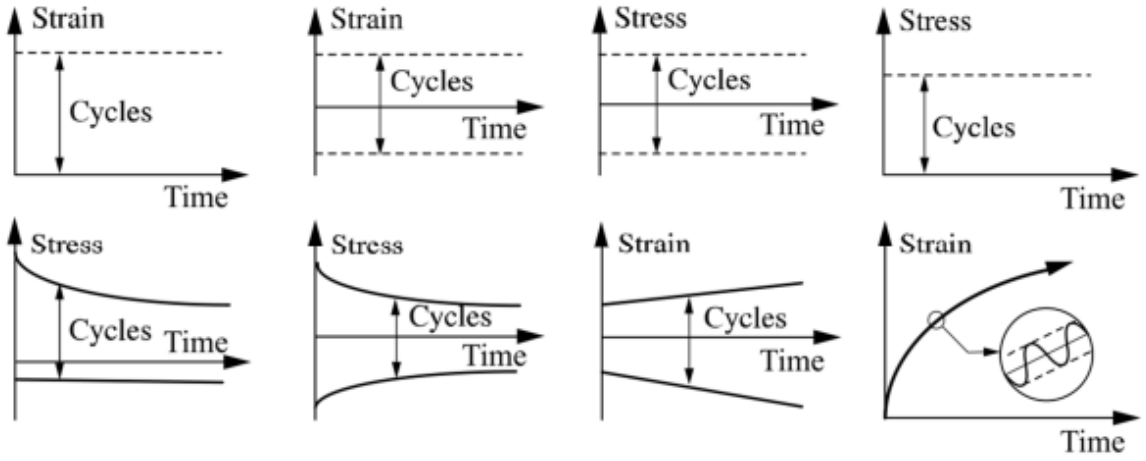


(Source: DI BENEDETTO and CORTÉ, 2005).

The testing geometry and loading path also contribute to the material response to homogeneity: two and four-point prismatic bending, indirect tensile, and uniaxial tension-compression. Among these, the uniaxial tension-compression is the only test that produces a homogeneous stress-strain state at all sample points (DI BENEDETTO *et al.*, 2004; MANGIAFICO, 2014; ISAILOVIC, 2018). If a testing protocol does not result in constant stress and strain at any given point of the sample, then it is not fully stress or strain-controlled, but force or displacement-controlled (MANGIAFICO, 2014).

### *2.2.1 Simplified Viscoelastic Continuum Damage (S-VECD)*

The Viscoelastic Continuum Damage model (VECD) is based on the Potential Work Theory (PWT). According to PWT, the damage is quantified using parameters such as stiffness

and, for the specific case of viscoelastic materials, pseudo-stiffness (SCHAPERY, 1990).

Damage is calculated primarily by the variation of these parameters. For asphalt mixtures in direct tension state, an internal state variable "$S$" is used for the evolution of microcracks (KIM, 2009). The pseudo-stiffness or integrity "$C(S)$" variable is then expressed by a power law as in Equation 7.

$$C(S) = 1 - C_{11}S^{C_{12}} \quad (7)$$

Where:

$C_{11}$ e $C_{12}$ = Power law fitting constants;

$C\ (S)$ = integrity;

$S$ = damage.

Previous works have characterized material integrity using monotonic tests (KIM and LITTLE, 1990; PARK *et al.,* 1996; LUNDSTRÖM and ISACSSON, 2003), but no real fatigue property is defined using this type of test since there is no cyclic loading and damage.

The use of cyclic tests caused a new calculation problem since a prohibitive amount of data was generated to determine the decrease in materials integrity. Therefore, a simplified version of the former VECD was developed as the Simplified Viscoelastic Continuum Damage (S-VECD) for the sinusoidal loading (UNDERWOOD *et al.*, 2009 and 2012).

According to Underwood *et al.* (2009 and 2012), a difference between S-VECD and VECD stands in the calculation method. S-VECD assumes that fatigue occurs only during tension and the pseudo-strain can be determined as the product of modulus and pseudo-strain. The method also assumes that the integrity between cycles decreases linearly ignoring a possible modification during the compression part of the cycle.

Using this method, as well as VECD, the expected fatigue results is the Damage Characteristic Curve, and the integrity parameter ($C$) is normalized by the Dynamic Modulus Ratio ($DMR$) further described in Section 3.3.8. The damage during cyclic tension is then calculated from Equations 8 and 9, used to obtain the same $C\ vs.S$ curve independent of loading type, frequency, or test temperature, but exclusively due to the tested material.

$$C = \frac{\sigma}{\varepsilon^R \times DMR} \quad (8)$$

$$\Delta S_n = \left(-\frac{DMR}{2}(\varepsilon_{ta}^R)^2(C_n^* - C_{n-1}^*)\right)^{\frac{\alpha}{\alpha+1}}(\Delta t_R)^{\frac{1}{\alpha+1}}(K_1)^{\frac{1}{\alpha+1}} \quad (9)$$

Where:

$C$ = pseudo stiffness;

$\sigma$ = axial stress;

$\varepsilon^R$ = pseudo strain;

$DMR$ = dynamic modulus ratio;

$\varepsilon_{ta}^R$ = pseudo strain amplitude;

$K_1$ = shape factor;

$\alpha$ = rate of damage evolution.

Furthermore, Nascimento (2016) states that it is possible to model the behavior from test results with Equation 10. Fatigue behavior is observed using strain as an input to different maximum cycles or analyzing maximum strain levels to a given cycles number using the Wöhler curves.

$$N_f = \left( \frac{\left(\frac{1}{2}\left(\varepsilon_{ta}^R\right)^2 C_{11}\left(\frac{(\alpha-\alpha C_{12}+1)\left(\varepsilon_{ta}^R\right)^{2\alpha} K_1}{f_R^{2\alpha}}\right)^{\frac{C_{12}}{\alpha-\alpha C_{12}+1}}\right)}{Y\left(\frac{C_{12}}{\alpha-\alpha C_{12}+1}+1\right)} \right)^{\frac{1}{\Delta+1-\frac{C_{12}}{\alpha-\alpha C_{12}+1}}} \quad (10)$$

Where:

$Nf$ = number of cycles until failure;

$f_R$ = reduced frequency.

The Fatigue Factor of Mixtures ($FF_M$) parameter is also calculated to observe which asphalt mixture should present better properties. It is defined as the area under the Wöhler curve between 100 and 200$\mu S$ as described in Equation 11 (NASCIMENTO, 2015):

$$FFM = \frac{\log(N_{f,100})+\log(N_{f,200})}{2} \times [\log(200) - \log(100)] \quad (11)$$

### *2.2.2 Failure criteria*

Due to the definitions of fatigue, multiple failure criteria are described in the literature such as phase-angle abrupt drop; a predefined modulus loss such as 30, 50, and 70% of its initial value; the maximum released pseudo-strain energy. Among these failure criteria, the modulus decrease is usually criticized due to significant variations in fatigue life when different modulus loss is used, specimens' variability comes into the analysis or the loading

scheme is altered (HOPMAN *et al.* 1989; SABOURI and KIM, 2014; BABADOPULOS, 2017).

Sabouri and Kim (2014) adopted a failure independent of loading mode, the $G^R$ defined in Equations 13 to 14 in a log-log scale. When plotted, the $G^R$ *vs.* $N_f$ curve is fitted as Equation 14 in log-log space.

$$W_{max}^R = \frac{1}{2}(1-C)\left(\varepsilon_{0,ta}^R\right)^2 \quad (12)$$

$$G^R = \frac{W_{max}^R}{N_f} = \frac{\int_0^{N_f} \frac{1}{2}(1-c)\left(\varepsilon_{0,ta}^R\right)^2 dN}{\left(N_f\right)^2} \quad (13)$$

$$G^R = Y\left(N_f\right)^{\Delta} \quad (14)$$

Where:

$G^R$ = mean rate of pseudo strain released energy;

$W_{max}^R$ = maximum accumulated pseudo-strain energy release;

$\Delta$ = exponent from $G^R$ fitting;

$Y$ = constant of $G^R$ fitting.

The $D^R$ parameter in Equation 15, developed by Wang *et al.* (2018), is another failure criterion that is also independent of loading mode, and based on pseudo-strain released energy, resembling $D^R$.

$$D^R = \frac{\int_0^{N_f}(1-c)dN}{N_f} \quad (15)$$

The main difference as stated by Wang *et al.* (2018) is that $G^R$ is determined in a log-log scale, while the $D^R$ is calculated with a linear regression in an arithmetic scale. In addition, $D^R$ passes through the origin, making it necessary to calculate only its slope, whereas $G^R$ requires both the slope and the intercept of the linear regression to be determined. Moreover, fewer tests are required for $D^R$ when compared to $G^R$. According to the referred authors, the main advantage is fewer errors during extrapolation of curves since one occurs in log-log scale and the other in arithmetic scale. This mostly leads to lower possible deviations when using a program such as FlexPAVE™, former LVECD – Layered Viscoelastic Pavement Analysis, for Critical Distresses (ESLAMINIA *et al.*, 2012) to simulate a real structure.

However, the same parameters are necessary to characterize fatigue. Thus, the choice of $D^R$ or $G^R$ parameter should be evaluated for specific analysis or reporting needs.

## 2.3 Water on asphalt pavements

Among other factors, it is well known that moisture is key to granular materials stability in pavements, as studied by Bastos (2013) and Araújo (2019) for conditions and materials of the state of Ceará, Brazil. Therefore, draining systems, drainable asphalt mixtures and a project that allows water to flow through the structure without damage are necessary.

Specifically, for asphalt layers, Ribeiro (2011) investigated the effects of moisture damage on different additives for asphalt mixtures especially Cashew Nut Liquid (LCC). Ferreira (2013; 2015) analyzed permeability of asphalt mixtures which according to Azevedo (2007) is partially responsible for the water imprisoned at the surface and under layers.

When water effects are evaluated on a complete pavements structure, there are many ways in which this moisture might encounter the material layers especially the surface layer (PEREIRA, 2003; SILVA, 2005; AZEVEDO, 2007; RIBEIRO, 2011; BEZERRA, 2018). Figure **13** exemplifies how the different mechanisms listed below might occur.

- Direct precipitation through cracks on surface layer;
- Lateral percolation from sidewalks or slopes;
- Water ascension due to groundwater reserve;
- Residual materials moisture before construction.

Figure 13 – Water in contact with asphalt pavement.

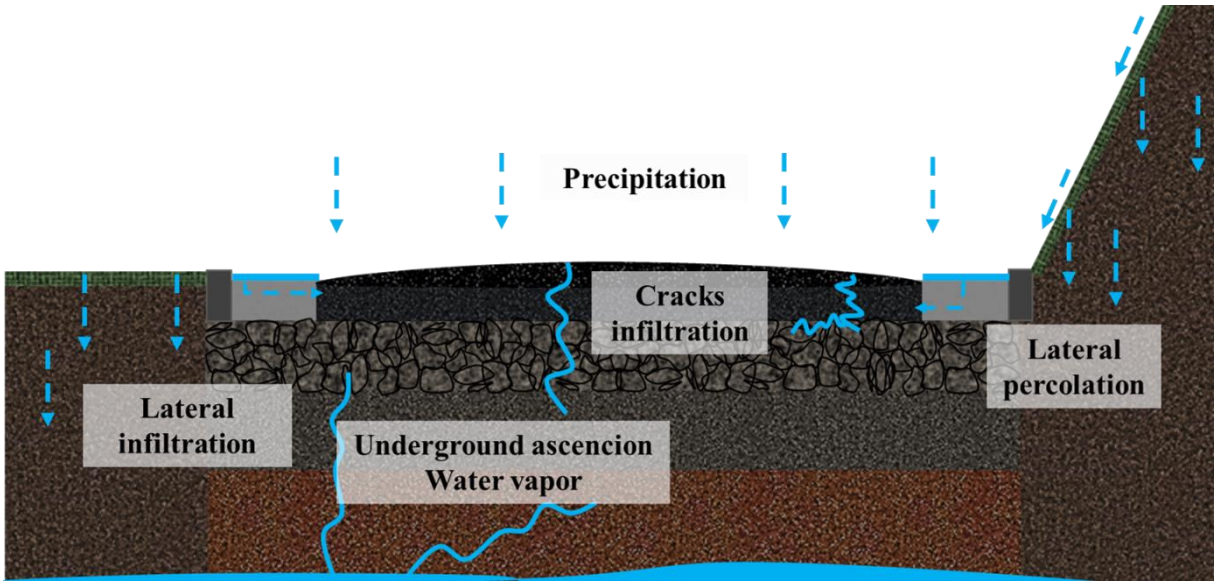


(Source: Adapted from Azevedo, 2007).

### *2.3.1 Moisture damage mechanisms*

Hicks (1991) states that asphalt pavements' durability depends on several factors, moisture resistance being a key factor and it might be linked to the adhesion or cohesion mechanisms. Due to the severity of these problems, different distresses might come in place such as deformation, potholes, cracking, and raveling.

According to Caro *et al.* (2008), damage is "*the degree of loss of functionality of a system*", and moisture damage is defined as "*the degradation of mechanical properties of the materials due to the presence of moisture in a liquid or vapor state*". Other definitions rely on adhesion failure modes which are the final steps from the complete damaging process. This process is divided in two main steps that constitute the moisture damage mechanism: moisture transport and the response of the system. The authors relate different attributes, moisture states and system responses as follows:

- System Attributes: Surface energy; chemical properties; aggregates form properties; air voids; construction issues;
- Moisture states: unsaturated flow, saturated flow, diffusion;
- Response of the system: detachment/debonding, displacement, dispersion, film rupture/microcracks, desorption, spontaneous emulsification.

Other authors (KIGGUNDU and ROBERTS, 1988) still suggest that additional mechanisms and a combination of them play a significant role in moisture damage such as: pH instability, and the effects of climate/environment on the materials combination. Beside these factors, according to Terrel and Shute (1989) different theories are often used to describe adhesion in the aggregate-binder system: chemical reaction, surface energy, molecular orientation, and mechanical adhesion. Even though the most likely to occur is a combination of effects instead of a single theory, the chemical reaction theory is one of the most accepted or discussed to promote aggregate-binder adhesion.

Little and Jones (2003) discuss that despite aggregate or binder have a charge (positive or negative), due to the nonuniform charge distribution, they might act as having charges which promotes the initial adhesion to the aggregate-binder system. However, according to Hicks (1991), silicious aggregates tend to be classified as hydrophilic or prone to stripping. Therefore, the hydrogen bonds connecting the Carboxylic Acid Group (-COOH) and the Silanol (-SiOH) from aggregates are expected to break when in contact with water. On the other hand, when Hydrated Lime exists in the mixture, the $Ca(OH)_2$ molecule dissociates and $Ca^{2+}$ ions bond to COOH resulting in an insoluble calcium salt which leaves SiOH free to bond

with nitrogen (PETERSEN *et al.*, 1987).

Considering these properties, it is necessary to highlight that the Brazilian standard to determine the stripping potential of aggregate-binder is DNER 078 (1994). The procedure does not require any aging process, although asphalt mixtures produced in laboratory and incorporated on roads undergo a short aging process. This difference in testing conditions can mislead interpretations. Ongoing research at LMP/UFC observed that short term aged (2h in oven at the compaction temperature) aggregate-binder samples do not present loss in adhesion after the DNER 078 (1994) protocol (TAVARES FILHO *et al.*, 2023). Based on these findings it is expected that the standard test protocol results do not correlate to the Moisture Induced Damage Test (Modified Lottman Test) results and probably do not reflect what happens to the material after aging or during service life. This corroborates the need of additional study of aggregate-binder interface behavior and testing protocols that truly detect the water effects.

### *2.3.2 The use of Hydrated Lime as an anti-stripping additive*

Moura (2001) studied the use of hydrated lime in proportions of 1 and 2% as a replacement of stone dust. In this study, lime acted as an anti-stripping additive to gneiss aggregates compared to a liquid anti-stripping agent. The author observed that the use of 1% of lime or the liquid additive promoted a higher resistance to moisture damage when compared to the neat mixture. However, when 2% was added to the mixture, no significant damage was observed when comparing ITSR results.

Epps, Berger, and Anagnos (2003) indicate 1 to 2% of HL addition is enough to improve moisture resistance while some mixtures might need up to 2.5%, and some mixtures might have their asphalt content reduced due to the lime addition. According to Little and Epps (2006), the use of HL in asphalt mixtures has many benefits such as:

- Reducing stripping;
- Stiffening of binders and asphalt mixtures;
- Low temperature cracking improvement;
- Reducing oxidation susceptibility;
- Improving stability by altering properties of fines such as clays present in aggregates.

Due to these characteristics, different techniques were tested to add HL to asphalt mixtures such as: dry lime to the mixer drum, dry lime on dry or saturated aggregates, and lime slurry. From these possibilities, lime slurry tends to add another variable to the mixture: the higher moisture content on aggregates prior to heating, which could increase fuel consumption

as well as equipment acquisition.

Kim *et al.* (2008) tested different HL addition methods to the asphalt mixture and observed that these mixtures had better performance due to: stiffness increase, strength, and mastic's toughness against moisture damage due to the aggregate-binder bond improvements. However, the authors highlight that these benefits decay when multiple freeze-thaw cycles are performed on these mixtures.

Ribeiro (2011) evaluated the addition of HL to asphalt mixtures in dry condition prior to heating. The author observed that the addition of 2% of HL resulted in 0.5% binder content reduction as well as 0.7% lower air voids (AV) at 100 gyrations for mixtures design. As discussed by the author, similar results were found by Budny (2009) who tested Calcite and Dolomitic Hydrated Limes adding 1% of each HL to the evaluated mixture.

In a similar study, Bock *et al.* (2009) evaluated different adding techniques to add 1% of HL to the asphalt mixture as a replacement of stone dust: as a filler, dry over der coarse aggregates, dry over wet coarse aggregates, and as lime slurry. Similar results of binder content reduction were found by the authors as well as the higher ITSR results for the dry addition over dry coarse aggregates.

### *2.3.3 Moisture damage of asphalt binders*

As previously described, moisture damages asphalt materials acting as catalyst for other distresses. Vasconcelos (2010) developed a study on the diffusion of moisture in binders and fine aggregate mixtures using different techniques such as Fourier Transform Infrared (FTIR) - Attenuated Total Reflectance (ATR) spectrometry, and Gravimetric Sorption Measurements. The investigated process of diffusion consists in the transportation of part of a given system to another by molecular movements such as moisture in asphalt binders. When in humid environments, asphalt binders tend to absorb water which might modify physical and mechanical properties as well as affect the aggregate-binder interface. This phenomenon is influenced by pressure, temperature, and the physical state of water.

Some of the conclusions of the study were that the rate of diffusion is dependent on moisture exposure's history and increases with the time of exposure. Furthermore, the diffusivity increased due to the history dependence after every exposure cycle. These differences were addressed to microstructural modifications in the Binder. Also, residual moisture evidence was verified and, but aggregate-binder adhesion debonding effects are unknown.

An investigation by Lucas Júnior *et al.* (2021) was conducted with neat binder and binder with amino-based anti-stripping agents. Among the testing methods, rheological test was performed on conditioned binders. The conditioning method chosen was 24h water bath at 40ºC of binder samples prior to testing. The authors observed that while the anti-stripping agent reduced the binders' resistance to permanent deformation and stiffness for the dry condition, the moisture damaging protocol decreased these properties for both binders.

In another work, Akentuna *et al.* (2022) evaluated the moisture susceptibility of both asphalt binders and mixtures using Frequency Sweep (FS) and the Hamburg Wheel Test (Loaded Wheel Test – LWT) after different conditioning protocols. The authors have observed a rising difference between the reference and conditioned samples related to the severity of the conditioning protocol. One of the main observations was the increase in stiffness for binders observed in FS results. For LWT results, the opposite was found, in an increased rutting depth for asphalt mixtures after moisture damage.

Furthermore, Akentuna *et al.* (2023) emphasized the effects of both asphalt binders and mixtures using different conditioning protocols: multiple freeze thaw cycles in accordance AASHTO T 283 procedure, different MiST levels following ASTM D 7870 protocol. For binders, the stress sensitivity in MSCR (Multiple Stress Creep and Recovery test) was observed to decrease probably due to stiffness increase as cited in Akentuna *et al.* (2022). For asphalt mixtures, the same decrease in moisture resistance was observed when the severity of the conditioning protocol increased. Despite that, when compared to Indirect Tensile Strength Ratio (ITSR), the authors did not observe an agreement to the other Ratios evaluated on tests.

### *2.3.4 Moisture damage at the aggregate-binder interface*

For materials interface, Cui *et al.* (2014) used peel tests in both dry and wet conditions to evaluate aggregate-binder adhesion. They used the same 40/60 bitumen combined to four aggregates divided in basic and acid respectively: (i) limestone and marble; (ii) two different granitic. Moreover, the authors evaluated the use of different anti-stripping agents: two silane-based, a commercial amino-based anti-stripping and a styrene-butadiene-styrene (SBS) polymer.

With these combinations, the authors could assess both mineral composition and porosity properties as well as additive effects on adhesion. The peel test used consists of peeling the adhesive layer (asphalt binder) adhered to an aluminum peel arm from the mineral substrate

and evaluating the steady state residual force after reaching peak values. This test was performed. The conditioning method used by the authors was immersion in distilled water at 20°C for multiple periods up to 10 days.

The authors observed that when compared, chemical composition is more relevant than porosity for adhesion. As for the additives used, silanes were better suited for silica-rich granites, amino-based anti-stripping had impressive results for limestone and one of the granites, the SBS modification not only promoted a better adhesion, but also increased the fracture energy.

In other study, Sudarsanan *et al.* (2020) applied the time-temperature superposition principle to the Pull-Off Asphalt Bond Strength (ABS) of tack coats applied to a metal surface using the Binder Master Curve shift factors obtained from the Dynamic Shear Rheometer (DSR). In addition to the viscoelastic effects on the ABS test with the construction and adjustment of a Master Curve, these authors recommended an analysis on other surfaces in which the texture imitates reality, such as aggregates or asphalt mixtures. Another finding from the authors is the adhesive rupture probability in lower temperatures which could invalidate test results.

Cala and Caro (2021) developed a predictive quantitative model for assessing the asphalt-aggregate adhesion quality based on aggregate chemistry. They established a new Pull-Off test in which the adhesiveness was evaluated directly from a small binder film applied to the stone. The authors observed correlations from the oxides' percentage to the moisture damage susceptibility and proposed different analyses considering aggregates textures, asphalt binders, additives, and aging.

Considering asphalt binders, mineral substrates, and asphalt mixtures discs, Lucas Júnior *et al.* (2021) verified the effects of moisture conditioning associated with the Digital Image Processing techniques (DIP). The authors evaluated a pure and a modified binder containing amino-based anti-stripping agent using ABS and DSR rheological tests. They affirm that moisture affected the binders at the same intensity regardless of the additives presence. Besides, a better correlation ($R^2 > 0.75$) was verified for conditioned samples than for dry ones ($R^2 < 0.50$) on IDP and ABS analysis for asphalt mixtures discs.

Nazzal *et al.* (2021), using Atomic Force Microscopy (AFM) determined the adhesive and cohesive binding forces and correlated these results from micro to macro scales. These authors used different additives to produce warm asphalt mixtures with a Performance Grade (PG) 64-22 binder and the same binder modified ("M" suffix) with SBS to achieve a PG 70-22M. The obtained results indicate that the presence of the polymer was the main impact on the cohesive or adhesive forces. Nevertheless, cohesive forces of binders are less susceptible to

the moisture effect. In addition, the correlation between ITS and the cohesive force was $R^2 > 0.90$ on both conditioned and not conditioned samples.

Maia *et al.* (2021) motivated by the aggregate-binder interface problem studied the properties of traditional bituminous mixtures containing acidic aggregates and a neat binder modifying the nature of the filler (granitic crushed rock or limestone) or adding a specific chemical component such as cellulosic fiber pellets. The authors evaluated four aggregate-filler-binder combinations, not only for adhesion, but also moisture induced damage and rutting properties. Their results indicate that the use of fiber pellets promote better adhesion. Similar results considering ITSR were observed for both fiber pellets and limestone filler and this trend was also observed for rutting. These findings point out that not only rupture testing are impacted by moisture resistance but also rutting resistance could be enhanced with an anti-stripping agent, whether it is a mineral filler or chemical additive. This is also corroborated by conclusions from Mohammad *et al.* (2000).

Alkofahi and Khedaywi (2021) performed a literature review on the state-of-the-art in adhesiveness of asphalt mixtures. The authors highlight several variables related to the study and the impacts of aggregate, binder, and additives selection additionally to the pavement's construction and operation aspects, as well as field testing. Among the main conclusions on the state of the art of the theme, one might cite (i) adhesiveness (or moisture damage) could be the cause of pavements distresses in many countries; (ii) the CaO and $SiO_2$ contents are relevant to adhesiveness; (iii) Hydrated Lime is considered one of the cheapest and best adhesiveness improving agent; (iv) the binders film thickness is a key point to understand the damage resistance; (v) the development of a simple and precise test to evaluate adhesiveness is essential.

Although moisture damage or moisture conditioning tests were not the aims of the work, Orozco (2021) developed a new test to evaluate thin asphalt films between rocks. The test consisted of evaluating different films thickness in a uniaxial tension-compression state to induce homogeneous loading to the sample using a Hydraulic Press to determine Pull-Off Strength and LVE properties. Some of the main contributions of this new kind of test were an indicative that asphalt binder is almost incompressible mainly in lower frequencies with a Poisson ratio of approximately 0.498; the possibility of performing pull-off tests in thin films in both strain and stress rate controlling.

### *2.3.5 Moisture-induced damage in asphalt mixtures*

There are many moisture tests and conditioning methods, besides the many

modifications performed by researchers in specific works. The literature points out different adhesiveness-improving additives, methods to evaluate conditioned specimens, and moisture effects on different scales. Hunter and Ksaibati (2002) mention Lottman, Static Immersion, Tunnicliff and Root, Boiling, Immersion-Compression, Texas Freeze-Thaw Pedestal Test, and Modified Lottman that evaluate the mixtures resistance to moisture.

Besides different conditioning methods, Ribeiro (2011) examines the response regarding moisture-induced damage of liquid from cashew (LCC) comparing it to Hydrated Lime. For the asphalt mixture containing Pure Binder, the author evaluated two alterations to the "Modified Lottman" procedure as well as the standard considering 7% Air Voids (AV) and -18ºC freezing temperature.

Ribeiro (2011) modified the AV to 4% and cooled the samples only until 10ºC since -18ºC is not a Brazilian representative temperature. To evaluate the additives, only the standard procedure was performed. The author affirms that the 10ºC cooling retains ITS above 80% for pure mixtures, equivalent to using 2% of LCC or 2% of Hydrated Lime, even when these mixtures were conditioned with the -18ºC freezing.

Barra *et al.* (2012) studied the effects of fatigue in 3 conditions: dry, 60% saturated samples immersed in water and 60% saturated immersed in water after a pre-conditioning of 3 blocks of 5 days immersion at 60°C followed by 3 days in an oven at 60°C without water. The authors used a testing protocol of 2 points bending (2PB) in trapezoidal samples at 10°C and 25Hz and displacement control, and the adopted failure criteria was the drop of displacement force to half of its initial value.

According to the findings for two asphalt mixtures: one with neat binder and granitic aggregated and another mixture with limestone filler, Barra *et al.* (2012) observed that limestone filler promoted and increase in fatigue life in all conditions evaluated. The authors affirm that this behavior is due to the filler's mineralogy and chemical properties.

Furthermore, the saturation conditioning of asphalt mixtures presents low capacity of modifying binders' viscosity, thus a long-term of water effect would be necessary to act as an anti-stripping. This opposes the observation for a pre-conditioning involving multiple immersion and temperature effects, as temperature highly impacts the effects of water on asphalt mixtures.

For the use of the additives, Anitelli (2013) states that the use of Styrene-Butadiene-Styrene (SBS) polymer or HL makes the asphalt mixtures more resistant or at least similar to the control mixture considering the ITS Ratio (ITSR). Medeiros *et al.* (2017) studied the use of Hydrated Lime as filler material in the proportions of 0, 2, and 4%. The ITSR and Resilient

Modulus tests were evaluated as well as an Image Digital Processing (IDP) tool. The results indicate that the use of Hydrated Lime in 2% or 4% is satisfactory to obtain ITSR above 70%.

According to Lucas Júnior (2018), evaluating adhesiveness, the DIP analysis presents a good correlation to the Moisture Induced Damage test. The author evaluated Phonolitic and Granitic Aggregates with the variation of binder type: 50/70 $mm^{-1}$ penetration binder, 50/70 + anti-stripping liquid agent, 50/70 + plastic bag residue. Moreover, the author reinforces that the use of anti-stripping liquid agent improves the results of adhesiveness, ITSR, and Tension-Compression Fatigue. However, the author did not perform analysis on conditioned samples for Complex Modulus (|E*|) or Tension-Compression Fatigue. These are recommendations from the author.

Barboza Junior (2018) evaluated the effect of moisture on stiffness, ITS, and rutting of asphalt mixtures containing 50/70 binder, and Polymer Modified Binder (PMB) 60/85 with or without the use of Hydrated Lime. The author emphasizes that the use of PMB 60/85 and Hydrated Lime might improve the durability of pavements. It is also described that there is a need for more research in Brazil about rutting, viscoelastic, and fatigue analysis considering moisture damage. However, the author highlights that the Uniaxial Repeated Load Test might not be the better protocol to evaluate the effects of moisture on rutting. Fatigue testing is also recommended on conditioned samples.

Considering the effects of water on asphalt mixtures, Brondani (2019) investigated the effects of two moisture damage cycles on |E*| and only one cycle to ITSR. Although the evaluated mixtures presented a loss of resistance after conditioning, the author relates that these mixtures had the minimum 70% of ITSR which is one of the admitted limits. The author mentions that for |E*|, the variation on characterization curves is more significant after the first conditioning cycle. This consideration was made based on the 2S2P1D model. She also highlights the distancing of characterization curves that reinforces the higher susceptibility of 50/70 Binder to moisture, as already described in the literature.

Lamothe *et al.* (2019) evaluated uniaxial homogeneous tension-compression Fatigue tests in both dry and partially saturated with water (PSW) conditions. The conditioning method used by the authors consisted of the application of vacuum in samples for 30 minutes at 22°C followed by 90 minutes immersion in water. After this conditioning, a latex membrane was used to preserve its saturation level prior and during testing. The indicated no significant variation at initial modulus ($|E^*|_0$). A reduction in fatigue life was observed for PSW samples with high differences magnitudes between samples, and the difference was addressed probably at the microstructural level between aggregate-binder interface damage. Despite that, when

using the Corrected Damage parameter ($D_{IIIC}$) (DI BENEDETTO *et al.,* 2004), dry and PSW samples would fail around 23% of $D_{IIIC}$, and no significant difference was observed.

In another study, Cardona *et al.* (2021) proposed a Tension-Compression analysis on conditioned samples using a new moisture-induced damage conditioning method. The method consists of a water bath at 60ºC for 168h, surface drying followed by -18ºC freezing for 24h inside a plastic bag with 100mL of water, and finally 30h of climate chamber heating at 40ºC. According to the authors, this method accelerates moisture-induced damage without causing microcracking due to saturation forcing. Among the evaluated asphalt mixtures, the dispersion of Wöhler curves results complicated the evaluation of a tendency other than materials' degradation on two of the three evaluated mixtures.

In a similar study, Almeida *et al.* (2018) evaluated an asphalt mixture regarding both rheology using |E*| and fatigue using 2PB. The core of the testing protocol also relies on immerse versus dry testing with and without preconditioning cycles.

Although, a different conditioning method than the used by Barra *et al.* (2012) was chosen as well as the use of a Damage Factor (D) in the Huet-Sayegh rheological model to evaluate the influence of water. Almeida *et al.* (2018) performed 5 blocks of 18h at a 60°C water bath followed by 6h in an oven without water at 60°C to condition samples. For fatigue testing, the authors also used two temperatures, 10 and 20°C at 25Hz. The authors concluded using the cited conditioning method that the combination of water and temperature considerably modifies rheological properties of asphalt mixtures. That indicates that asphalt layers behavior in regions with tropical climates would be notably altered under traffic's action. On the other side, the observed damage in viscoelastic properties is not linear as it is influenced also by other parameters such as AV content. As for fatigue, the coupled effects of temperature and water decreased ε6 strains by 16 to 27% respectively due to temperature and temperature with preconditioning and water immersion.

On another work, Brondani *et al.* (2022) investigated the effects of Moisture Induced Damage at |E*| using the conditioning protocol in AASHTO T 283 (2021) for a total of 21 asphalt mixtures with different aggregates mineralogy, type of binder and penetration as well as content, and Nominal Maximum Aggregate Size (NMAS). A new index (Dynamic Modulus Area Ratio – DMAR) derived from |E*| master curves alterations in dry and conditioned samples was also proposed. The findings using the DMAR and ITSR did not present good correlations probably due to the loading scheme and the destructive characteristics of ITSR compared to LVE characterization. Although, the use of the new index presented good results to perceive the entire modulus spectra variation, so in the future it could be used in

performance testing as well as field analysis to evaluate stiffness differences.

Different to conventional fracture or fatigue investigations, Frossard *et al.* (2022) used Semi Circular Bend (SCB) tests to determine fracture parameters of different aggregate/fillers used in asphalt mixtures when subjected to moisture induced damage. The authors used natural aggregates combined with slag aggregates (SA) and fillers from natural aggregate (NA), slag aggregate, hydrated lime (HL), electrostatic precipitator (EP) due to their different chemical composition.

One of the authors' observations was that without moisture damage, all five designed mixtures had similar fracture behaviors, opposing to their results after the damaging protocol. It was observed, as expected, a higher reduction for natural aggregates, followed by SA, EP, mix of SA and NA powders and HL for maximum loading force. These results indicate that some fillers are more susceptible to moisture damage and are likely to maintain or lose ductility, becoming brittle materials. From the testing protocol, Frossard *et al.* (2022) indicated that TSR and SCB's maximum force parameter have a good correlation.

## 2.4 Final considerations

The previous topics presented a review of the literature from linear viscoelastic properties, fatigue damage and water effects on pavements and its material damage susceptibility. Some highlights are provided below:

- Asphalt pavements surface layer encounters water by different means at different stages of service life: residual moisture of constituents, construction mistakes, precipitation, percolation, groundwater ascension, and water vapor;
- Most asphaltic materials studies considering water conditioning (or moisture damage) protocols usually focuses on one scale of analysis: binder, aggregate-interface, fine aggregate matrix, or asphalt mixture;
- Moisture effects (or water conditioning) might influence results from the binders and mixture scales with different proportions;
- The quantification of aggregate-binder interface studies has potential whether with the use of widely known techniques such as Pull-Off testing or the development of new tests;
- Conditioning protocols might vary due to local standards and therefore testing results might not be comparable. Hence, both |E*| and fatigue results can determine scattered data or a significant reduction in LVE or fatigue-life properties.

# 3 MATERIALS AND METHODS

## 3.1 Summary of experimental program

This thesis aims to evaluate different asphaltic materials in three scales: binder, aggregate-binder interface, and mixture. Therefore, a broad experimental plan consisting of existing testing protocols: ASTM D 6575 (2015), AASHTO T 342 (2011), AASHTO TP 107 (2014), AASHTO T 361 (2016), AASHTO T 391 (2020), AASHTO T 283 (2021), AASHTO T 240 (2021). Figure 14 shows a summary of the selected experimental program to achieve all objectives of this thesis.

Figure 14 – Experimental program summary.

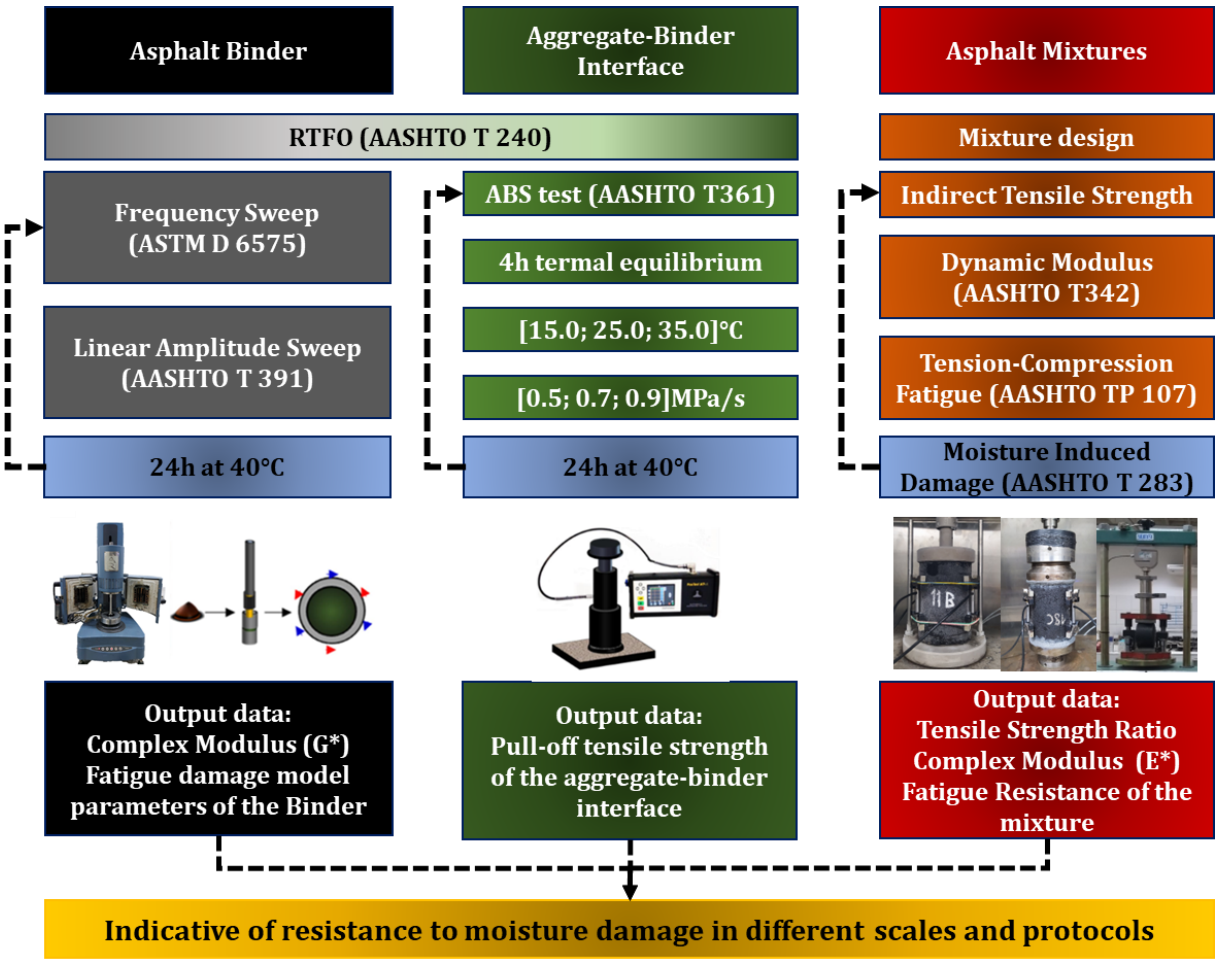


(Source: Author).

## 3.2 Materials

### *3.2.1 Asphalt binder*

The used binder in this research is characterized by Penetration as 50/70mm$^{-1}$, and is produced in Fortaleza, Ceará. It is classified by Performance Grade (PG) as 64-XX and is widely used in paving works in Brazil. Table **1** presents the binders empirical characterization. The lower temperature is not specified for the binder herein used as the temperature gradients in Brazilian Northeast aren't wide enough to require this specification.

Table 1 – Neat binder characterization.

| Tests | Neat Binder | Limits |
|---|---|---|
| **Penetration at 25.0ºC (mm$^{-1}$)** | 46 | 50-70 |
| **Softening point (ºC)** | 49 | Min. 46 |
| **Brookfield viscosity at 135ºC (cP)** | 399 | Min. 274 |
| **Mixing range (ºC)** | 150-156 | Max. 177 |
| **Compaction range (ºC)** | 140-144 | Max. 177 |

(Source: Author).

### *3.2.2 Anti-stripping additives*

As this research focuses on evaluating Fatigue Cracking resistance after moisture conditioning, two different commercial anti-stripping agents were selected as follows:

- Amine-based anti-stripping liquid agent;
- Hydrated Lime (HL) classified as HL-1 (higher $Ca(OH)_2$ content).

These additives were not characterized in the thesis since it does not contemplate different anti-stripping liquid agents, HL origins, or other adhesion promoters to compare their efficiency. These materials were selected to understand how different anti-stripping agents would behave along with the used methodology. For further information on HL production in Ceará and hydration reactions to the material it is recommended to read Araújo (2009) which describes the application of HL to stabilize soils.

The anti-stripping amine-based agent used in this thesis was added to the binder at the proportion of 0.7% weight/weight. For the rheologic characterization, a sample of 300g of binder was modified using a mixing apparatus at 130°C for 30 minutes with an average 1000 RPM speed, as observed in Figure 15. This process was not performed for HL as the addition was made directly over the aggregates before heating.

Figure 15 – Anti-stripping amine-based agent and binder mixing process.

(Source: Author).

### *3.2.3 Aggregates*

This work used aggregates available in Fortaleza's metropolitan area, in the state of Ceará, Brazil, due to the availability and applicability of the Thesis results to local specifications (Figure 16).

Figure 16 – Quarry located in maps and aggregates piles.


(Source: Adapted from Google Maps and personal picture).

The used aggregates are classified as Gneiss and were collected from three different Nominal Maximum Aggregate Size crusher piles with 19.0, 12.5 and 4.8mm. Figure 17 shows

the aggregates grading curves. For anonymity purposes, the name of the Quarry is not presented. The basic characterization of aggregates was performed according to Brazilian specifications as presented in Table 2.

Figure 17 – Aggregates gradation.

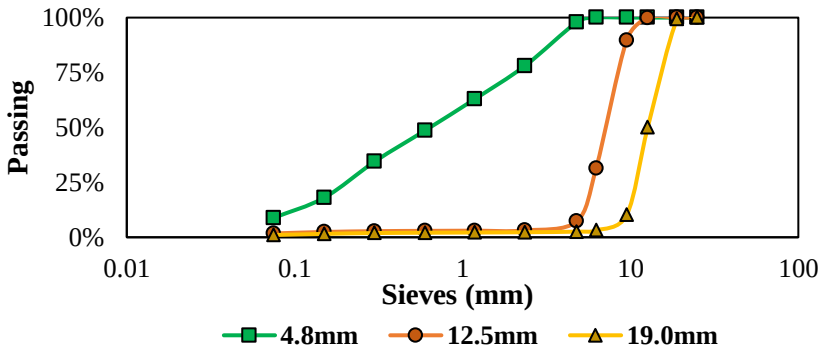


(Source: Author).

As observed in Table 2, Gneiss aggregates show poor adhesiveness properties as the aggregated from this quarry are characterized as acidic (Lucas Júnior *et al.*, 2021).

Table 2 – Aggregates basic characterization.

| Tests | Standard | 19.0mm | 12.5mm | 4.8mm |
|---|---|---|---|---|
| **Los Angeles abrasion (%)** | **DNER 035/98** | 31 | 35 | - |
| **Absorption (%)** | **DNIT 411/2019 and 412/2019** | 0.45 | 0.80 | - |
| **Specific Gravity (g/cm³)** | **DNIT 411/2019 and 412/2019** | 2.665 | 2.664 | 2.775 |
| **Adhesiveness test** | **DNER 078/94** | Unsatisfactory (Neat Binder) Satisfactory (+0.7% anti-stripping liquid agent) | - | - |

(Source: Author).

In addition to 19.0, 12.5, and 4.8mm aggregates for asphalt mixtures production, larger rocks from the Quarry were collected (Figure 18) to perform the ABS testing with the following combinations.

- Gneiss, and neat 50/70 binder;
- Gneiss, and neat 50/70 binder with anti-stripping liquid agent.

Figure 18 – Rocks at quarry and prismatic cut.

(Source: Author).

## 3.3 Methods

### *3.3.1 Asphalt mixtures design*

The asphalt mixtures design followed the Superpave methodology considering 4.0% target Air Voids (AV) at 100 gyrations for the reference mixture (M1). All mixtures follow DNIT 031 (2006) standard inside the C-Range gradation limits (similar to Superpave 12.5mm NMAS). Figure 19 presents the proposed gradation curve obtained combining the aggregates as 20% of 19.0mm, 35% of 12.5mm, and 45% of 4.8mm aggregates.

Figure 19 – Project gradation.

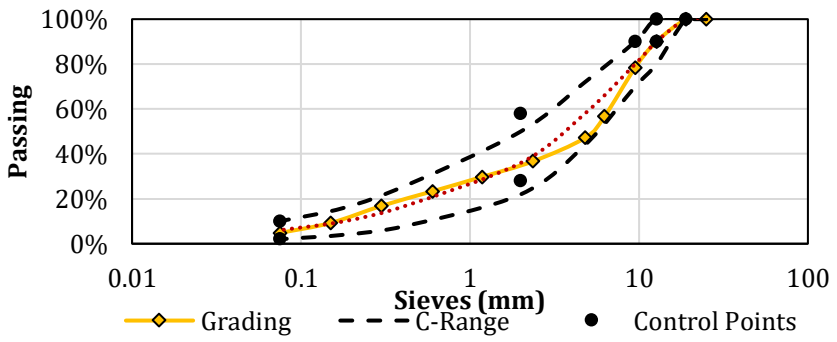


(Source: Author).

As observed in Table 2, the used aggregates would demand an anti-stripping agent to attend to the minimum requirements described at DNER 078 (1994). Therefore, both anti-stripping amine-based agent and HL are used in this work with gradation, binder origin and content fixed values to keep as many variables as possible constant.

Considering the selected materials, the asphalt mixtures produced are:

- M1: gneiss, and neat 50/70 binder – Reference Mixture;
- M2: gneiss, and 99.3% 50/70 binder + 0.7% anti-stripping amine-based agent;
- M3: 99.0% gneiss + 1.0% Hydrated Lime, and neat 50/70 binder.

It is highlighted that for M2, the anti-stripping liquid agent content was chosen after testing which percentage promoted better results at an anti-stripping test. Therefore 0.7% of anti-stripping liquid agent in relation to the binder weight in the mixture was used. The HL addition was evaluated in different proportions from 1.0 to 2.0% of the aggregates' weight into the mixture to produce M3, but the chosen percentage was 1.0% to prevent too low Air Voids (AV). The used method to incorporate HL into the mixture was the removal of 1.0% in weight of the 4.0mm aggregates to incorporate 1.0% of HL before mixing the material with the aggregates prior to heating the group to the mixing temperature.

A general production process of the asphalt mixtures is divided into: determining 3 initial binders contents to test which one results in a mixture with 4% AV at 100 gyrations, 4.0%, 4.5%, and 5.0% were used; separate aggregates following the gradation proportions to produce 3 small compacted specimens of 1200g to calculate the Maximum Bulk Gravity ($G_{mb}$) in Equation 16, and 2 loose mixture samples of 1500g to determine the Maximum Measured Gravity ($G_{mm}$) in Equation 17; the aggregates are heated to 10°C higher than the mixing temperature, while the binder is heated to the mixing temperature; they are then mixed until a homogeneous mixture is obtained; the loose mixture is placed inside an oven at the compaction temperature during 2h to simulate a short aging period of the mixture; after aging, the 3 small samples are compacted and the loose mixture is cooled until room temperature.

$$G_{mb} = \frac{W_{dry}}{W_{saturated} - W_{submerged}} \times 0.9971 \quad (16)$$

$$G_{mm} = \frac{MW_{dry}}{MW_{dry+}\, CW_{submerged} - MW_{submerged}} \times 0.9971 \quad (17)$$

Where:

$W_{dry}$ = dry specimen weight (g);

$W_{saturated}$ = saturated specimen weight (g);

$W_{submerged}$ = submerged specimen weight (g);

$MW_{dry}$ = loose mixture dry weight (g);

$CW_{submerged}$ = submerged cylinder weight (g);

$MW_{submerged}$ = submerged cylinder with loose mixture weight (g).

As previously mentioned, the same grading curve was used, and the asphalt content was kept for the 3 mixtures. Therefore, M1 was designed with 100 gyrations, M2 also attended 4.0% AV with 100 gyrations, but M3 was produced with only 40 gyrations to achieve 4.0% AV due to the HL effect. Considering the aforementioned procedure, Table 3 summarizes the asphalt mixtures characteristics.

Table 3 – Asphalt mixtures design specifications.

| **Asphalt Mixture** | **M1** | **CV (%)** | **M2** | **CV (%)** | **M3** | **CV (%)** |
|---|---|---|---|---|---|---|
| **Binder content (%)** | 4.4 | - | 4.4 | - | 4.4 | - |
| **Air voids (%)** | 3.9 | 4.6 | 3.8 | 9.0 | 4.2 | 1.7 |
| **Void bitumen ratio (%)** | 72.6 | 1.3 | 72.8 | 1.7 | 70.9 | 0.7 |
| **# Gyrations** | 100 | - | 100 | - | 40 | - |
| **Gmb** | 2.368 | 0.2 | 2.362 | 0.4 | 2.341 | 0.1 |
| **Gmm** | 2.463 | 0.0 | 2.456 | 0.1 | 2.444 | 0.1 |

(Source: Author).

It is observed from results in Tables 3 and 2, that the low absorption of the aggregates most likely caused a lower Binder Content of 4.4% to be enough for the mixtures design. Besides that, the 1% of HL would also reduce the need of Binder.

### *3.3.2 Moisture conditioning of asphalt binders*

To address moisture damage on asphalt binders, two different conditioning periods were evaluated before deciding which one to perform as standard to the research presented herein. The first conditioning was achieved using 25.0mm asphalt samples of 1.0g approximately on silicon molds submerged in distilled water at 40.0ºC for 72h as Figure **20** shows.

Figure 20 – Moisture conditioning of binders.

(Source: Author).

This procedure copies the conditioning method used to address stripping on coarse aggregates as stated by DNER 078 - Adhesiveness Test (1994). Despite this criterion, 24h conditioning at 40.0ºC was also tested as it is a more practical period when multiple replicates are required for binders or aggregate-binder interface. After the conditioning step, the binders were let at room temperature so the residual surface water could evaporate, then all conditioned samples were kept in a sealed recipient to prevent contamination.

### *3.3.3 Frequency Sweep*

For the stiffness characterization, the Frequency Sweep – FS (ASTM D7175, 2015) test is performed on the same DSR to reduce variability possibility. The FS is performed in a wide temperature and frequency ranges varying from 4.0 to 82.0ºC and from 0.16 to 25.0 Hz. All binders were short-term aged using the Rolling Thin Film Oven (RTFO) (AASHTO T 240, 2021).

The test is divided into two steps: in the (i) step one, at lower temperatures [4.0, 16.0, 28.0, 40.0] ºC at 8.0mm plate-plate geometry with a 2000.0$\mu$m gap is used, and in the (ii) step two, at higher temperatures [46.0, 52.0, 58.0, 64.0, 70.0, 76.0, 82.0] ºC at 25.0mm plate-plate geometry with a 1000.0$\mu m$ gap is used. This division is necessary due to the equipment's maximum torque. The procedure is illustrated in Figure 21.

Figure 21 – Frequency Sweep test representation.

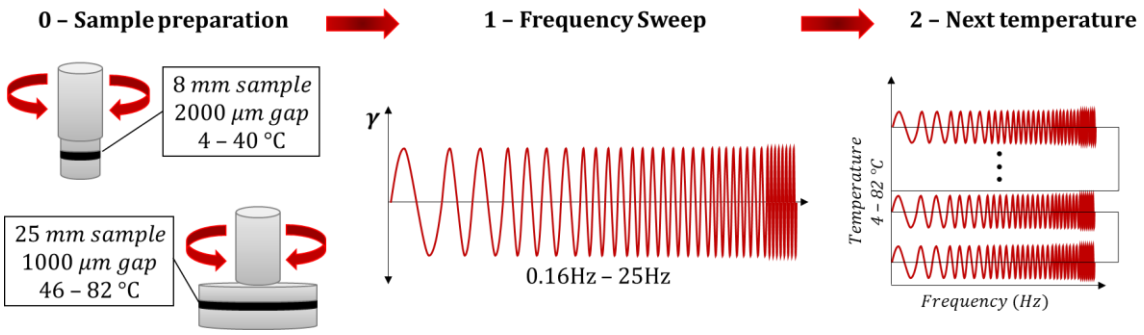


(Source: Author).

Therefore, the construction of a Master Curve at a reference temperature gives the stiffness behavior of the binder. The procedure for that is simple as the DSR software has a

function to shift test results to any given reference temperature and calculate the shift factors ($a_T$). However, a step-by-step process using spreadsheets is also possible such as for asphalt mixtures (Section 3.3.7).

As dry and wet tests are performed, the stiffness differences are analyzed by Complex Shear Modulus |G*| values. This should answer if the binder is truly affected by water during the conditioning protocol used in this work.

### *3.3.4 Linear Amplitude Sweep*

For fatigue binder characterization, the Linear Amplitude Sweep – LAS (HINTZ and BAHIA, 2013; AASHTO T 391, 2020) test is performed on a TA AR 2000 Dynamic Shear Rheometer at 25ºC. The use of this test temperature is due to the better output of LAS testing at 25ºC compared to 19ºC for a neat PG 64-XX binder (SAFAEI and CASTORENA, 2016). As Frequency Sweep, LAS tests are conducted after binders' aging protocols.

AASHTO T 391 (2020) requires both RTFO or RTFO + Pressure Aging Vessel (PAV) aging protocols. Although, as these test results will be compared to asphalt mixtures only short-term aged, and this thesis does not evaluate different aging protocols, it was chosen that only RTFO aging would be performed. Beside the same aging consideration, it is observed that fatigue evolution might occur from early stages of asphalt layer service life due to traffic loading.

According to AASHTO T 391, the LAS test consists of a Frequency Sweep test at 0.1% strain from 0.2 to 30.0Hz at constant temperature followed by an amplitude sweep from 0.1 to 30% strain at 10Hz represented in Figure 22.

Figure 22 – LAS test representation.

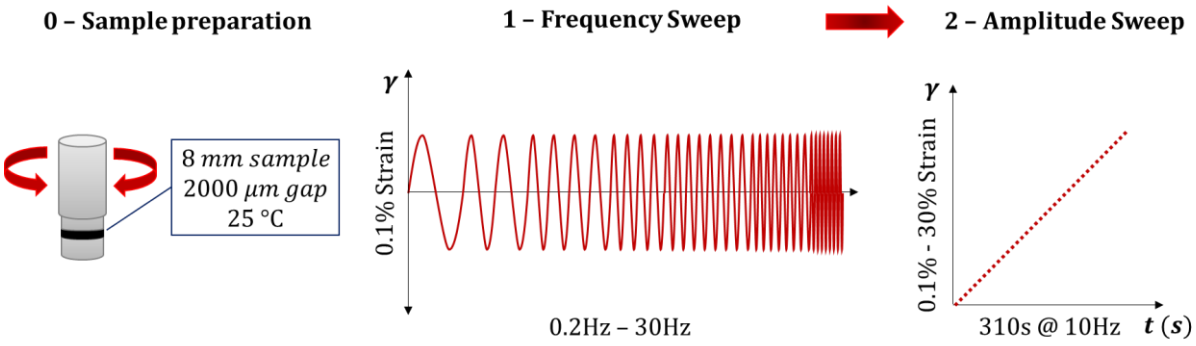


(Source: Author).

LAS results as the Damage Characteristic Curve with the C1, C2 parameters and the crack length ($a_f$) are determined until the failure cycle and fitted to the S-VECD model (SAFAEI *et al.*, 2014). The last parameter usually is obtained at the maximum Pseudo Strain Energy Release (PSE) and maximum torque observed at the DSR data (WANG *et al.*, 2015). The alpha (α) parameter derives from the frequency sweep results and corresponds to a measurement related to the material's ability to relax stress (HINTZ *et al.*, 2011). All calculations for damage during the LAS test derive from the $a_f$ parameter calculated in Equations 18 to 20, and the different output data charts are presented in

Figure **23**.

$$r^4 = \frac{k.2.h}{\pi.|G^*|_0} \quad (18)$$

$$r_n^4 = r_i^4.\frac{k_n}{k_i} \quad (19)$$

$$a_f = r_i - r \quad (20)$$

Where: k = ratio of torque and deflection angle;

$h$ = sample height;

$|G^*|_0$ = undamaged complex modulus;

$r_n$ = is radius at cycle N;

$r_i$ = is sample initial radius;

$k_n$ = torsional stiffness at cycle N;

$k_i$ = initial torsional stiffness;

$a_f$ = crack length.

Figure 23 – LAS resulting parameters graphics.

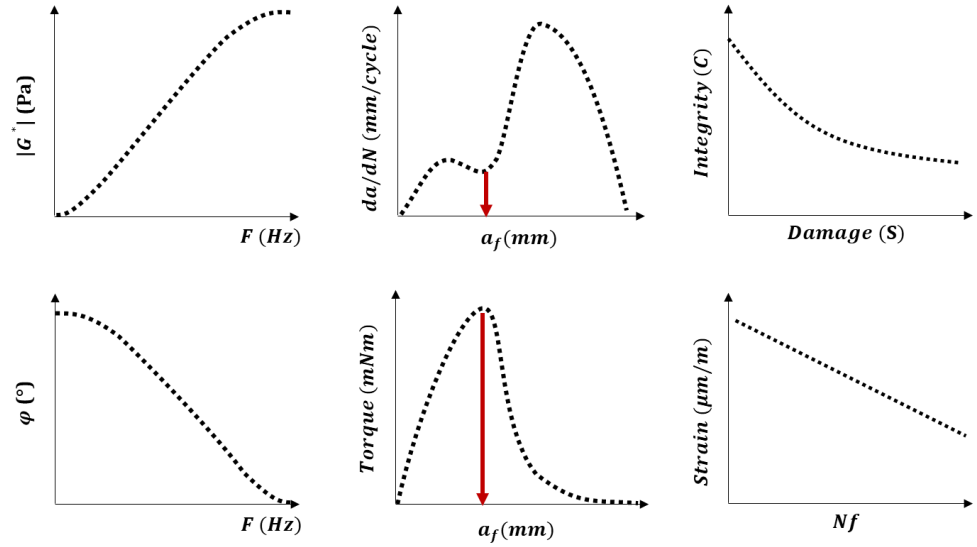


(Source: Author).

As the test allows fatigue parameters to be determined in a fast way, Wöhler Curves are also constructed. Therefore, a simple analysis is performed with both fixed failure cycles number ($N_f$) or fixed strain levels. To classify different binders, a tool developed by Nascimento *et al.* (2014) is the Fatigue Factor of Binder ($FF_B$). It is defined as the area under the Wöhler curve between 1.25 and 2.50% strains as described in Equation 21.

$$FFB = \frac{\log(N_{f,1.25\%})+\log(N_{f,2.5\%})}{2} \times [\log(0.025) - \log(0.0125)] \quad (21)$$

Considering the different binders' parameters, it is possible to perform a comparison between dry and wet results. The same way, a ratio between those parameters can be determined. This is performed for both Wöhler Curves and $FF_B$.

### *3.3.5 Pull-Off Test*

The Asphalt Bond Strength – ABS (AASHTO T 361, 2016) test with hydraulic equipment evaluates the materials' adhesion (Figure 24). Since it measures the pulling-off maximum tensile strength, the "pulling-off" expression will be used throughout this thesis.

The test is performed using metallic stubs and a prismatic aggregate substrate with approximate dimensions of [14.0 × 10.0 × 3.0] cm (Figure 24). The preparation procedure, as described at AASHTO T 361 (2016), consists of the following steps:

i.Placing the aggregate substrate at an ultrasonic bath with distilled water for 1h to remove any

residual dust or contaminants;

ii. Heating the substrates and metallic stubs at the mixing temperature for 1h;

iii. Preparation of binder samples in circular molds, approximately 0.4g each and 8mm in diameter;

iv. Placing these samples on a hot stub surface, approximately 20mm in diameter, with caution to guarantee the complete melting of the binder and the stub surface covering. This group is then pressed against the substrate for approximately 10s for adhesion.

v. The (iv) step is repeated until all samples are prepared. It is necessary to keep space to fit the tension apparatus between stubs;

vi. The substrate and stubs are left to stand at room temperature (25.0ºC) for 24h before testing. An automatic hydraulic tension equipment performs the test, and the maximum value is registered as the Pull-off strength (Figure 25). If water conditioning is used, the samples are kept under water at the desired temperature during this 24h interval.

Figure 24 – Metallic stubs, prismatic substrate and sample ready for testing.


(Source: Author).

After the dry tests, a second batch of samples is conditioned in a water bath at 40ºC for 24h. The same period and temperature are chosen to prevent different effects between scales.

Figure 25 – ABS representation.

(Source: Author).

Besides the standard pull-off rate and temperature, this test was also performed with other combinations to evaluate the viscoelastic effect considering: [0.3; 0.7; 0.9MPa/s] and temperatures of [15.0; 25.0; 35.0ºC]. This way, the obtained tension points are translated to a single equivalent condition in a Pull-Off Master Curve also capturing the moisture effects and the use of a commercial anti-stripping agent.

After testing dry and wet samples, it is possible to determine the Retained Pull Off Strength ($RPOTS$) of samples as the ratio between wet and dry samples.

Due to the elevated number of tests, only the 24h water bath (Figure 26) was used as a conditioning method. As for thermal equilibrium, after the 24h at 25.0ºC for dry samples or 40ºC in the water bath for conditioned samples, a 4h period at test temperature was used as a conditioning period if the test was conducted at a different temperature such as 15.0ºC and 35.0ºC.

Figure 26 – ABS samples in the water bath.

(Source: Author).

### *3.3.6 Moisture Induced Damage Test and conditioning protocol of Asphalt Mixtures*

The Brazilian specification DNIT 180 (2018) determines the procedure to evaluate asphalt mixture resistance to moisture damage. This test requires 6 samples of asphalt mixtures with 7.0±1.0% AV with an approximate dimension of 6.0 cm height × 10.0 cm diameter. The testing preparation and procedure are described in the following steps:

i. Measure all specimens and determine their AV;
ii. Divide into 2 groups of 3 specimens each;
iii. Submerge 3 samples in a container connected to a vacuum pump. Apply a vacuum between 97.0mmHg and 502.5mmHg for 5 to 10 minutes;
iv. Weight the 3 specimens to determine the volume of absorbed water. This volume determines the Saturation level (S) and should be between 55% < S < 80%. If S < 55%, the second step must be repeated, but if S > 80% then the specimens should be discarded;
v. Cover the 3 saturated specimens with plastic film, put them inside a plastic bag with 10mL of distilled water and seal the bag;
vi. Place the 3 sealed bags in a freezer at -18°C for 16h, then remove the specimens from the bags and submerge them in a water bath at 60°C for 24h. After this period, place them in water bath at 25°C for 2 to 3h.
vii. The 3 non-saturated specimens are only conditioned at 25°C for 2h to 3h dry.
viii. The 2 groups are then tested for Indirect Tensile Strength. The ratio between conditioned samples ($ITSc$) and non-conditioned ($ITS$) determines the Indirect Tensile Strength Ratio ($ITSR$), as observed in Figure **27**.

Figure 27 – Indirect Tensile Strength test.

(Source: Author).

Despite DNIT 180 (2018) only determines the procedure for small samples, an

adaptation is performed to condition taller samples. The AV of Dynamic Modulus and Tension-Compression Fatigue were chosen to be inside a range of 4.0±1.0%. This ± 1.0% admitted range is the same used for the Brazilian standard Moisture Induced Damage test of 7.0±1.0% AV specimens.

To perform the water bath at 60ºC, the saturated samples were kept in 2000mL Beakers inside an oven (Figure **28**) and the water temperature was verified at different periods to observe if the samples were in thermal equilibrium with low variations. This was done to avoid laying samples during a heating process, which could deform the samples.

Figure 28– Water bath at 60°C inside an oven.


(Source: Author).

To perform Uniaxial Dynamic Modulus and Tension-Compression Fatigue tests, all conditioned samples are kept at room temperature for at least one week to prevent excessive residual moisture (Figure **29**). This minimum period was determined to prevent adhesion problems with the Epoxy adhesives used to prepare samples. The same samples used in dry dynamic modulus tests were used to perform conditioned dynamic modulus.

Figure 29 – Samples at room temperature for 1 week.

(Source: Author).

### *3.3.7 Uniaxial Compression Complex Modulus*

The Brazilian Standard for the determination of the Dynamic Modulus (|E*|) of asphalt mixtures is DNIT 416 (2019), which describes a protocol similar to the one in AASHTO T 341 (2011). The test is performed using 3 cylindrical specimens of 150.0±2.5mm height × 100.0±2.0mm diameter at the desired AV content.

These specimens receive metal pieces glued with Epoxy adhesive spaced 120° each pair. This allows the instrumentation of Linear Variable Differential Transducers (LVDTs) to the sample. The set of glued and instrumented sample is then placed inside the Thermal Chamber of the Universal Testing Machine (UTM-25) centered to the actuator as Figure **30** illustrates.

Figure 30 – Dynamic modulus test instrumentation.


(Source: Author).

A cyclic sinusoidal loading is applied in compression mode varying from a minimum contact value of 5.0% of the maximum stress. The stress level is defined to the axial strain that remains inside the Linear Viscoelastic (LVE) limits between 50 and 150$\mu\varepsilon$. A target value of 34$\mu\varepsilon$ for half wave amplitude is used, therefore a level of 75$\mu\varepsilon$ from peak to valley.

The test is divided into three main parts (i) thermal conditioning, described in

Table **4**; (ii) fingerprint; and (iii) dynamic modulus:

i. Thermal conditioning: all samples are kept inside the thermal chamber until temperature equilibrium is reached, according to
ii.
iii. Table **4**.
iv. Fingerprint: one sample is tested using 50% of the maximum stresses applied to a known

asphalt mixture. This step results in axial strains for the specific loading pattern, but since it is assumed, they are in a linear domain, a proportional estimation is performed to determine the admitted maximum stress for $34\mu\varepsilon$.

v. Dynamic Modulus: using the maximum stress estimated during the fingerprint stage, the test is performed according to the frequencies and cycles defined also in

vi.

vii. Table **4**.

Table 4 – Dynamic Modulus test specifications.

| **Test temperature ± 0.3 (ºC)** | **Minimum temperature equilibrium duration** | | **Frequency (Hz)** | **Cycles** |
|---|---|---|---|---|
| | **Ambient** | **Previous test** | 25 | 200 |
| **-10.0** | Overnight | Overnight | 10 | 200 |
| **4.4** | Overnight | 4 h | 5 | 100 |
| **21.1** | 1 h | 3 h | 1 | 20 |
| **37.8** | 2 h | 2 h | 0.5 | 15 |
| **54.0** | 3 h | 1 h | 0.1 | 15 |

(Source: Adapted from DNIT 416, 2019).

In the end, the main output data are |E*| and phase angle ($\varphi$). |E*| represents the modulus and $\varphi$ the delay between the applied stress and calculated strain during sinusoidal loading, which describes the viscoelastic property of asphalt mixtures. These data are used for the construction of the Dynamic Modulus Master Curve at a given reference temperature using the Time-Temperature Superposition Principle (TTSP).

The master curve is constructed by changing the reference frequency of data. It uses a shift factors ($a_T$) calculated with different expressions, such as the Williams-Landel-Ferry or WLF Equation described in Equations 22 and 23. The intermediate temperature of 21.1°C is used as the reference temperature in the present work.

$$\log(a_T) = \frac{-C_1(T-Tr)}{C_2+(T-Tr)} \tag{22}$$

$$f_{red} = f \cdot a_T \tag{23}$$

Where:

$a_T$ = *shift factor* dimensionless;

$C1\ and\ C2$ = model constants dimensionless and in K respectively;

$T$ = tested temperature (K);

$Tr$ = reference temperature (K);

$f$ = tested frequency (Hz);

$f_{red}$ = reduced frequency (Hz).

As this thesis evaluates not only dry, but also wet specimens, all master curves are analyzed by comparing the behavior variations such as: absolute modulus variation, calibration constants divergence, and the ratio between wet and dry samples. This ratio is then determined during the test as $|E^*|_R$ (Equation 24):

$$|E^*|_R = \frac{|E^*|_{wet}}{|E^*|_{dry}} \quad (24)$$

Where:

$|E^*|_R$ = Dynamic modulus ratio (dimensionless);

$|E^*|_{Dry}$ = Dry dynamic modulus (MPa);

$|E^*|_{Wet}$ = Wet dynamic modulus (MPa).

### *3.3.8 Tension-Compression Fatigue*

The fatigue resistance of asphalt mixtures can be determined by different testing protocols, but a configuration that is known to only damage the sample with pure direct tension is the Uniaxial Tension-Compression test. As there is no current Brazilian standard for this test, the AASHTO TP 107 (2018) protocol with some adaptations is followed. The main difference to the current protocol is related to the determination of the specimens' initial strain levels.

This work still uses the Table **5** suggestion described in AASHTO TP 107 (2014). As for the desired initial strain levels, this research uses actuator displacement-controlled tests instead of strain-controlled ones. The number of testing samples and strain levels used in this thesis was six specimens for each asphalt mixture in both dry and wet conditions with three strain levels.

Table 5 – Initial strain levels.

| **Case** | **$\varepsilon_{os}$ (CP2)** | **$\varepsilon_{os}$ (CP3)** |
|---|---|---|
| 500<$Nf$<1,000 | $\varepsilon_{os1}$-100 | $\varepsilon_{os1}$-150 |
| 1,000<$N_f$<5,000 | $\varepsilon_{os11}$-50 | $\varepsilon_{os1}$-100 |
| 5,000<$N_f$<20,000 | $\varepsilon_{os1}$+50 | $\varepsilon_{os1}$-50 |
| 20,000<$N_f$<100,000 | $\varepsilon_{os1}$+100 | $\varepsilon_{os1}$+50 |
| 100,000<$N_f$ | $\varepsilon_{os1}$+150 | $\varepsilon_{os1}$+100 |

(Source: AASHTO TP 107, 2014).

The test uses cylindrical samples molded at the desired AV content and the height is reduced to 13.0cm to eliminate the extreme portions where most AV accumulates. Therefore, almost only the middle part of the specimen, in which the LVDTs are positioned, is left to be tested. Using this configuration, the chances to capture the initiation of cracking are more likely than using uncut specimens.

To prepare the samples, metal pieces are glued 120° apart around their vertical surface to position the LVDTs. After this step, the specimens are then put in another gluing apparatus to attach the endplates at the extreme surfaces, as illustrated in Figure **31**. Then the specimens should stand at the apparat for at least 4h, but only tested after 16h to guarantee a minimum Epoxy adhesive curing period and strength. This longer waiting period ensures that the rupture occurs in the specimen, not the adhesive layer.

Figure 31 – Glued pieces and endplates.

(Source: Author).

The endplates are two different pieces connected to the UTM-25. One connects to the actuator and the other one to the crosshead. In this way, the entire apparatus works as a single object to distribute tension and compression due to the actuator's vertical displacement (Figure 32).

Figure 32 – Fatigue specimen instrumented at UTM-25.

(Source: Author).

After preparing the sample, they must achieve thermal equilibrium inside the UTM-25 thermal chamber for at least 4h before testing. The experiment temperature depends on the Binder's PG, but as the used binder in this work is similar to others already analyzed at LMP, the 19°C temperature was chosen. During thermal conditioning and testing, a Dummy specimen is kept inside the thermal chamber to monitor the core and surface temperature variation. There are limits to temperature variations, as the target must fluctuate in a range of 0.5°C and the difference from core to surface temperatures should not exceed 1.0°C.

To perform the test, after fixing the specimen into the press, there are 3 main steps:

i. Looseness and amplitude test: a sinusoidal loading of 15 cycles at 10Hz with 0.1mm of actuator displacement amplitude is performed. The output signal is then analyzed to examine if the specimen needs to be tightened, due to the presence of looseness points or use a bigger displacement because of the poor signal response. This is an important step since other problems, such as Proportional, Integral and Derivative controllers' values, might influence the preciseness of a sinusoidal signal. Any deviation of this shape must then be fixed, otherwise, the test is invalid. With the acquired data, the user can determine the new displacement level to generate the initial strain level desired for the test.

ii. Tension-Compression |E*| fingerprint: the step consists of applying positive (compression) and negative (tension) symmetrical stress levels. First, known mixture stress values are used reduced to 50% as target stress in a fingerprint test to maintain the strain levels within the LVE range. With the strain levels resulting from this test, the new stress levels are determined and used to achieve $34\mu S$ after 5 to 10 minutes of rest. Unlike the standard compressive |E*| testing, the Tension-Compression |E*| is performed in a reduced number of cycles, as its use in this step is solely to determine the specimens' |E*| and compare to the Uniaxial

Compression |E*| of the mixture. This comparison evaluates if it is in an acceptable range using the Dynamic Modulus Ratio (DMR) in Equation 25.

$$DMR = \frac{|E^*|_{fingerprint}}{|E^*|_{LVE}} \quad (25)$$

Where:

$|E^*|_{fingerprint}$ = Tension-Compression |E*| (MPa);

$|E^*|_{LVE}$ = Uniaxial Compression |E*| (MPa).

iii. Tension-Compression Fatigue: the fatigue test initiates after 25 to 45 minutes of the |E*| fingerprint. This rest period is necessary, so the strains and the previous loading history are recovered. To initiate the experiment, the user defines the target displacement value obtained at the "Looseness and amplitude test". The press then performs cyclic loading at 10Hz inducing tension and compression stresses to the sample. There are different possible failure criteria to stop the test such as a predefined modulus reduction, the drop of phase angle, and the evolution of microcracks to macrocracks. The tests carried in this work were stopped at the occurrence of microcracks coalescence to macrocracks that completely divided some specimens.

All data acquired from the test is then analyzed using MATLAB and a set of spreadsheets to determine the parameters in AASHTO TP 107 (2018). With this procedure, the dissipated energy, phase angle drop due to cyclic loading, material's damage and integrity are determined. With these parameters, a behavior analysis is performed by comparing dry and wet results. Not only $C\ vs. S$ results are compared, but also $G^R\ vs.\ N_f$, and Wöhler Curves. For Wöhler curves with constant $N_f$, the wet and dry ratio is also determined to evaluate a range of possible damage acceleration expected during Fatigue Life. The same is performed with FFM.

### *3.3.9 Summary of conditioning protocols*

As a comparative chart, Figure 33 summaries of the methods used to condition samples of (a) asphalt binders, (b) aggregate-binder interface, and (c) asphalt mixtures. Sample preparation prior to these conditioning protocols were explained in the previous sections.

Figure 33 – Moisture conditioning of (a) binders, (b) aggregate-binder, and (c) mixtures.

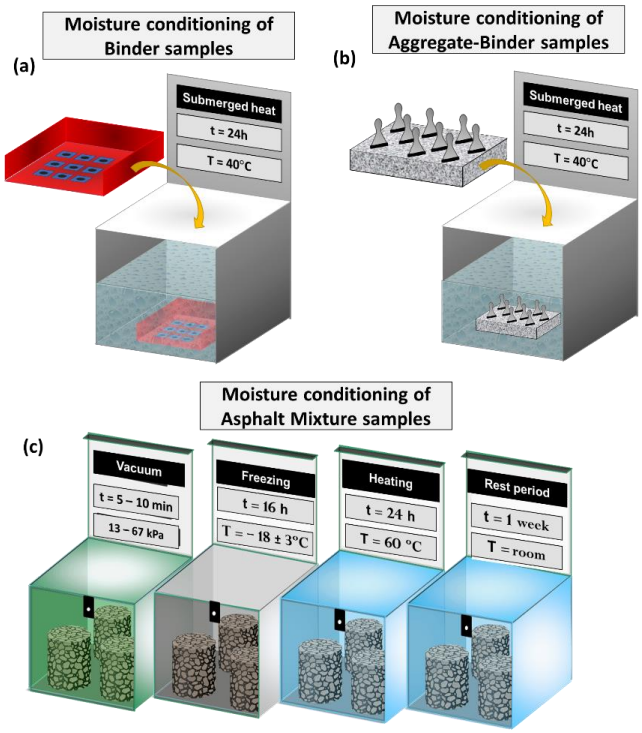


(Source: Adapted from Lucas Júnior *et al.*, 2019).

## 3.4 Simulation Software

Brazilian specifications require a project's service-time analysis using the MeDiNa software (DNIT, 2023). However, the method currently calibrated for this software considers: diametral compression Resilient Modulus and Indirect Tensile Fatigue tests for elastic analysis. Thus, it is not possible to use this method with the data acquired from: Dynamic Modulus and Tension-Compression Fatigue.

Two analysis programs, CAP3D-D (HOLANDA *et al.,* 2006; SANTOS, 2020; VALE *et al.*, 2022) developed at the Pavements Mechanics Laboratory – Federal University of Ceará (LMP/UFC), and FlexPAVE™ (ESLAMINIA *et al.*, 2012; WANG *et al.*, 2018) developed at the North Carolina State University (NCSU), are used herein to evaluate the mechanical response of the tested mixtures in both dry and conditioned states.

The following subsections are meant to briefly describe how each tool work from the user point of view for simulation purposes. For further understanding of the software, the reader is encouraged to consult the referred works. Figure 34 illustrates the general expected simulation and the expected results.

Figure 34 – Simulated conditions for CAP3D-D and FlexPAVE™.

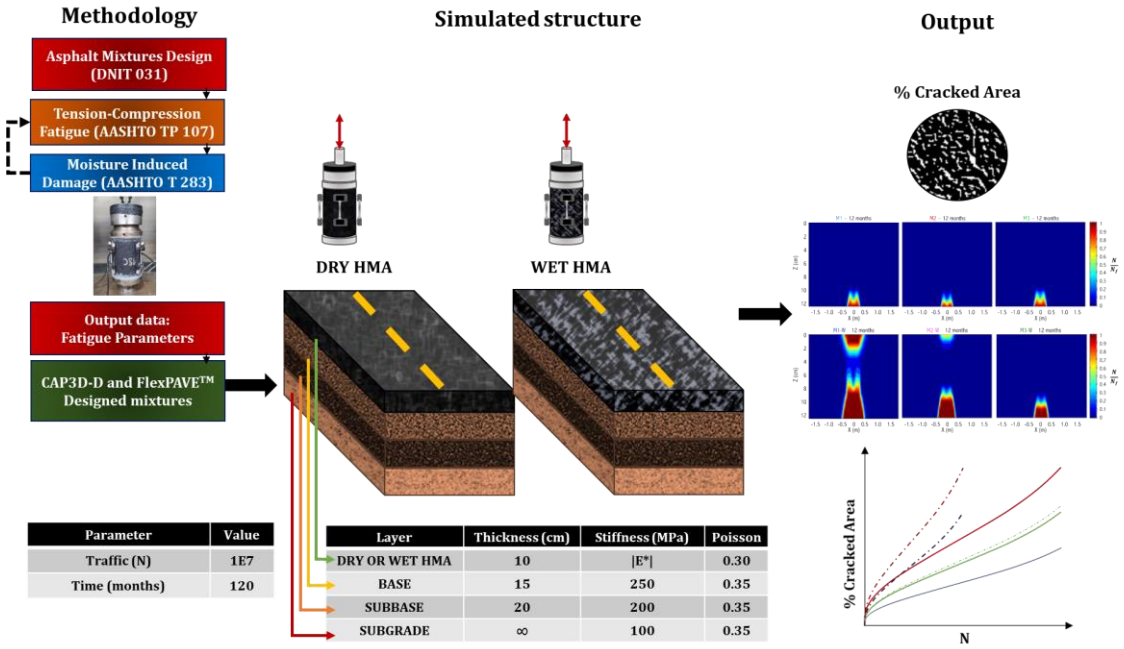


(Source: Author).

### *3.4.1 CAP3D-D*

The CAP3D-D software has been in constant improvement over the years and has been used by different authors for both rutting (BASTOS, 2016; BASTOS *et al.,* 2018, VALE *et al.*, 2022) and fatigue (SANTIAGO, 2017; SANTIAGO *et al.,* 2018; SANTOS, 2020; LUCAS JÚNIOR, 2021) analysis. Figure 35 illustrates the software user graphic interface.

Figure 35 – CAP3D-D user interface.

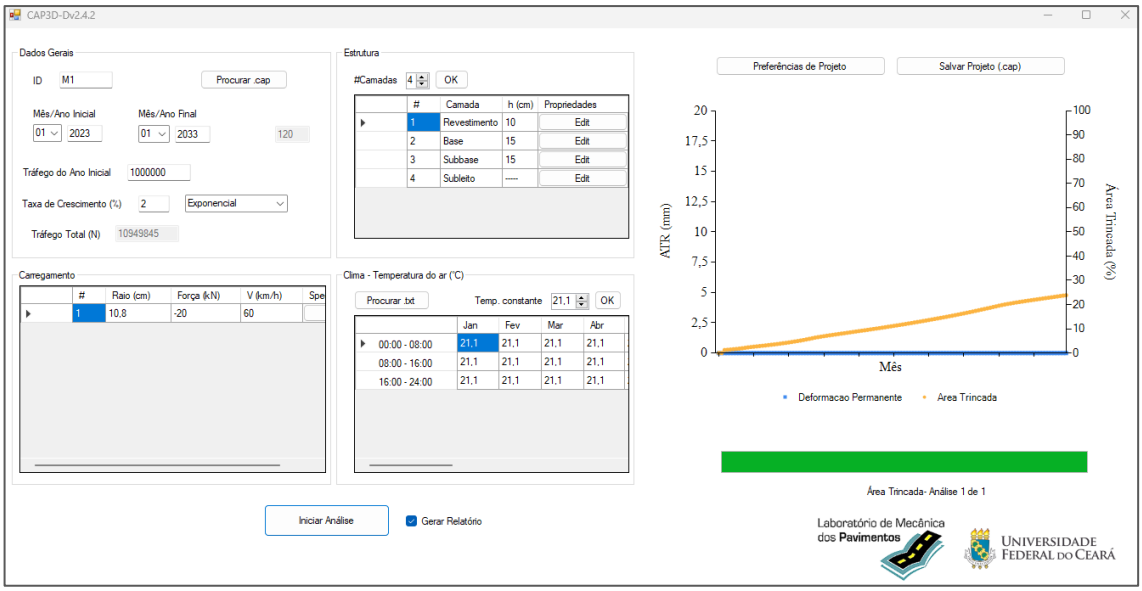


(Source: Author).

According to Santos (2020), the program uses the Finite Element Method (FEM) with a 240 Gauss points mesh to perform structural analysis; these Gauss points are distributed in 60 elements, and 30 of them are directly below the loading source. CAP3D-D can evaluate different models such: planes, axis symmetrical, and tridimensional. Despite the possibility of using both $C\ vs.S$ and $G^R\ vs.\ N_f$ for Tension-Compression Fatigue and a Sigmoidal model with polynomial TTSP shift factors for |E*|, or Indirect Tensile Fatigue (ITF) and Resilient Modulus, CAP3D-D uses elastic-linear analysis to calculate stress, strain, and displacements at the asphalt layer considering primarily Tension-Compression and |E*| due to the calibrated Transfer Function.

Besides structural analysis, the program also incorporates temperature effects as a function of air temperature and heat transfer capacity of the entire layer and a current work is improving thermal analysis (FONSECA, 2023). However, it is also possible to use constant temperature or import specific data into the analysis. Another concept incorporated in the analysis is traffic speed which represents the equivalent frequency of loading in the simulation as well as the vehicle simulation to loading.

CAP3D-D uses the concept of damage accumulation as the damage existing in the nodal points of the mesh calculated as the ratio of $N$ and $N_f$. This accumulated value is used to determine the average damage ($D_{avg}$). However, this damage evolution occurs at different times, so it needs to be analyzed at an equivalent period in which Damage is equal to 35% ($T_{0.35}$). Therefore, Equation 26 calculated a shift factor to the month in which damage reaches 35% of cracked area. This result is used to calculate the reduced Damage ($D_{reds}$) in Equation 27 the output if finally used in the Transfer Function (Equation 28) to calculate the cracked area (%AT).

$$S = 0.00281(T_{0.35}) + 0.657 \tag{26}$$

$$Dred_s = D_{avg} \cdot S \tag{27}$$

$$\%AT = 17506.3\left(\frac{N}{N_f}\ red_s\right)^5 \tag{28}$$

### *3.4.2 FlexPAVE™*

FlexPAVE™, formerly known as the Layered Viscoelastic Continuum Damage program (ESLAMINIA, 2012), is also in constant upgrade since its initial versions and works

in a slightly different way than CAP3D-D. One of the main differences between the two softwares is the Damage Contours generated at FlexPAVE™, which indicate the expected beginning of cracks in the asphalt layer and their evolution during the simulated service-life. Figure 36 shows the user interface and a damage contour example.

Figure 36 – FlexPAVE™ user interface and Damage Contour.

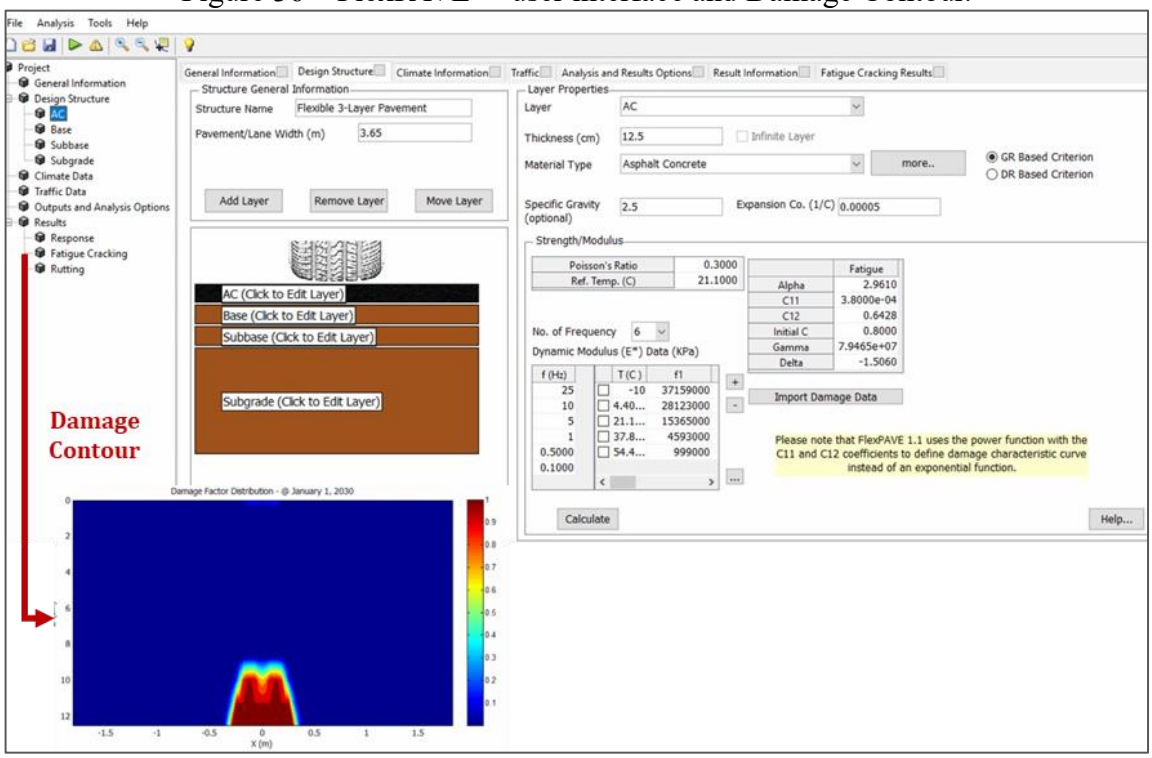


(Source: Author).

According to Wang *et al.* (2018) and the User Manual (FLEXPAVE 1.1 ALPHA, 2018), the program can be used for different pavements distresses such as rutting, thermal cracking and the focus of this thesis: fatigue cracking. It also uses the Finite Element Method (FEM) in a three-dimensional structure to calculate stresses and strains due to loading assisted to the Fast Fourier Transform which reduces computation timing. Different from CAP3D-D, FlexPAVE™ accepts different data formats for both |E*| (Prony Series, raw values, or Sigmoidal function with polynomial TTSP) and Fatigue ($C\ vs. S$ and $G^R\ vs.\ N_f$ or $D^R$ failure criteria). For temperature considerations, the software works both with constant temperature, year database or imported data.

The fatigue damage evolution is calculated using the concept of Damage Factor of the analyzed area which, for the $G^R$ failure criteria is defined by the Minor`s Law as the ratio of the current cycle ($N$) to the failure cycle ($N_f$) in Equation 29. This damage Factor is then used to calculate the %Damage of the simulated structure as a ratio of the sum of damage in

each nodal element by the total area (Equation 30). This last value is finally used in a transfer function to determine the cracked area as %Cracking (Equation 31).

$$Damage\ Factor = \frac{N}{N_f} \tag{29}$$

$$\%Damage = \frac{\sum_i^M (Damage\ Factor)_i \cdot A_i}{\sum_i^M A_i} \tag{30}$$

$$\%Cracking = \frac{50}{1+C_{f1}e^{\left[C_{f2}\left(logC_{f3}-log\%Damage\right)\right]}} \tag{31}$$

Where: $C_{f1}, C_{f2}, and\ C_{f3}$ = are calibration factors equal 0.342, 13.97, and 16.38 respectively.

# 4 RESULTS AND DISCUSSIONS

## 4.1 Rheological Characterization

The testing campaign conducted in this research was thought to compare different methods of evaluating binders' behavior as it relates to moisture damage. Even though Frequency Sweep and LAS tests have different parameters and purposes, it is expected that they lead to similar results.

### *4.1.1 Frequency Sweep*

Both neat binder (NB) and binder with anti-stripping agent (NB+D) had similar behaviors for |G*| values, as observed in Figure 37(a) and 37(b). Both figures also indicate that NB and NB+D outputs are similar when placed under moisture damage. The |G*| variation at all temperatures is similar for both binders, as observed in the right axis as the plotted line of "Ratio |G*|", which stands for the ratio between |G*| values considering the non-conditioned sample as the reference value (Equation 32).

$$Ratio\ |G^*| = \frac{|G^*_{wet}|}{|G^*_{dry}|} \tag{32}$$

As indicated by the values inside boxes for each temperature in Figure 37, the modulus Ratio is as high as 135% at lower temperatures (4°C), and drops to 108% at higher temperatures (82°C) for NB. When NB and NB+D results are compared, it is noticed that the anti-stripping liquid agent reduces |G*| from 8% at lower temperatures (4°C) to 23% at 28°C, but no significant variation was observed from 40°C to 82°C. When all values are observed as well as Master Curves are compared (Figure 38), no significant divergence is noticed. The same trend of stiffness reduction is observed for wet samples when NB+D is compared to NB. The stiffness loss is 14% at 28°C, 8% at 70°C, and 5% at 82°C. Despite the reduction, both NB and NB+D still shared the same PG.

Figure 37 – NB and NB+D dry and wet comparative results.

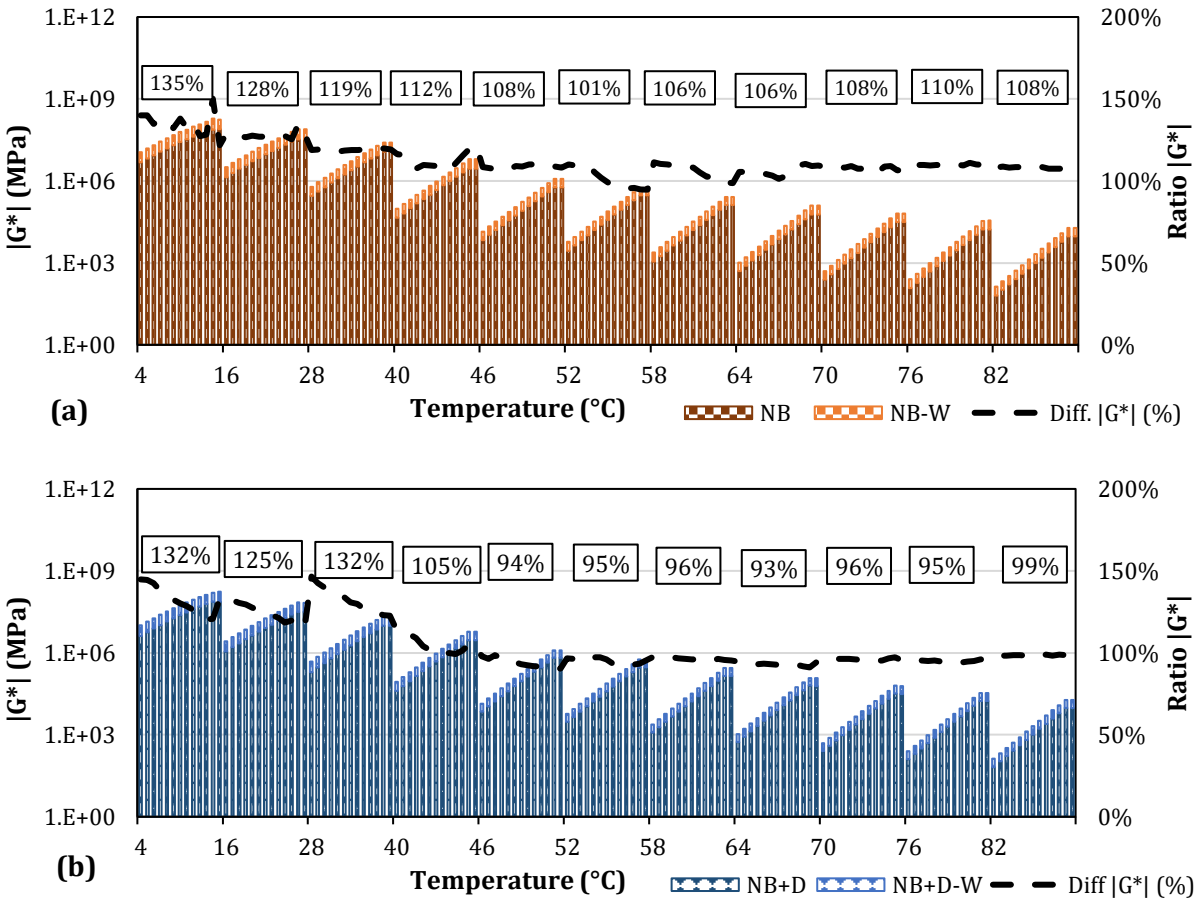


(Source: Author).

Contrary to what one would expect, both binders after 24h moisture conditioning at 40°C presented higher values of stiffness than without moisture conditioning. In fact, this result disagrees with the ones presented by Júnior *et al.* (2021). The results were consistent to the studies by Akentuna *et al.* (2022 and 2023) which have indicated that moisture damage increased the observed stiffness.

Considering the results, it seems like the conditioning method used affects mostly the binder's properties. An average value of 12.8% higher |G*| after moisture damage was observed for NB, and 5.8% for NB+D.

Figure 38 – Dry and wet |G*| and φ comparison.

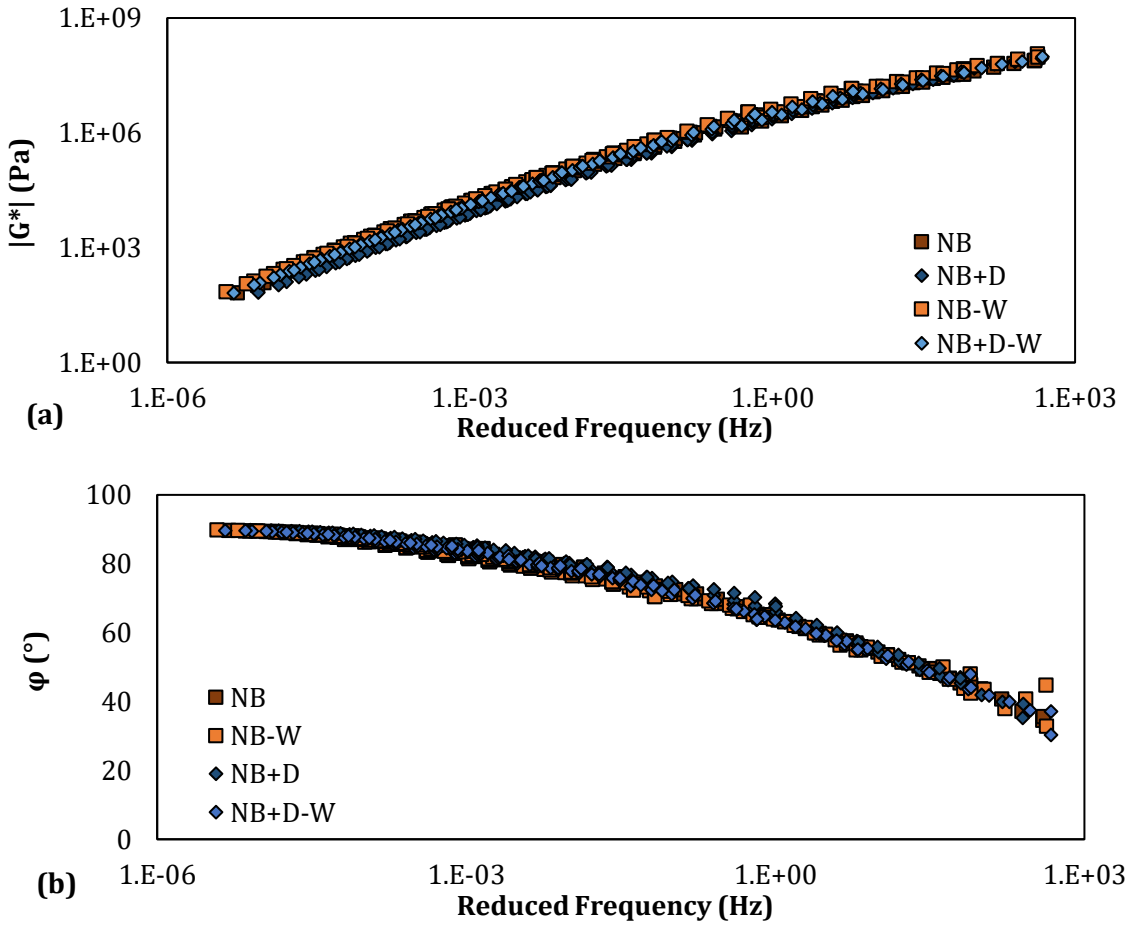


(Source: Author).

Although 40°C is a significantly lower temperature than the 163°C used in RTFO, aging is one of the expected reasons for higher |G*| values for wet samples. Thus, it is believed that the aging (40°C) has possibly hidden the damage caused by moisture. The other hypothesis is just a normal sample-to-sample divergence. However, similar results of higher stiffness were observed for Akentuna *et al.* (2022) when using different conditioning protocols. Therefore, it is assumed that this is the expected behavior for FS results after moisture conditioning.

It is highlighted that different portions of binders were divided into containers, to prevent aging due to heating the same binder multiple times. The containers with binder that underwent moisture conditioning were only heated before preparing the molds as described in Section 3.3.2 while the containers of dry samples were heated just to separate samples prior to testing.

### *4.1.2 Linear Amplitude Sweep*

LAS tests were conducted on the first try at 19ºC, but the output data and test signal were unsatisfactory. As LAS uses both crack length and maximum pseudo strain energy to determine the failure cycle, these data made it almost impossible to clearly determine whether it was truly the cracking point.

Thus, since fatigue results can be translated to other temperatures, 25°C was chosen as the test temperature. As it is a PG 64-XX binder, it is likely that at lower temperatures an adhesion problem happens during the test.

However, the used methodology to determine the failure cycle was the PSE with S-VECD modeling. As observed in Figure 39(a), the materials' characteristic curves are almost the same, and in Figure 39(b) the Wöhler curves are overlapping. This indicates that all tested samples presented low variation in behavior. However, isolating NB and NB+D results in dry and wet conditions, a slightly higher integrity decay is observed, as well as lower Wöhler curves. The water conditioning might have slightly altered the binders' resistance to fatigue.

Figure 39 – (a) C vs. S and (b) Wöhler curves for dry and wet binders.

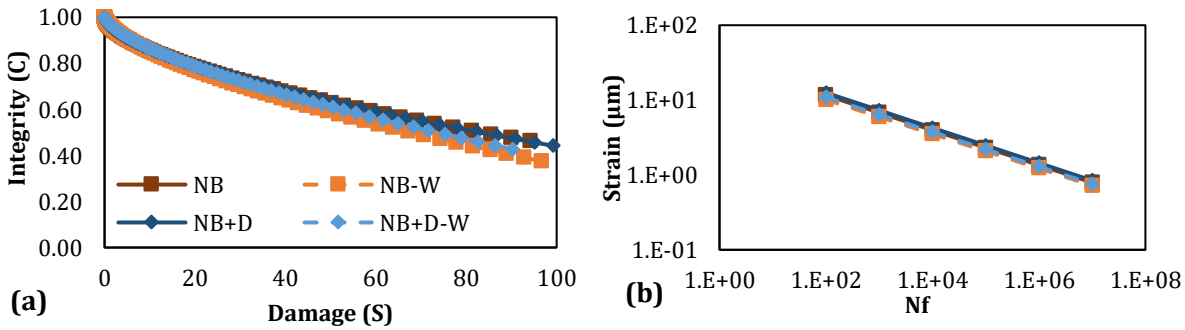


(Source: Author).

When comparing binders' resistance to fatigue, the $FF_B$ becomes easier to analyze than Wöhler Curves, especially when they have very similar behaviors. As the used materials are similar, this is the better comparison method as it uses specific data from Wöhler Curves to determine the index (NASCIMENTO, 2015).

It is observed in Figure 40 that there is no significant difference between dry and wet samples. NB had only a 3.4% reduction, while NB+D was 2.5%. Between binders, NB+D is 0.9% better in dry conditions and 1.9% in wet conditions than NB. This suggests that no real difference is observed for fatigue of binders due to the used conditioning method.

Figure 40 – Fatigue factor of dry and wet binders.

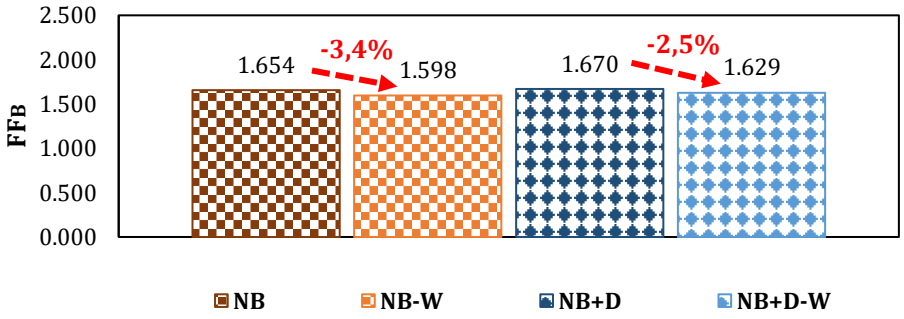


(Source: Author).

The same assumption is made when comparing LAS parameters (Table 6). Figure 40 suggests that there is no significant difference between binders, just a small variation between dry and wet conditions, as observed for $FF_B$. As observed in the present research, LAS captures some differences between dry and wet results, but they are not significant.

It looks as if the behavior is the same for all binder samples when comparing different parameters: $C1$ and $C2$ fitting coefficients from $C\ vs.S$; damage evolution constant ($\alpha$); A and B fitting coefficients for Wöhler Curves (Intercept and Slope, respectively).

Considering Frequency Sweep (Section 4.1.1) and LAS results, different temperatures and testing frequencies are better to capture moisture damage to binders than a single condition, even if this difference becomes smaller at some points.

Table 6 – LAS parameters.

| | $C1$ | $C2$ | $\alpha$ | $A$ | $B$ |
|---|---|---|---|---|---|
| **NB** | 3.75E-02 | 5.86E-01 | 2.142 | 3674581.605 | -4.285 |
| **NB+D** | 3.41E-02 | 6.08E-01 | 2.131 | 4777198.915 | -4.262 |
| **NB-W** | 3.43E-02 | 6.35E-01 | 2.181 | 2434387.165 | -4.363 |
| **NB+D-W** | 3.01E-02 | 6.55E-01 | 2.163 | 3021886.706 | -4.326 |

(Source: Author).

## 4.2 Asphalt Bond Strength (ABS) - Aggregate-binder interface testing

For the ABS testing campaign, it is common to use only one temperature and rate of pull-off on triplicates due to the test's variability associated to sample preparation and surface conditions. However, based on binders' viscoelastic properties, it was expected that variations in pull-off rate and temperature should determine different maximum applied stresses.

Therefore, a failure envelope would be observed, such as a construction of a "Master Curve of Pull Off testing" or "Failure Tensile Envelope". Along with VEL properties,

it was expected that the acid aggregates used in this research would result in a poor adhesion property for NB when compared to the NB+D, since adhesiveness is strongly related to the aggregate mineralogy.

The used range rates of 0.5, 0.7 and 0.9 MPa/s were a conservative choice based on the equipment's limitations around the usual value of 0.7MPa/s. On the other hand, the temperatures range of 15, 25 and 35°C was chosen to match usual values of Dynamic Modulus tests (Section 3.3.7). These 9 combinations in tension stress and rate for two binders, 2 conditions, and triplicate samples resulted in 108 pull-off tests.

### *4.2.1 POTs and RPOTs results*

ABS tests on dry NB results are in accordance with the expected LVE behavior: lower $POTS$ values for higher temperatures. Although an irregular trend is observed considering the pull-off rates, Figure 41(a), wet results (NB-W) have the same trend. They follow no pattern of higher or lower values at the same pull-off rate.

Using $R_{POTS}$ as an indicator, it is observed in Figure 41(a) that the general aggregate-binder adhesion properties were satisfactory for NB since the minimum average was 85% at 25°C considering all stress rates (0.5; 0.7; and 0.9MPa/s). An average value of 96% $\boldsymbol{RPOTS}$was observed for NB considering all data.

For NB+D, dry results are similar to what was observed for NB. A higher $POTS$ at 15°C followed by lower POTS at 35°C, with an irregular trend with respect to pull-off rates, as indicated in Figure 41(b). For wet results, at 0.7MPa/s and 15°C an irregular result was observed with higher $POTS$. Despite the fact that triplicates were used in all tests, this result might still be due to some test variability. However, $\boldsymbol{RPOTS}$ results considering all temperatures average, 106%, the average of box values in Figure 41(b), indicate that the aggregate-binder adhesion properties are not altered significantly as the average $R_{POTS}$ for NB+D (106%) and NB (99%) do not differ significantly.

Figure 41 – ABS test results on wet and dry samples of (a) NB and (b) NB+D.

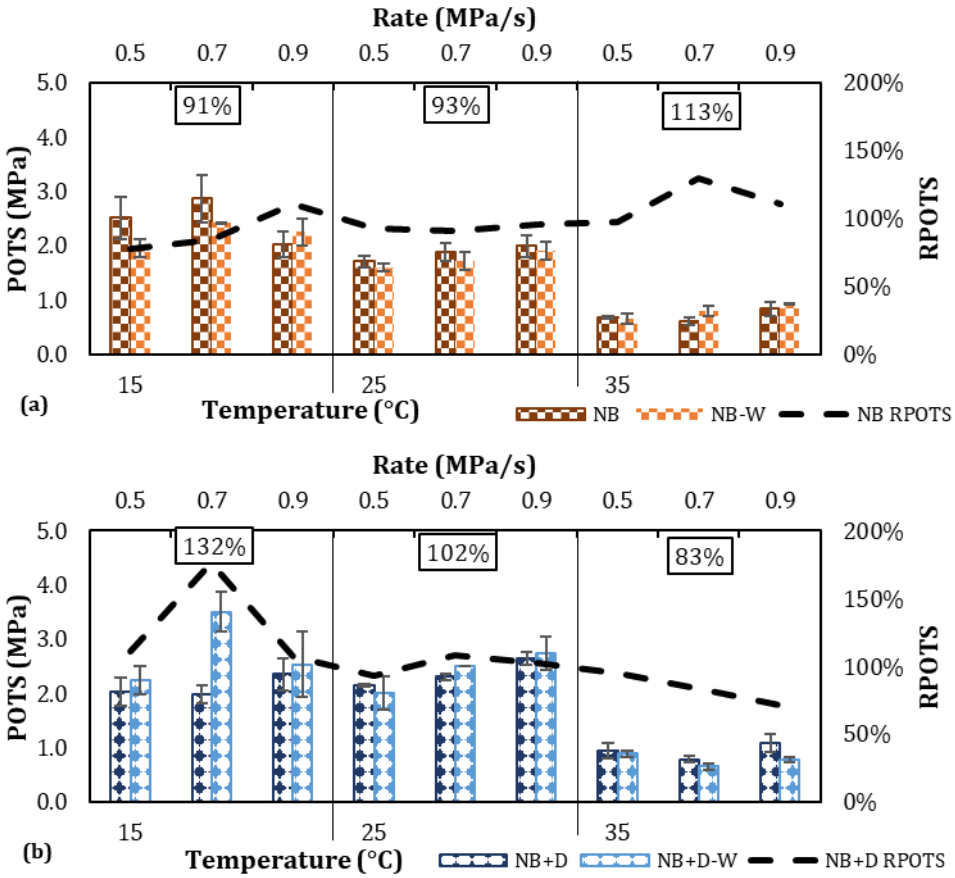


(Source: Author).

If outlier values from both NB and NB+D at 15ºC are excluded from the analysis (0.9 and 0.7MPa/s rates respectively), NB ***RPOTS*** drops to 96% and NB+D ***RPOTS***drops to 98%. Still, NB+D indicates that the test captures the effects of the anti-stripping agent keeping a ranking of moisture resistance as: NB+D > NB. However, the approximation of ***RPOTS*** results from NB and NB+D are strange compared to results of other authors (LUCAS JÚNIOR *et al.*, 2021). Even though moisture effects at the binder scale have history dependence (VASCONCELOS *et al.*, 2011), the low reduction after moisture conditioning is probably due to the thermal equilibrium for 4h which might have altered the aggregate-binder state.

These results preserve the test's expectations to observe both moisture susceptibility of the aggregate-binder interface, and LVE properties observations incorporated as a complex combined behavior to the pull-off test on the mineral substrate. However, it is believed that rates and temperatures in the present study can be reconsidered. A lower value than 0.5MPa/s could be used and an intermediate temperature, such as 30ºC, may be considered in future works. Another observation is that the binders' creep behavior may have caused a drastic decrease in POTS for both dry and wet samples. Therefore, such an effect is not the result of a true interface

rupture, but something that can be affected by the creep behavior driven by the binder.

Despite the findings reported, the used combinations indicate the importance of knowing the binders' behavior to adhesion tests in other conditions for better aggregate-binder properties evaluation. For failure classification, most of them remained adhesive-cohesive. Especially at 35°C, despite the cohesive classification, longer binder filaments were created which indicates a state transition instead of fracture, which did not happen at lower temperatures. At 15°C, it was observed that some specimens failed not at the aggregate-binder interface or at the middle of binder film, but at the binder-stub interface which was also observed by previous authors (SUDARSANAN *et al*., 2020), like what could happen in lower temperature testing to LAS (SAFAEI and CASTORENA, 2016). Data from binder-stub failures were removed from the analysis as they could interfere with failure interpretation. Figure 42 illustrates the observed differences with respect to failure classification. It reinforces the idea that the testing method should use two aggregate plates with a binder adhesive layer in between them.

Figure 42 – Failure in different temperatures.

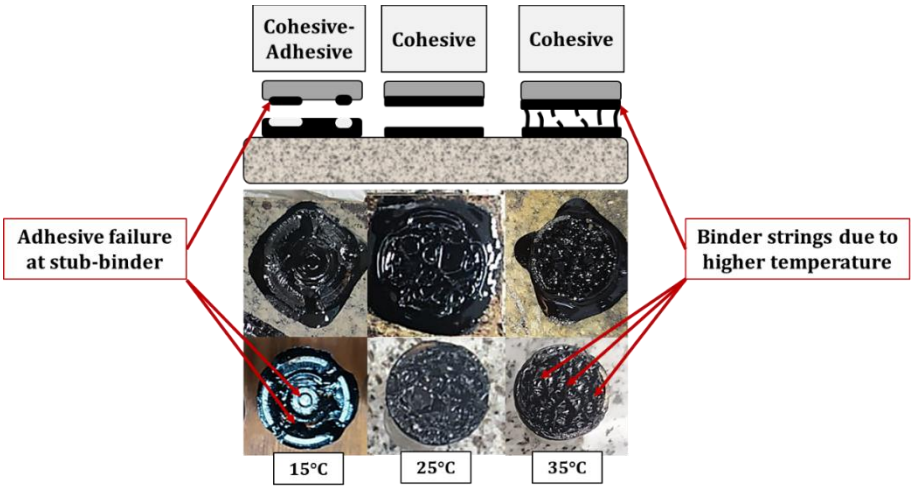


(Source: Author).

### *4.2.2 Failure envelope construction*

Since no strain measurement is possible with the used method to determine POTs, no inference considering a limiting strain due to temperature or rate of pull is possible. Even though the diameter and approximate height of samples is determined by Stubs' volume, it is not clear how high the pulling device elevated the stub before the rupture was determined. Therefore, it is only possible to construct a failure envelope considering the maximum tensile stress.

This failure envelope is thought to be constructed in a strict linear shift of experimental points. This procedure follows a similar path to what is done when determining shift factors for |E*| or |G*|. It is reasonable to think that, since no clear trend was observed as purely increasing or decreasing values among pull-off rates, this curve might not have a perfect fit, but the trend might still be observable as a maximum stress variance was observed for different temperatures.

The first step is the construction of isotherms in a log-log space using the maximum stress in kPa and pulling-off rate ($R$) in (MPa/s) as Y and X axis (Figure 43(a)). Then, the 25°C intermediate temperature is set as the reference temperature. The intercept (b) and slope (a) of log-log isotherms are then determined. With the isotherms, the extreme points are determined as coincident values for the regression expression to determine a single alignment of values (Figure 43(b)). This expression (Equation 33) is used then to calculate the shift factors ($a_T$).

$$\log(a_T) = \frac{b1 - \frac{a1}{a2} b2 - \left(1 - \frac{a1}{a2}\right)\log(\sigma)}{a1} \tag{33}$$

Where:

$a_T$ = the experimental shift factor;

b1 = the intercept of reference isotherm;

b2 = the intercept of the second isotherm;

a1 = the slope of the reference isotherm;

a2 = the slope of the second isotherm;

$\sigma$ = the selected coincident value of slopes (MPa).

Using the shift factors, the log of pulling-off rate (log R) is shifted obtaining a trend of aligned values, and finally a trend line is also determined. Such line, which is a linear regression for the log-log space, is the failure envelope (Figure 43(c)).

Figure 43 – Shift of experimental data to determine the failure envelope.

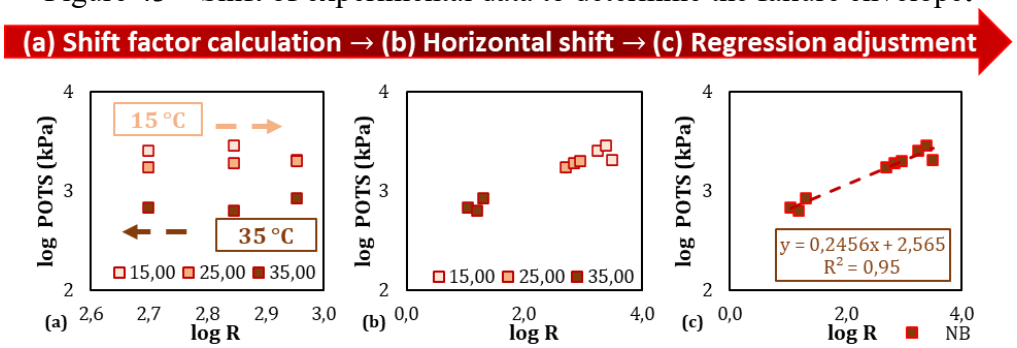


(Source: Author).

This process was performed for both NB and NB+D data presented in Section 4.2.1. The resulting failure envelopes for both dry and wet conditions and a comparison of NB are observed in Figure 44 (a), (b), and (c).

Using this methodology to determine whether data is well adjusted, it becomes clear that an intermediate temperature between 25 and 35°C should be used due to the lack of data an around $log\ R\ = 2$. However, both lines present a good $R^2$ value, *i.e.*, above 0.95. Due to the log-log space, both regression lines in Figure 44 (a) and (b) look the same.

However, raw experimental data (Section 4.2.1) show that they are different. Although a hypothesis for this similar result is the effect of the thermal equilibrium period chosen to be 4h. It is expected that during these 4h samples have probably lost some of its moisture. Thus, misleading maximum tensile strength results were obtained.

Figure 44 – Failure envelopes for NB in (a) dry, (b) wet and (c) both conditions.

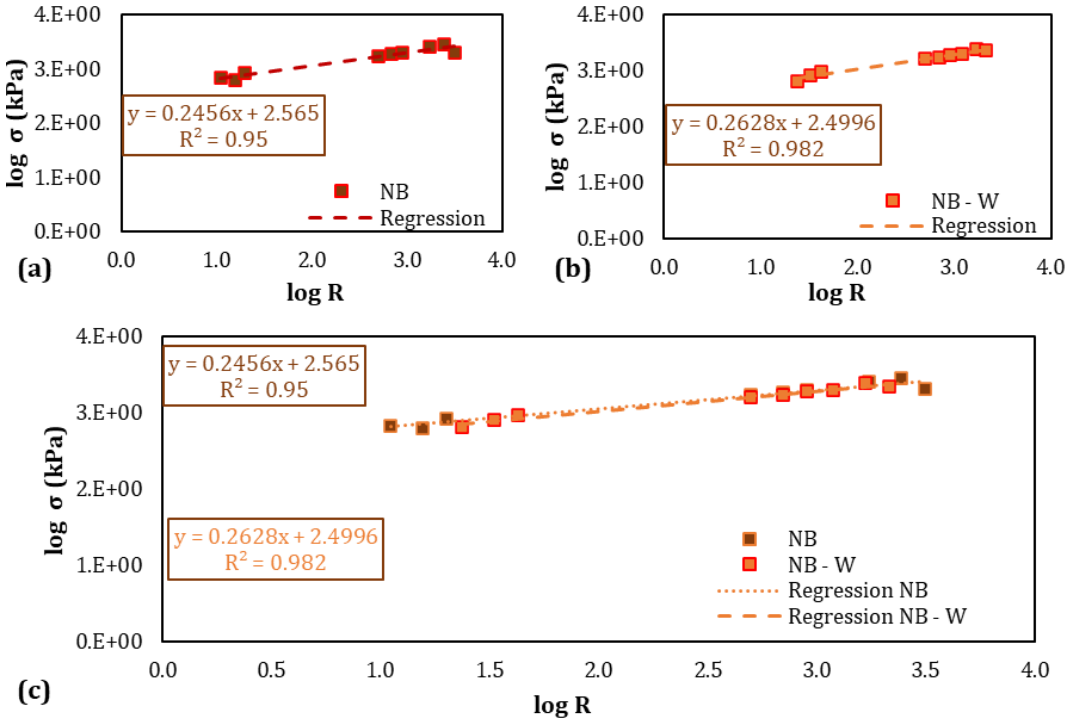


(Source: Author).

The resulting failure envelopes for both dry and wet conditions and a comparison of NB+D are observed in Figure 45 (a), (b), and (c). The same trend observed for NB is visible for NB+D, therefore a temperature between 25°C and 35°C should also be tested. Both lines present a good $R^2$ value, above 0.86. Although no significant difference was observed for the NB experimental fitting curves, the trend is altered for NB+D.

NB+D appears to be affected by water conditioning, and this effect is more noticeable at higher temperatures since anti-stripping liquid agent loses its resistance. This is better understood when analyzing the slope of dry and wet samples of NB+D.

Different from NB results, NB+D have presented very different raw data. A hypothesis for this behavior is also due the conditioning period of 4h associated to the anti-stripping liquid agent behavior of resistance loss. The observed divergence in response possibly caused the slopes to shift when comparing neat binder. In consequence, NB+D and NB+D-W lines are not aligned, different than NB lines. This might also suggest that Pull-Off tests are not precise enough for this kind of analysis when multiple rates and temperatures are evaluated.

Figure 45 – Failure envelopes for NB+D in (a) dry, (b) wet, and (c) both conditions.

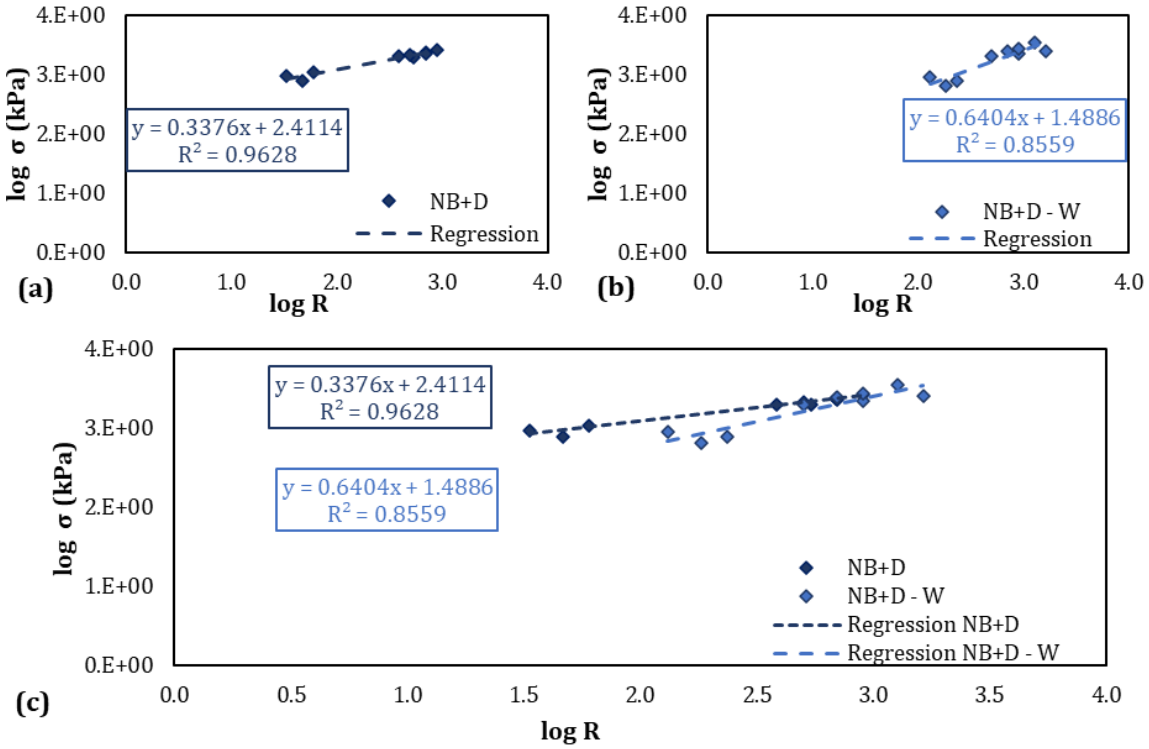


(Source: Author).

Figure 46 – Correlation between dry and wet POTS for (a) NB and (b) NB+D.

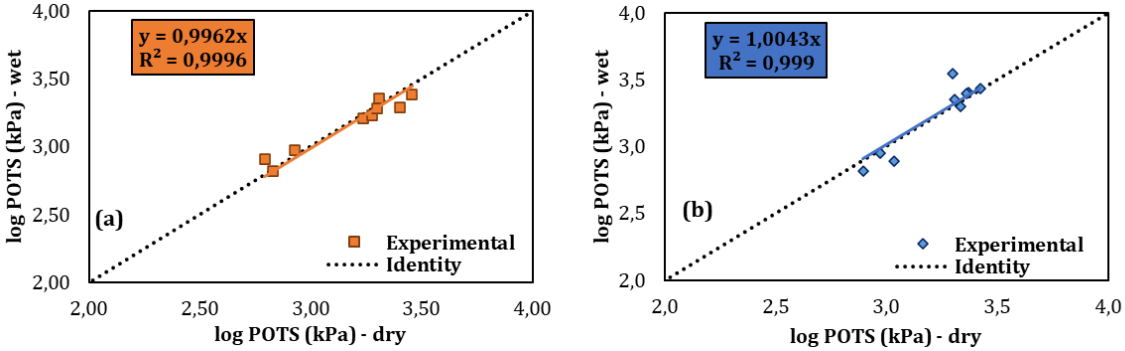


(Source: Author).

The comparison of all regression lines (Figure 46) suggests something already observed, that the effects of adding anti-stripping agents are probably better observed when considering a mineral substrate and water conditioning. However, this difference is not as high as expected.

The used method to determine the single envelope was successful, but no $a_T$'s could be calculated using WLF equations to adjust a single model. This probably was due to the lack of more temperatures with truly overlapping values, the test's variability or WLF should be used to LVE |E*| or |G*| values, not maximum $POTS$ values the LVE range.

Figure 47 – Failure envelopes (a) separated by binder, and (b) collapsed data.

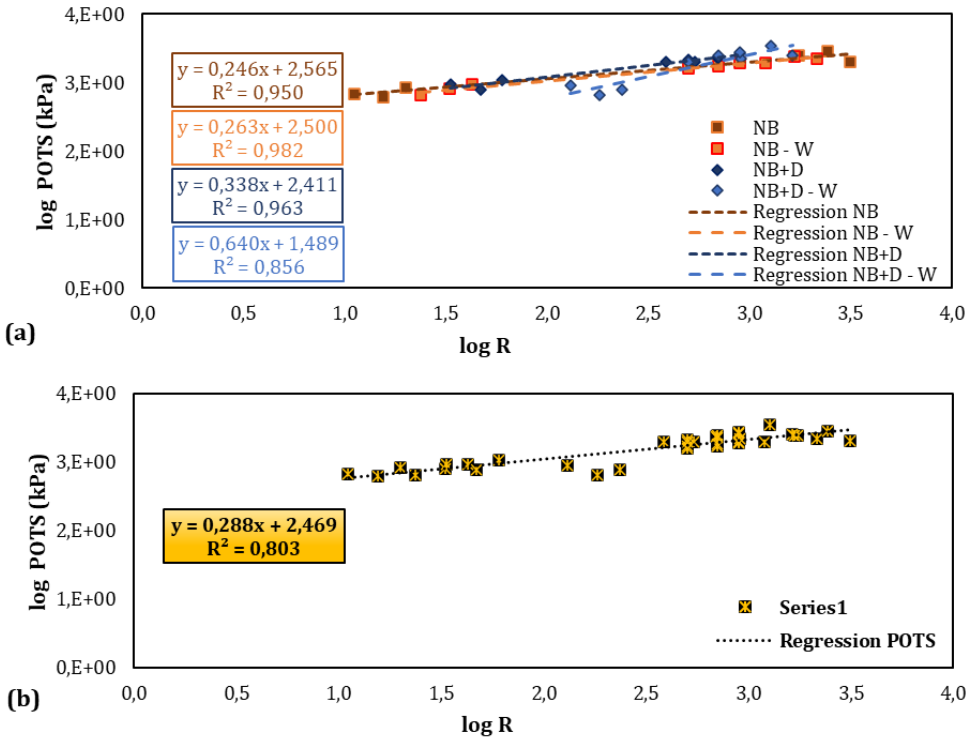


(Source: Author).

This result suggests two main hypotheses:

(i) Anti-stripping liquid agent probably degrades during the mixing process due to the higher temperatures (150 ºC), but not completely. This was not verified during this research, but it is a recommendation for future works, to determine how different anti-stripping agents preserve their properties with and without aging, before and after mixture temperatures used in asphalt mixing plants;

(ii) The used protocol variability is higher than expected to determine a single failure envelope that captures the water effect. This hypothesis is mainly related to almost no variation observed for the NB when compared to NB+D which should have had better results.

### 4.3 Asphalt mixtures design

The Brazilian specification DNIT 031 (2006) describes some acceptance criteria for asphalt mixtures, from materials quality to the final mixture layer constructed. Therefore, quantitative quality aspects must be controlled, such as the minimum Indirect Tension Resistance and Moisture Induced Damage Resistance.

Figure 48 illustrates the asphalt mixtures ITS values obtained at 25ºC, as described by DNIT 136 (2018) with 4% AV. The minimum admitted value is 0.65MPa, although the literature states that this criterion by itself is not enough.

All three designed asphalt mixtures (M1 – Neat Binder, M2 – Neat Binder + amine-based anti-stripping liquid agent, and M3 – Neat Binder + Aggregates + Hydrated Lime) attended the minimum requirements above specified. M1 had the higher ITS value of 1.62MPa, followed by M2 with a slightly lower value of 1.44MPa, and finally the M3 with 1.07MPa.

This behavior could also be because M3 was compacted with only 40 gyrations, while M1 and M2 achieved 4.0% AV with 100 gyrations, making them probably more stable than M3. This finding is in accordance with what the literature described of amine-based anti-stripping liquid agent reduction in ITS.

If M1 is taken as the reference mixture, M2 has an 11.0% loss in resistance and M3 loss is 34.0%. Since the test was conducted at 25°C, considering values |G*|, this would be expected as anti-stripping liquid agent reduced |G*| by 17% between 16°C and 28°C.

Figure 48 – Indirect tensile strength results.

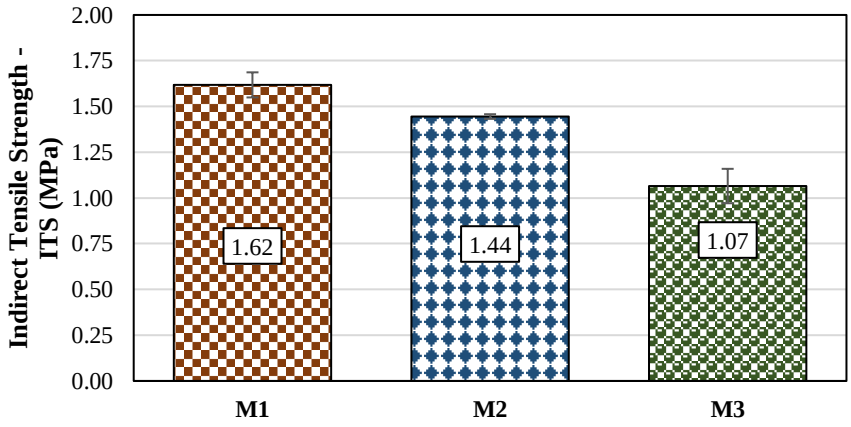


(Source: Author).

A similar trend is observed when comparing the ITSR values (Figure 49). It is highlighted that this test was performed with a higher AV of 7%. The unconditioned samples have presented values of 1.20MPa for M1, 1.16MPa for M2, and 0.94MPa for M3, while the conditioning resulted in 0.78MPa for M1, 0.85MPa for M2, and 1.22MPa for M3.

When comparing only ITS dry samples considering M1 as a reference value, M2 and M3 behave 4% and 22% lower than M1. However, if only ITS conditioned values are observed, M2 and M3 results are 9% and 56% higher than M1, respectively.

If only ITSR values are observed, M1 presented a 35% loss of resistance, M2 a 27%

loss, and M3 gained 30%. This was expected based on the literature for HL (MOURA, 2001; KIM *et al.*, 2008; BUDNY, 2009) as well as the bonds created with $Ca^{2+}$ and water which promotes adhesion between the aggregate and the binder to be maintained after moisture damage (PETERSEN *et al.*, 1987).

Figure 49 – Indirect Tensile Strength Ratio.

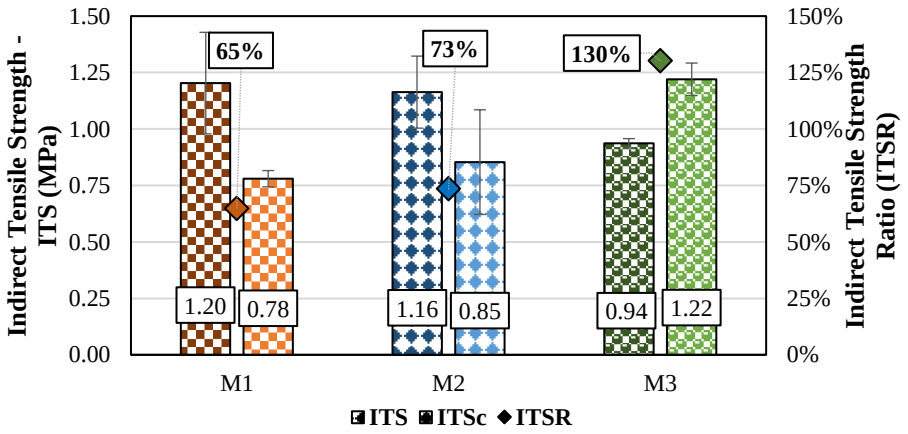


(Source: Author).

Even though fatigue damage begins at the microscale, sometimes it is considered to start at air voids working as initial cracks, other times in aggregates fractures or poor adhesion points (CARO *et al.*, 2008). Considering that the AASHTO T 283 (2021) protocol intends to accelerate adhesion problems and other authors also mention cracking induction (CARDONA *et al.*, 2020), one could expect the observed behavior in ITSR to also occur during fatigue life. Therefore, it is expected that the standard characterization usually overestimates the real performance, as damage might occur at higher rates due to the water effects. Some authors have observed that some conditioning procedures might significantly decrease fatigue life of asphalt mixtures (BARRA *et al.*, 2012; ALMEIDA *et al.*, 2018).

### 4.4 Asphalt mixtures uniaxial repeated loading tests

This testing program was designed to determine the |E*| and fatigue parameters of asphalt mixtures as the usual testing protocols. These tests were also performed with conditioned samples. However, neither Dynamic Modulus nor the Tension-Compression Fatigue tests are required in Brazil as mandatory tests. Despite that, these testing protocols allow a better understanding of materials' behavior for temperature and frequency combinations of modulus and indicative of cracking growth due to cyclic tensile loading.

Different softwares such as FlexPAVE™, and CAP3D-D (HOLANDA *et al.,* 2006; SANTIAGO *et al.,* 2018 and 2019; VALE *et al.*, 2022) use LVE parameters and Tension-Compression fitting coefficients to simulate a real structure fatigue life. Thus, it would be necessary that the user chooses whether to consider conditioned data or not.

The testing herein described are intended to understand the implications of a severe moisture-induced damage protocol on LVE properties and fatigue life parameters. With these data, real structures simulations can be performed as well as a deeper understanding of the expected fatigue life of asphalt mixtures variance considering the worst limiting scenario of a previously damaged material.

### *4.4.1 Uniaxial Compression Complex Modulus*

Dynamic Modulus test was performed as described in Section 3.3.7 for all mixtures in both conditions: dry and wet. It was originally thought to perform the test on separate triplicate samples for each condition, but as this test does not damage the sample when performed within the LVE limits, the same specimens were used for wet tests. This methodology was followed to avoid possible divergence sources.

In Figure 50 it is possible to observe experimental values to the nominal testing temperatures and loading frequencies for all mixtures on both conditions and the percentage loss of |E*|, determined as the ratio of the difference between dry and wet samples to the dry samples as described in Equation 34.

$$Loss\ of\ |E^*| = \frac{\left|E^*_{dry}\right| - |E^*_{wet}|}{\left|E^*_{dry}\right|} \tag{34}$$

For all mixtures, it is noticeable that this difference increases when temperature rises and mixtures behave in a similar ranking trend as observed for ITSR with M1 < M2 < M3. But contrary to what it is expected, when comparing dry and conditioned results, M3 has shown some increase in |E*| only at -10ºC and almost no variation at the other temperatures except for 54ºC.

Figure 50 – Experimental values of dry and wet |E*| comparison.

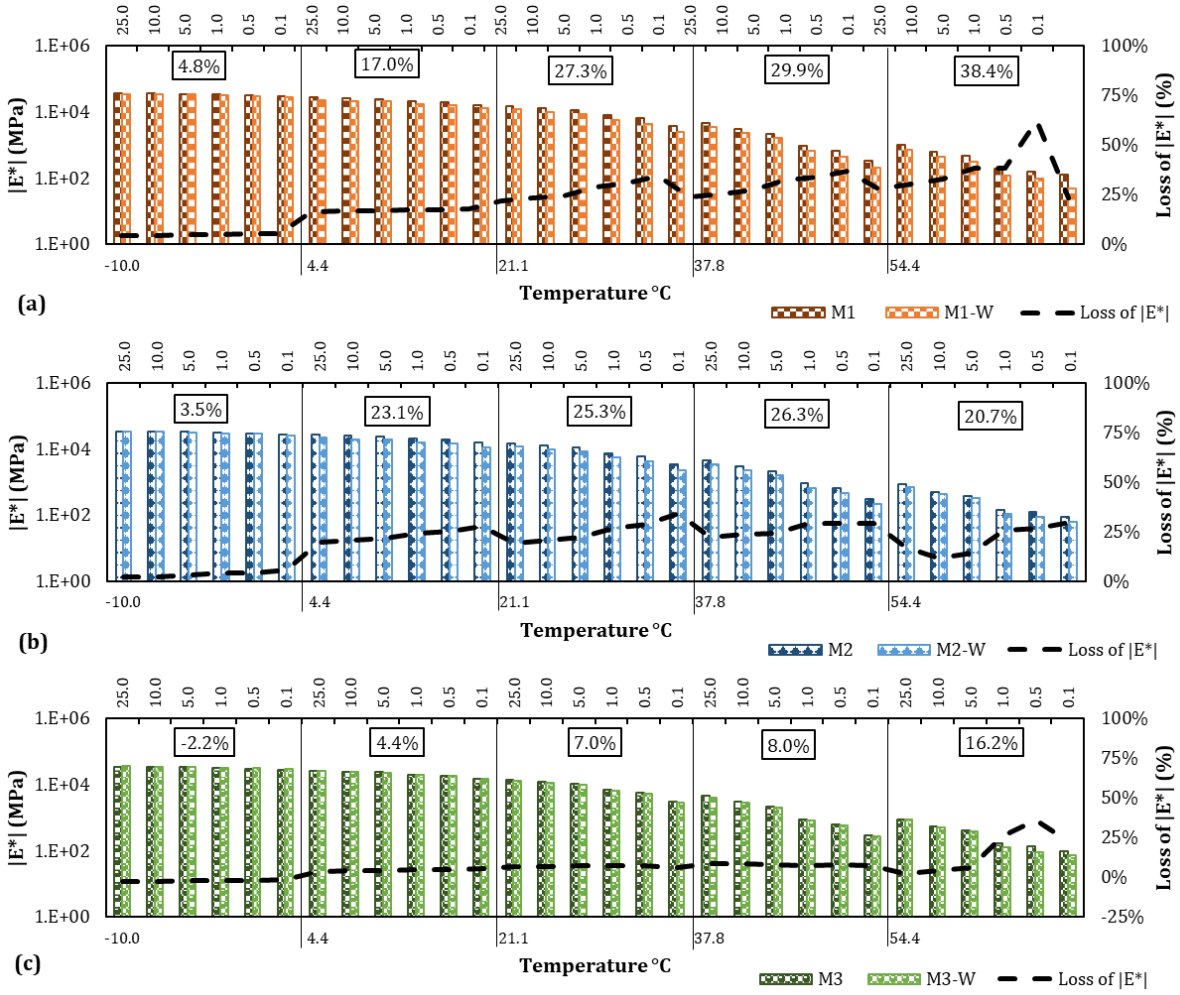


(Source: Author).

When analyzing the raw data, the dry mixtures' stiffness led to a rank in which M1 > M3 > M2. After moisture-induced damage, this trend is modified to M3 > M1 > M2. It is necessary to observe that these are just absolute modulus values. Figure 51 presents a comparison where it is clearer that M1 has a higher modulus than the other mixtures when dry, but M3 is the one with the highest modulus after conditioning for almost all frequencies and temperatures. Except for M3 at -10ºC, all other 14 out of 15 scenarios (5 temperatures for 3 mixtures) present increasing loss in stiffness with temperature. This is also observed for lower frequencies for each temperature, as expected due to the time-temperature superposition principle. This trend is also observed for master curves adjusted at the 21.1°C reference temperature as well as the 2S2P1D fitted model (Figure 52).

Figure 51 – (a) Dry and (b) wet modulus and ratio to M1 or M1-W values.

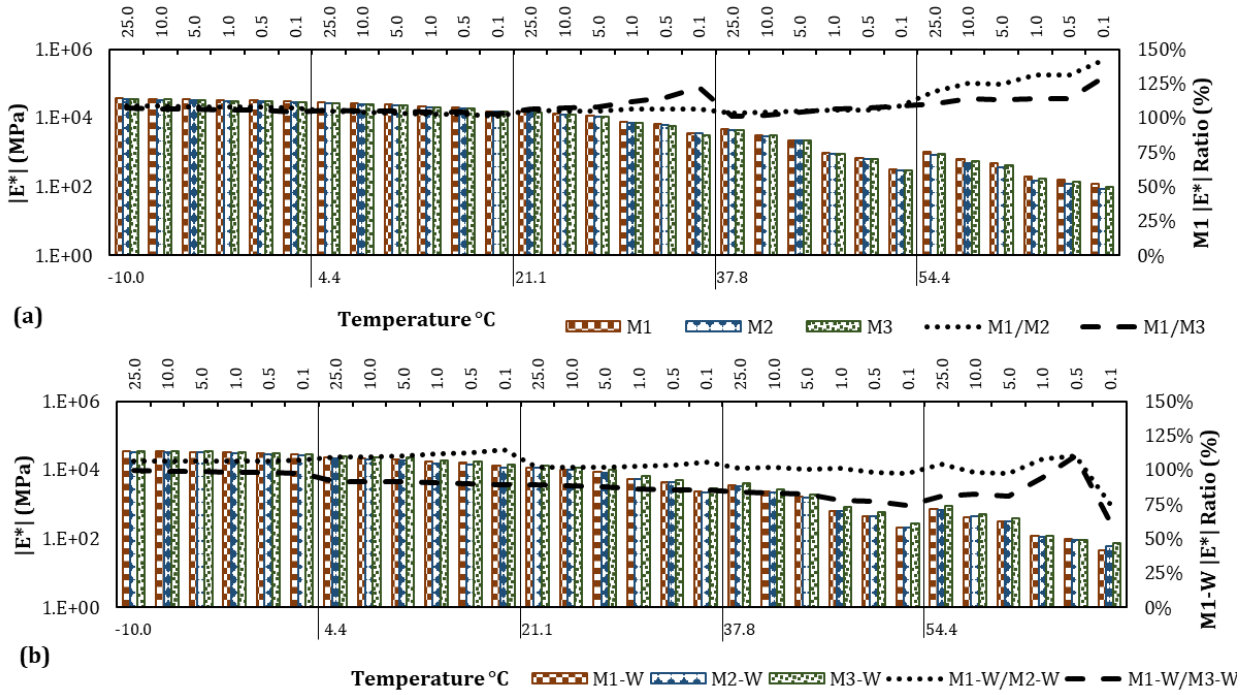


(Source: Author).

Figure 52 – Dry and wet experimental |E*| and 2S2P1D master curves.

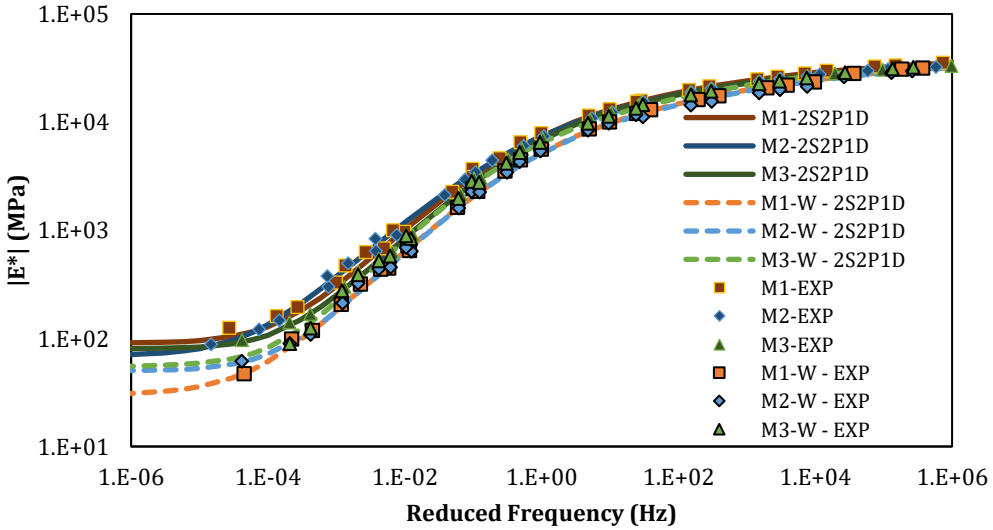


(Source: Author).

In Table 7 both WLF and 2S2P1D parameters are presented as they were fitted to determine the experimental master curves and Rheological Model. For all 3 mixtures, the main difference was verified on WLF constants and asymptotic modulus $E_{00}$ and $E_0$ which represent respectively the elastic behavior at lower or higher frequencies due the aggregates influence (elastic-behavior constituents).

On the other hand, the parameters $k, h, \delta, \tau$, and $\beta$ did not diverge significantly

on each condition (dry or wet) analysis. This is explained as an influence of the binder's viscoelastic behavior. At the 2S2P1D the binder's characteristics obtained by these constants define the master curves shapes.

All 2S2P1D constants were initially found using MS Solver, followed by fine adjusting. It is noticeable that WLF's Mean Squared Error (MSE) is higher than the 2S2P1D MSE.

After moisture damage, all parameters' values became closer than they were before conditioning, especially WLF constants. This indicates that for experimental purposes it is likely that at lower strains, the mixtures would still behave almost the same. But M3 behavior is almost the same after conditioning, and it is expected that it has a stiffer behavior compared to M1 and M2, which could lead to faster cracks growth as well as a lower thermal susceptibility.

Table 7 – WLF and 2S2P1D parameters.

| | C1 | C2 | MSE WLF | $E_{00}$ | $E_0$ | k | h | δ | $\tau_E$ | β | MSE 2S2P1D |
|---|---|---|---|---|---|---|---|---|---|---|---|
| **M1** | 19.32 | 147.10 | 2E-01 | 90 | 41000 | 0.20 | 0.62 | 2.30 | 0.05 | 300 | 2E-02 |
| **M2** | 25.82 | 188.94 | 9E-02 | 70 | 38000 | 0.21 | 0.59 | 2.25 | 0.06 | 450 | 2E-02 |
| **M3** | 16.28 | 126.65 | 6E-02 | 80 | 38000 | 0.21 | 0.62 | 2.05 | 0.04 | 200 | 9E-03 |
| **M1-W** | 14.84 | 113.94 | 5E-02 | 30 | 40000 | 0.20 | 0.62 | 2.75 | 0.02 | 200 | 2E-02 |
| **M2-W** | 15.63 | 120.31 | 2E-01 | 50 | 40000 | 0.20 | 0.63 | 2.95 | 0.03 | 300 | 2E-02 |
| **M3-W** | 15.63 | 120.31 | 6E-02 | 55 | 40000 | 0.22 | 0.66 | 2.96 | 0.06 | 300 | 2E-02 |

(Source: Author).

### *4.4.2 Uniaxial Tension-Compression Fatigue*

The fatigue testing program was defined to use duplicates to strain levels within the range of 250, 300 and 350$\mu\varepsilon$ for all analyzed mixtures at the dry and wet conditions. But due to the equipment's compliance factor of LVDTs' strain to the actuator's displacement, and variations in sample preparation, these exact values were not achieved.

For dry specimens, each mixture had samples with at least one of the following: rupture outside the capture range, unleveled gluing, and too few cycles until failure. For wet specimens, the main problem was the strain levels that had to be reduced to the range of 100$\mu\varepsilon$ to 300$\mu\varepsilon$ for M1 and 150$\mu\varepsilon$ to 300$\mu\varepsilon$ for M2. This modification was necessary due to faster cracking growth before 500 cycles in wet conditions.

Figure 53 presents all Damage Characteristic Curves (C *vs.* S) with their respective failure envelope determined by the $G_R$ *vs.* Nf failure criteria. All asphalt mixtures tested presented acceptable regression lines, with $R^2$ above 0.98 as well as DMR values above 0.8.

This means that the used samples represent well each of the analyzed mixtures, without greater deviations.

Figure 53 – Dry $\boldsymbol{C\ vs.\ S}$ of (a) M1, (c) M2, (e) M3 and $\boldsymbol{G^R\ vs.\ N_f}$ of (b) M1, (d) M2, (f) M3.

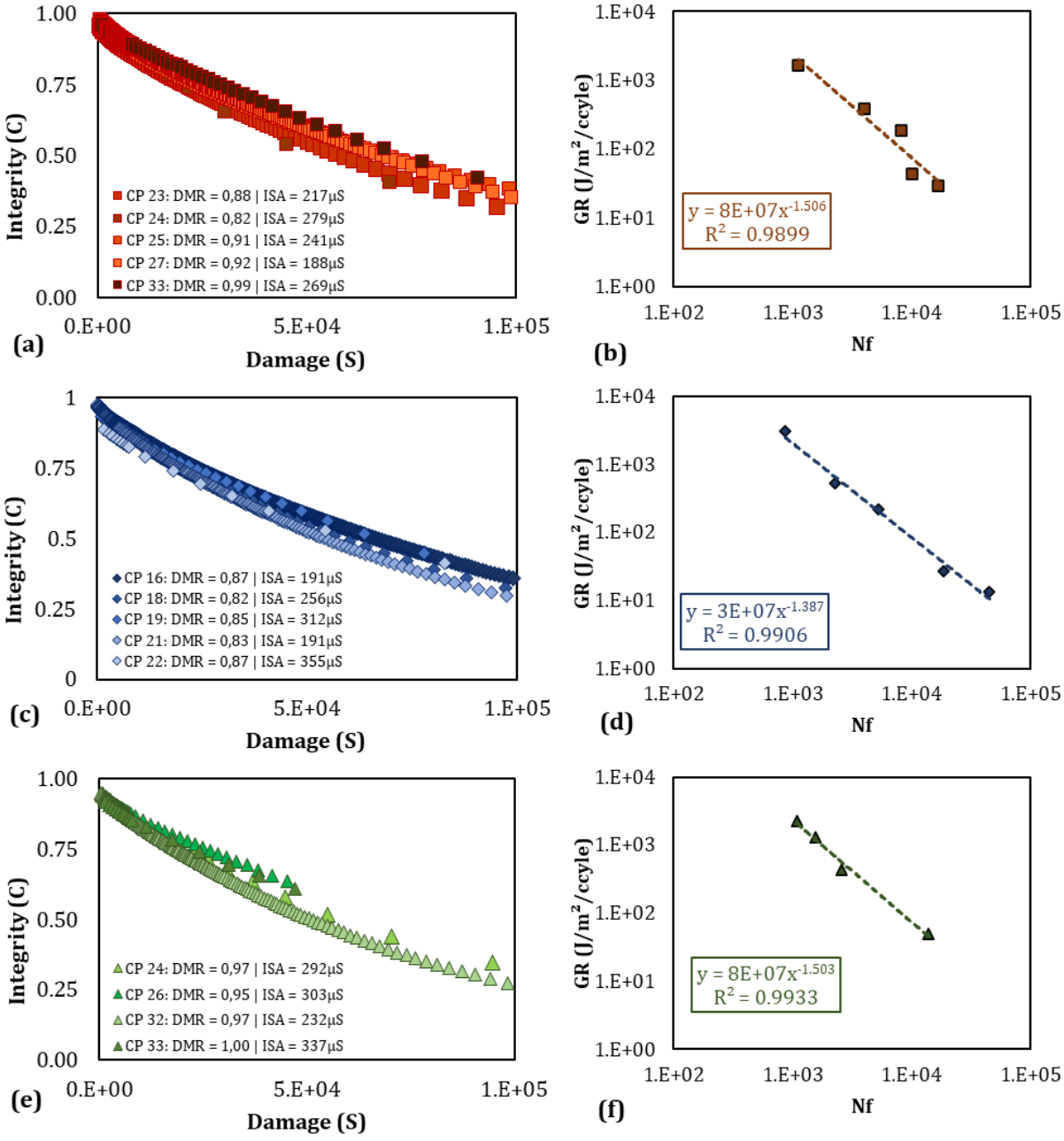


(Source: Author).

Figure 54 presents the same graphs for damaged mixtures. Although $\boldsymbol{G^R\ vs.\ N_f}$ graphs have great regression coefficients, fewer samples were tested and DMR values weren't as high as for undamaged samples. For M1, a total of 8 samples were prepared for testing, 3 of

them failed before 500 cycles, and one had unleveled endplates. Therefore, only 4 samples could be used, despite CP 34 DMR's the data were consistent with the other samples considering the failure criteria.

Figure 54 – Wet $\boldsymbol{C\ vs.S}$ of (a) M1, (c) M2, (e) M3 and $\boldsymbol{G^R\ vs.N_f}$ of (b) M1, (d) M2, (f) M3.

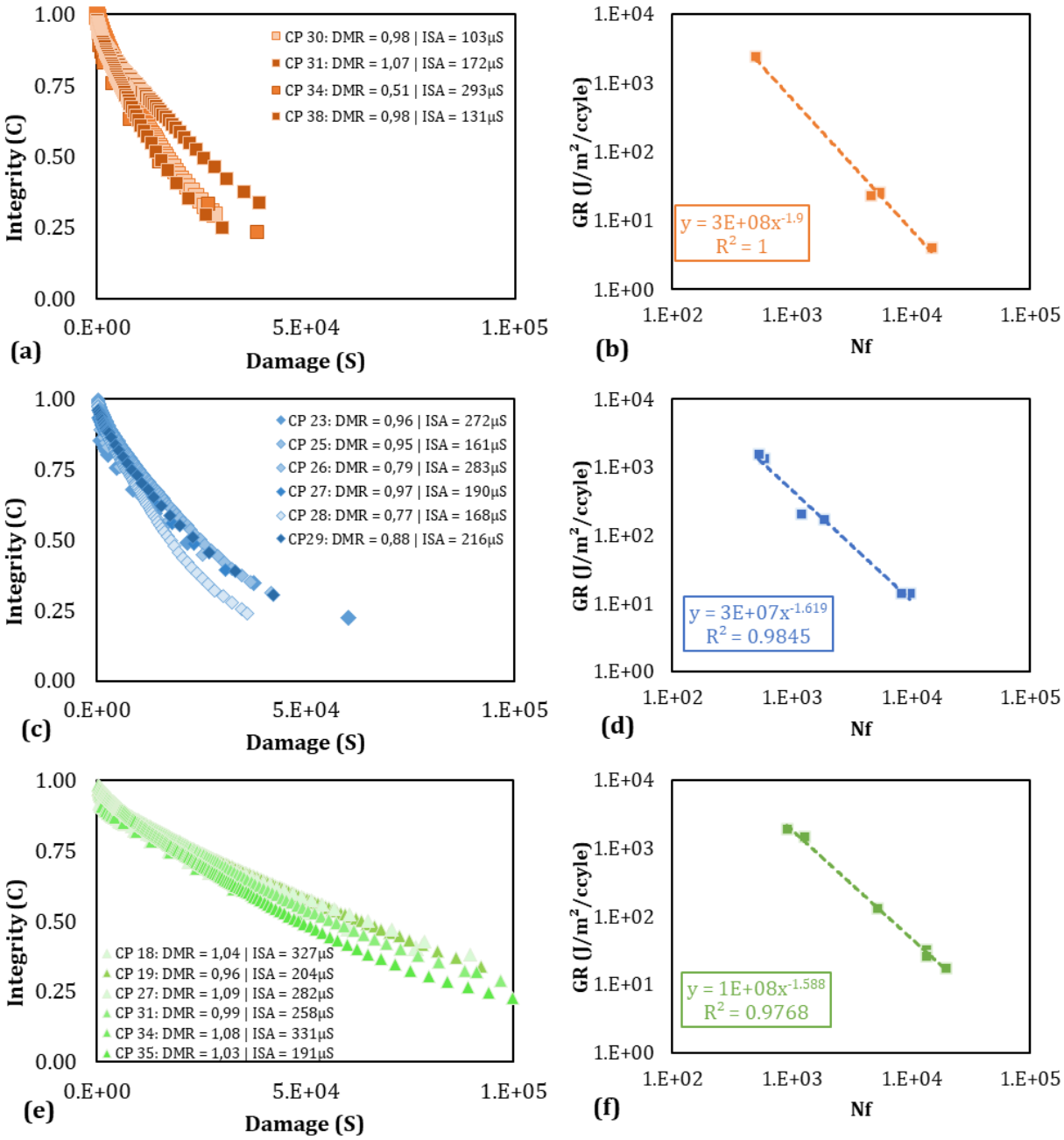


(Source: Author).

As observed in both Figures 53 and 54, the damage and $N_f$ axis were kept the same to observe shift in integrity's rate of decay. This is relatable when comparing the reduction

in Integrity and Damage values at failure mean values, $C_f$ and $S_f$, respectively, in Table 8.

Table 8 – $C_f$, $S_f$, and $DMR$ statistics.

| | $S_f$ | | | $C_f$ | | | DMR | | |
|---|---|---|---|---|---|---|---|---|---|
| | **Mean** | **SD** | **CV (%)** | **Mean** | **SD** | **CV (%)** | **Mean** | **SD** | **CV (%)** |
| **M1** | 167835.41 | 52643.67 | 31.4 | 0.20 | 0.07 | 34.7 | 0.90 | 0.06 | 6.7 |
| **M2** | 127096.91 | 60270.16 | 47.4 | 0.19 | 0.04 | 21.9 | 0.85 | 0.02 | 2.6 |
| **M3** | 177743.91 | 29311.31 | 16.5 | 0.18 | 0.04 | 23.2 | 0.97 | 0.02 | 2.4 |
| **M1-W** | 33886.29 | 5564.85 | 16.4 | 0.28 | 0.05 | 16.5 | 0.89 | 0.25 | 28.7 |
| **M2-W** | 41359.76 | 10157.70 | 24.6 | 0.30 | 0.06 | 21.2 | 0.89 | 0.09 | 10.0 |
| **M3-W** | 128963.28 | 27124.04 | 21.0 | 0.22 | 0.04 | 19.3 | 1.03 | 0.05 | 5.0 |

(Source: Author).

When observing just M3, a concern comes to mind: at a first look, it suggests that HL preserves asphalt mixture integrity and strength, but what would be the behavior when aged? That is an interesting question because HL after moisture damage resulted in almost no stiffness difference, but it is known that stiffness usually increases with aging. That behavior might lead to a reduction in viscous properties, approaching each time an elastic material.

To compare both model results, fitting curves of $C\ vs.S$ and Wöhler at fixed $N_f$ are plotted in Figure 55, which deserves special attention since it is where complete verification is possible. Undamaged mixtures behave almost the same in both approaches, while conditioned M1 and M2 significantly change their behavior while M3 almost does not change.

Figure 55 – Fitting of (a) $C\ vs.S$ model, and (b) Wöhler curves.

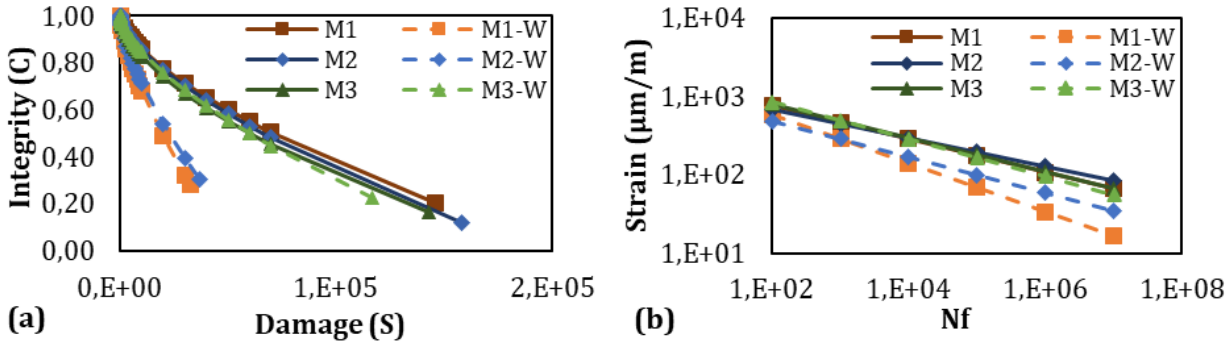


(Source: Author).

Considering all charts, it is seen that M1 and M2 have close reduction proportions but constant ranking. In opposition, M3 presented almost the same behavior. These observations are numerically noticed in Table 9 where all fitting coefficients are described.

Table 9 – Alpha values, and fitting coefficients of $C\ vs.\ S$, $G^R\ vs.\ N_f$.

| | | $C\ vs.\ S$ | | $G^R\ vs.\ N_f$. | |
|---|---|---|---|---|---|
| | $\alpha$ | $C11$ | $C12$ | $Y$ | $\Delta$ |
| **M1** | 2.961 | 3.82E-04 | 0.643 | 7.95E+07 | -1.506 |
| **M2** | 3.030 | 3.74E-04 | 0.649 | 2.99E+07 | -1.387 |
| **M3** | 2.896 | 7.39E-04 | 0.592 | 7.61E+07 | -1.503 |
| **M1-W** | 2.839 | 5.44E-04 | 0.691 | 3.00E+08 | -1.900 |
| **M2-W** | 2.882 | 5.54E-04 | 0.678 | 2.33E+07 | -1.576 |
| **M3-W** | 2.817 | 3.61E-04 | 0.658 | 1.09E+08 | -1.588 |

(Source: Author).

Especially comparing Wöhler curves in Figure 55(b), the $\varepsilon_6$ parameter (strain at 1E+06 cycles) provide an idea of how admitted traffic would decrease if these asphalt mixtures were to be used in a real structure. Their behavior follows the modulus reduction in which M1 has the greatest reduction of 68.7%, followed by M2 with a 54.5% reduction, and last by M3 with just 12.0% decrease. An interesting observation is that even though M2 resists higher strains when undamaged, the reduction after conditioning goes almost as deep as a pure asphalt mixture (Figure 56).

Figure 56 – Strain levels at 1E+06 $N_f$.

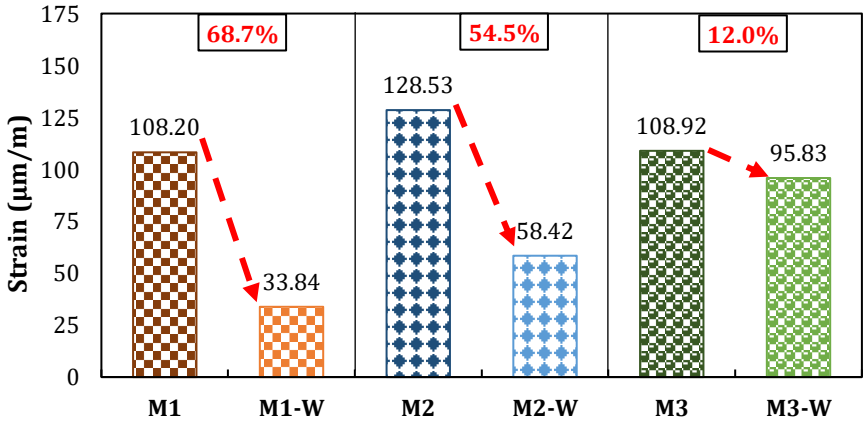


(Source: Author).

As a comparison of results, Figure 56 shows a similar trend for ITSR: M1 loses 45% of ITS, M2 loses 27%, and M3 gains 30%. For fatigue results, analyzing strain levels at $N_f$ of 1E+06, the admitted strain decreases way more than the mixture's ITS reduction. Still, M3 behaves almost with no variation after losing only 12% of its admitted strain-level.

At last, the $FF_M$ calculation is enough to highlight the trend discussed up to this point. For undamaged asphalt mixtures, the ranking would still be M2 > M3 > M1. But for moisture-damaged mixtures, the ranking would be rearranged as M3-W > M2-W > M1-W

(Figure 57). It is highlighted that the percentage reduction is different due to the same strain level used, a different approach that translates more directly to the expected stress levels.

Figure 57 – FFM of dry and wet mixtures.

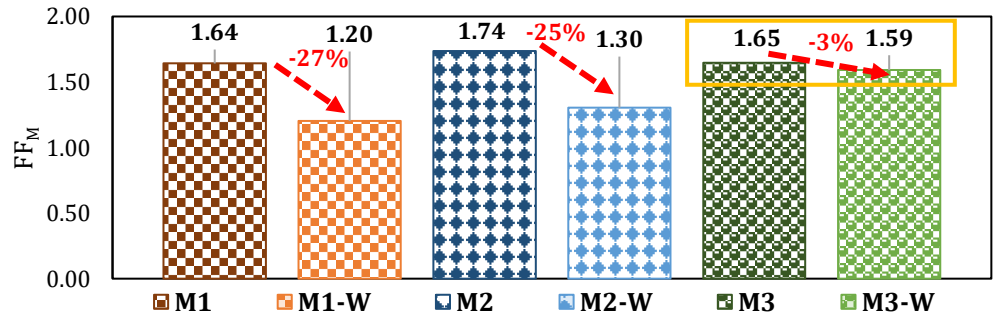


(Source: Author).

Another highlight from the results is the observation of a similar trend from Figure 48. M1 showed the greatest reduction in ITS, followed by M2, while M3 gained strength. In fact, comparing Figure 56 to both Figures 48 and 49, ITS results may be a good indicative of fatigue ranking despite of mixtures stability observed from just dry samples at 4% AV in Figure 48. When stability was mentioned for those results, they were linked to the compaction energy, as M1 and M2 samples needed 100 gyrations, while M3 just 40. It is worth noting that M2 used the amine-based anti-stripping liquid agent, which for the presented results have shown a reduction in resistance.

## 4.5 Asphalt mixtures simulation

### *4.5.1 CAP3D-D*

Despite the use of a complete structure, CAP3D-D only calculates the cracked area at the surface layer (asphalt layer). Therefore, the results presented here do not consider crack's propagation from other layers. For the simulation in CAP3D-D, the following scenario was used: fixed temperature of 30ºC, project duration of 120 months, annual traffic leading to a total N = 1E+07, 20kN of loading, and 60km/h speed.

As expected from Wöhler curves, all dry mixtures would perform well after 120 months of service life. Comparing Accumulated Damage (Figure 58) at 120 months, it is observed that M1-W presents an accumulated damage 6.5 times higher than M1, M2-W is 10.3 times higher than M2, and M3-W is 2.0 times higher than M3. Dry mixtures behave

significantly better than wet mixtures, and the ranking in damage accumulation changes. All dry mixtures would have an accumulated damage under 0.2. On the other side, the conditioned mixtures present damage from 0.2 to 0.6. From $FF_B$, it was expected that M3 behaved better than M1, but worse than M2.

Figure 58 – Accumulated damage in CAP3D-D.

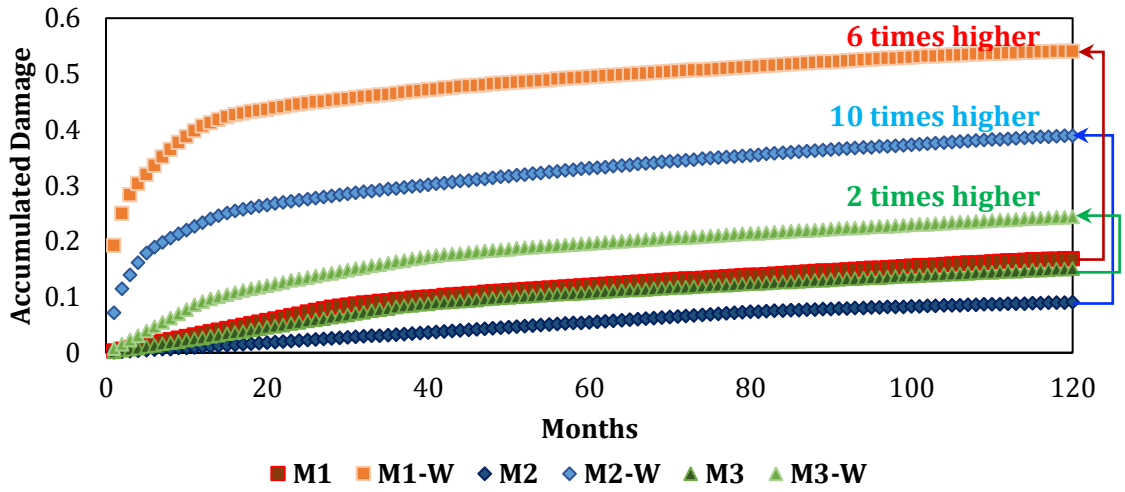


(Soure: Author).

Now considering the cracked area (Figure 59), all dry mixtures would be accepted under the 30% limit (DNIT, 2023). The neat mixture when conditioned (M1-W) presents 30% of cracked area already at the first 7$^{th}$ month and reaches 100% at 33 months. The mixture with the anti-stripping liquid agent when conditioned (M2-W) still preserves its integrity longer, reaching 30% of cracked area at the 36$^{th}$ month, and 100% at 117 months. Finally, the conditioned mixture containing HL (M3-W) does not reach 30% of the cracked area. However, this comparison needs special attention because both 30% and 100% cracked area were achieved in different moments for the mixtures as already presented. This is a greater indicative of fatigue resistance than the comparison of the total cracked area at the end of 120 simulated months. Besides, it is highlighted that M2-W seems to be the worst mixture considering moisture resistance due to its higher damage accumulation compared to the dry M2 mixture. That said, comparing all three mixtures in terms of cracked area, M1-W still is the worst mixture followed by M2-W, and finally M3-W which keeps its stability as previously discussed.

Figure 59 – Cracked Area in CAP3D-D.

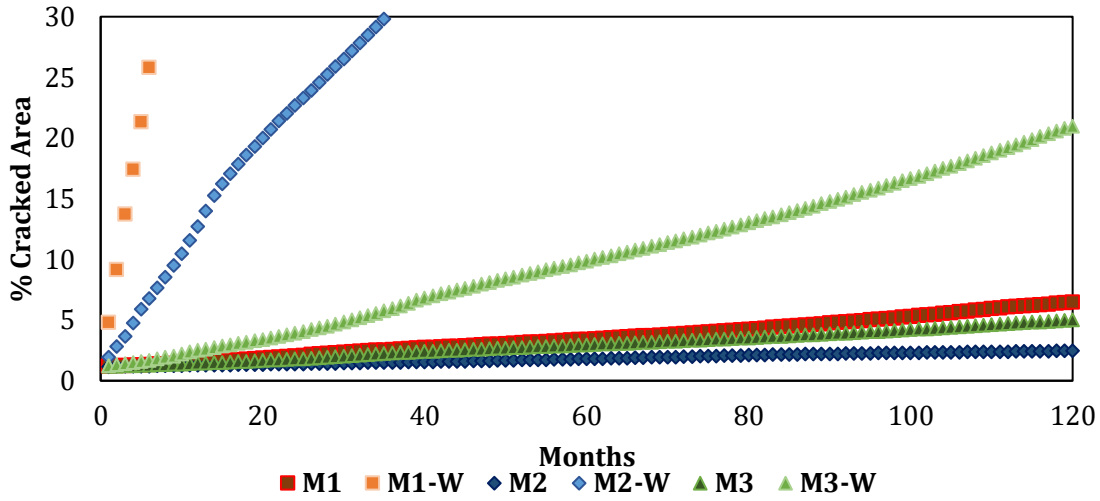


(Source: Author).

### *4.5.2 FlexPAVE™*

Using the FlexPAVE™ software calibrated with the Transfer Function proposed by Wang *et al.* (2021), different structures were simulated as previously described in the methodology section. Despite the presence of the whole structure, only fatigue evolution results of the asphalt layer are herein analyzed. For this simulation in FlexPAVE™, the following scenario was used: fixed temperature of 30ºC, project duration of 120 months, constant traffic of 274 vehicles a day leading to an N = 1E+7, 40kN of loading and in at 60km/h speed.

Figures 60 and 61 show, respectively, the damage factors ($N/N_f$) after 12 and 120 months of fatigue life simulation. In Figure 60, it can be observed that the mixtures M1 (NB) and M2 (NB+D) are already damaged in the first centimeter (center of the loading axis) from the bottom-up of the asphalt coating layer after only 12 months, while the mixture M3 (with HL) showed lower intensity points in the same location than the others. This result shows that the HL seems to delay the initiation and propagation of cracks in the asphalt mixture, possibly due to the improvement of adhesive characteristics between the aggregate and the asphalt binder.

Still in Figure 60, it is possible to see that when these same three asphalt mixtures (M1, M2, and M3) are moisture conditioned (M1-W, M2-W, and M3-W), the M1-W mixture showed a higher damage factor in both the lower and upper parts of the asphalt layer, followed by the M2-W mixture which showed higher damage factor in the lower part and a beginning of damage in the upper part. Contrary to that, M3-W only showed damage in its lower part of the

layer. All samples presented bottom-up cracking.

This result is important because it showed that the mixture with neat binder (M1-W) suffered considerable damage due to moisture conditioning. This is in line with what is expected in the literature (MOURA, 2001; LUCAS JÚNIOR *et al.*, 2019; FROSSARD, 2022), since acidic/gneiss aggregates (with high silica content) such as those used in this study tend to have adhesion problems with pure asphalt binders. In another analysis, M2-W presented a reduction in cracking under moisture conditions when compared to the control mixture M1-W. However, M3-W showed the best behavior against the damage caused by moisture.

These results seem to show that the difference between the amine-based antistripping agent and HL is that the former additive seems to improve the adhesive bond between the aggregate and the binder, while the latter acts much more on the cohesive properties of the mixture. Thus, when the mixture undergoes freezing (there is water expansion inside it) and heating as in the modified Lottman test, the better adhesion caused by the addition of the amine-based antistripping agent is not able to combat the damage caused by expansion/contraction, while the mixture with lime acts by conferring greater cohesiveness to the mixture, and this makes the mixture maintain greater integrity when in contact with this type of water conditioning.

Figure 60 – Damage factor ($\boldsymbol{N/N_f}$) at 12 months.

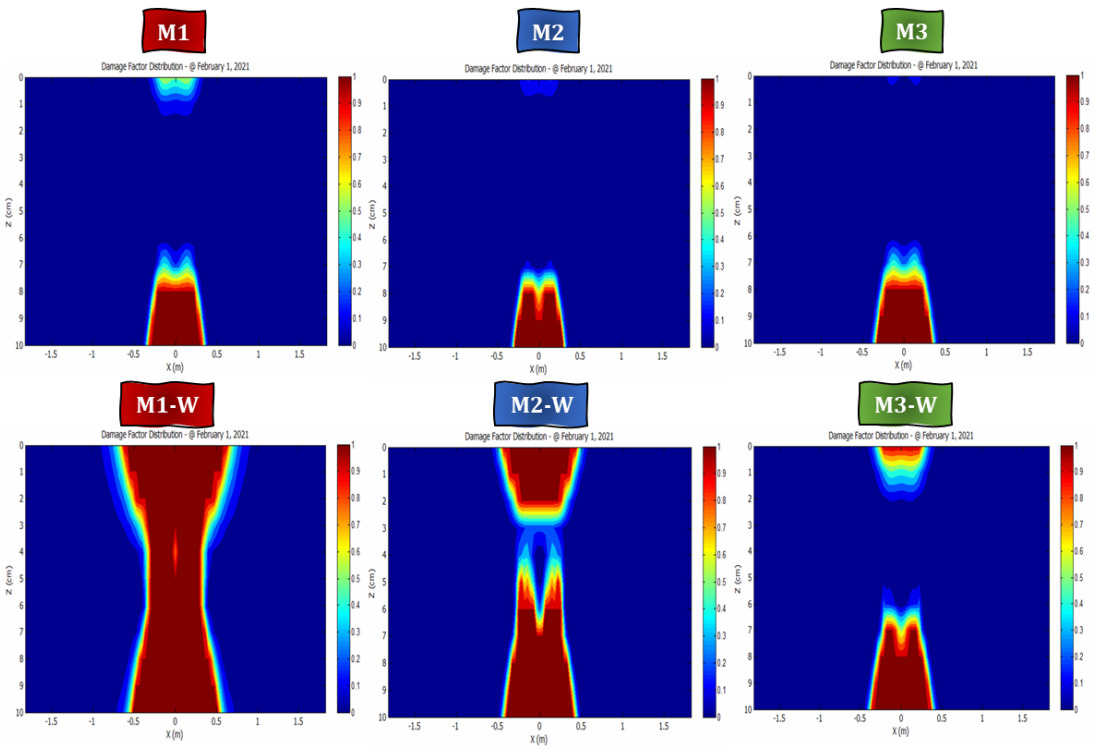


(Source: Author).

After 120 months of simulation (10 years of initial project), the mixtures continue to show the same tendency of damage that they presented at 12 months of simulation but with more intensity. In the dry condition, damage reached the lower 4cm and the upper 3cm of the asphalt layer for M1, while M2 and M3 showed similar behavior in relation to the damage factor ($N/N_f$), still M2 with better results than M3. On the other hand, when evaluated considering the conditioning, M1-W showed higher $N/N_f$ followed by M2-W, indicating that the amine-based antistripping agent even after 120 months of simulation continued to show better results than the neat binder. The mixture with HL (M3-W) showed less damage than M2-W and M1-W. As a comparison between Figures 60 and 61, it is possible to see that the M3-W mixture had a damage factor with the smaller variations after 120 months of simulation while the M2-W mixture had significant difference in the damage factor after 120 months of simulation, it shows that HL is much more effective in combating moisture damage than the amine-based antistripping agent.

Figure 61 – Damage factor ($N/N_f$) at 120 months.

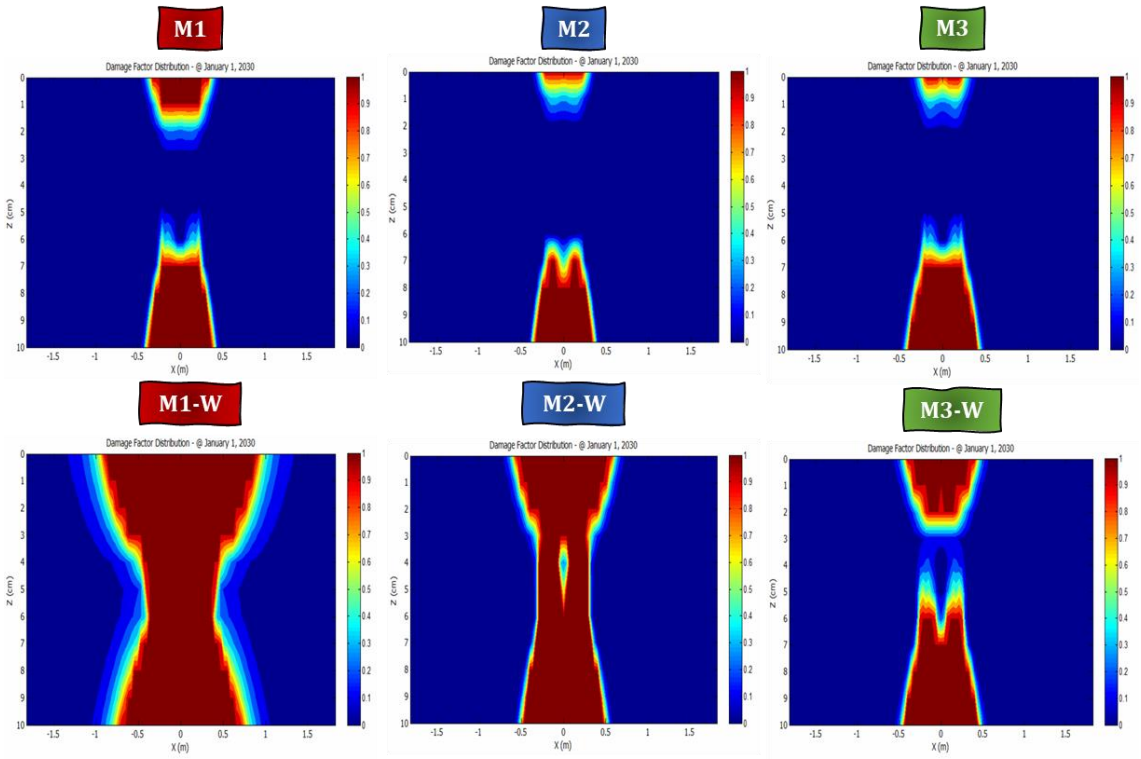


(Source: Author).

Figure 62 shows the evolution of the percentage of damage of the six asphalt mixtures analyzed up to a design time of 120 months. It is noted that in the dry samples, M2 (with amine-based antistripping agent) had the lowest %Damage (25.8%) after 120 months.

While the pure binder mixture (M1) had %Damage of 36.7%, followed by M3 (containing hydrated lime) with 31.8%. On the other hand, when the same mixtures were conditioned to moisture, they presented an increase in %Damage. The pure binder mixture conditioned to moisture (M1-W) was the most affected by water action, and the %Damage after 120 months increased 3.4 times, while the mixture with amine-based antistripping agent (M2-W) increased its %Damage by 3.3 times, and finally, the mixture with HL conditioned to moisture (M3-W) increased 1.6 times its %Damage. This result, considering the limitations of the number of mixtures analyzed and other aspects of the simulation, indicates that the cohesion provided by lime to asphalt mixtures seems to resist the effects of moisture better than the improvement in adhesiveness conferred by the amine-based antistripping agent.

Figure 62 – Damage of asphalt mixtures in FlexPAVE™.

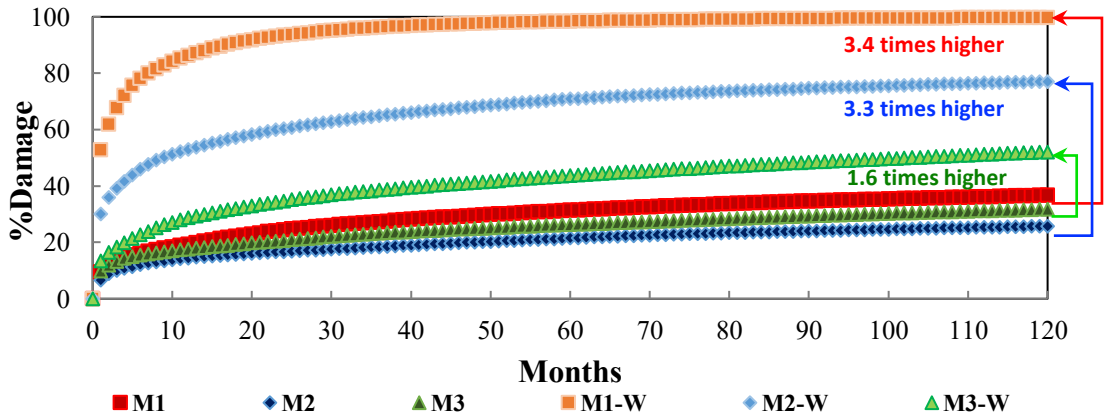


(Source: Author).

Figure 63 shows the percentage of cracked area after 120 months and 1.0E+07 simple axle cycles per dual wheel. It was noted that in the dry condition, the M2 mixture had the lowest cracked area with 48.9%, followed by the M3 mixture with 49.7% and M1 with 49.9%. When these same materials were conditioned to moisture, in the first month of simulation, M1-W already had 49.9% of the cracked area, M2-W presented 49.86% of the cracked area in the fourth month, and M3-W reached 37.55% only in the 45$^{th}$ month. This result shows that HL can significantly delay the beginning and propagation of cracks when in contact with water, and that the amine-based antistripping agent is a material to be evaluated to improve fatigue life in dry condition. Both the pure binder mixture (M1) and the amine-based antistripping agent mixture (M2) showed poor behavior in moisture-conditioned samples, while the lime mixture (M3) was the least affected by moisture.

Figure 63 – %Cracking at 120 months and 1E+07 cycles.

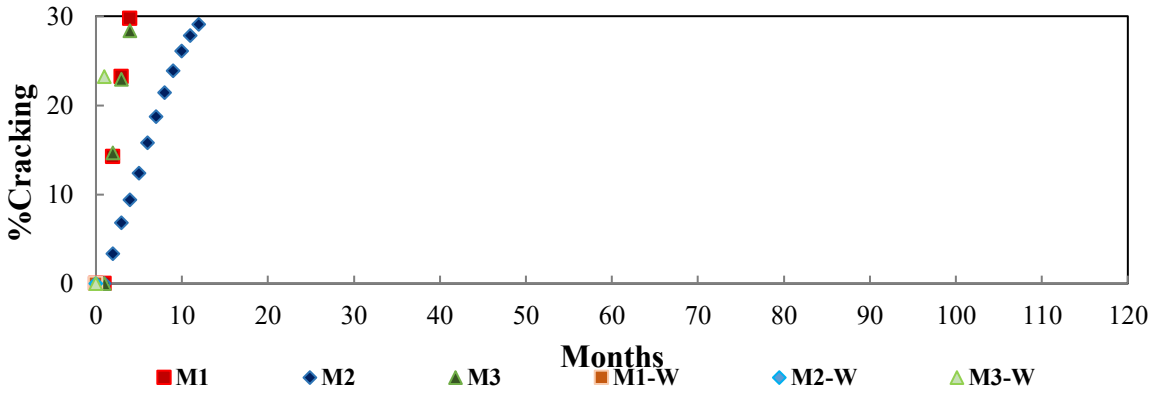


(Source: Author).

### *4.5.3 Comparison of analysis programs' output data*

The initial idea of using both programs was not a comparison of results, but a comprehension of how they would interpret conditioned results in the simulation. Both analyses are suitable to rank mixtures as they resulted in the same classification and captured the components' differences as well as moisture effects. CAP3D-D uses a national database and transfer functions while FlexPAVE™ uses an international database for the calibration.

As expected, these different Transfer Functions resulted in variations of cracked area between the two software. While CAP3D-D continues the analysis until the mixture reaches 100% of cracked area, FlexPAVE™ has a maximum cracked area of 50%. This difference leads to difficulties comparing results at 120 months between programs. As a direct effect, CAP3D-D output data seems more severe than FlexPAVE™ on the analyzed scenario. An alternative to avoid this problem would be the comparison of Accumulated Damage instead of cracked area.

## 4.6 Comparison amongst moisture damage protocols and scales

As observed from the results, the used method of analysis probably needs adaptation especially for the binders' scale. The minimum variation in FFB of dry and wet samples indicates that it is hard to determine moisture susceptibility of the binder. Therefore, the used conditioning protocol probably is not enough to induce damage to binders or at least for the binder considered herein and the LAS test. It is not possible then to clearly estimate the effects for the whole mixture for a conditioned scenario.

For the interface, the effects of moisture become clearer than for isolated binders.

Following the same rationale of ratio between conditioned and dry tests, it is observed that a ranking between the binders due to moisture does exist. Therefore, from this scale, results start indicating an expected behavior for material selection due to moisture susceptibility and a possible ranking between binders for the same mineral substrate.

Finally, for the asphalt mixture scale, the inferred materials' classification from the interface is observed among different testing methods (e.g., $ITSR$, $|E^*|$, and Tension-Compression Fatigue). However, if only $ITS$ are observed, wrong conclusions are made as the highest $ITS$ value led to the minimum expected service-life for fatigue. For this reason, the need of adopting modern tests such as Tension-Compression Fatigue to determine mixtures minimum behavior is reinforced. Besides, the moisture conditioning protocol from AASHTO T 283 (2022) is the most successful to induce damage to samples as demonstrated in Figure 49 for $ITSR$, Figure 51 for $|E^*|$, Figure 55 for $\varepsilon_6$, and Figure 56 $FF_M$. However, using these two last parameters ratio, an estimation of decrease in fatigue life becomes clearer as well as materials ranking which is then proved with simulated data in Figures 57-62 for both CAP3D-D and FlexPAVE™.

# 5 CONCLUSIONS

This thesis presented an analysis of moisture-induced damage in different scales of asphaltic materials considering isolated binders, aggregate-binder interfaces, and complete mixtures. This was done using an acid aggregate (considered prone to adhesiveness problems), neat binder, and the same binder with a commercial amine-based anti-stripping agent, as well as hydrated lime. The primary goal was to evaluate the fatigue cracking properties of asphaltic materials under the effects of moisture.

## 5.1 Main Observations

### *5.1.1 Moisture induced damage amongst scales and protocols*

- LAS does not seem to capture moisture effects clearly.
- The conditioning protocols used seemed suitable to determine moisture-induced damage for the materials and scales analyzed and similar results were observed for ranking purposes with clear responses starting from the interface scale.
- To understand the effects of moisture, the conditioning protocol choice is as important as the testing protocol itself. When using a given conditioning protocol, the selected test might capture the effects of moisture while other testing protocol might not be able.
- For materials' selection, ABS testing seems suitable to indicate a good combination of aggregate-binder for rupture purposes in the necessary temperature.
- $ITSR$ results compared to conditioned fatigue generate the same rankings between mixtures;
- Moisture conditioning reduces significantly the expected fatigue life of the asphalt mixtures and the consideration of only dry tests might overestimate the actual service-life of pavements.

### *5.1.2 Asphalt binders*

From the asphalt binders' perspective, the used protocol most likely did not really induce damage to the asphalts, or at least the observed variation could be discarded, especially for fatigue properties. Considering |G*|, the difference was the same for neat binder and binder with anti-stripping liquid agent, meaning that rheological characterization probably captures some anti-stripping effect of stiffness reduction but not enough to determine variations in behavior due to moisture. Therefore, their properties act strictly at the aggregate-binder

interface. Some of the hypotheses for these findings are related to the conditioning protocol used, as if this temperature and period is not enough to really induce any kind of damage. As for LAS results, it seems that capturing the effects of moisture on binders' fatigue is a more complex task than for asphalt mixtures.

### *5.1.3 Aggregate-binder interface*

At the aggregate-binder interface, a more significant modification in behavior was observed for the same conditioning method used for asphalt binders. Considering all pulling-off rates and temperatures, the most significant variable to alter adhesion-force was temperature, as the greater variation in maximum stress was observed for this variable. No clear trend is observed for raw data. When organized in a single curve, a trend in failure is observed as well as the need of one more temperature.

Therefore, the failure envelope was determined as the initial aim of the binder-aggregate interface testing. But, due to the lack of displacement measurements to calculate the strains, this curve is not related to stiffness as initially thought, but probably to failure ranking such as FFB and FFM or as an initial testing protocol to determine a range of variation in each binder-aggregate combination.

As a result of aggregate-binder interactions, it is reinforced that these tests must be conducted at both aggregate surfaces. Whether they are at an adaptation of Pull-Off Stubs or DSR spindles. Using such adaptations, both tensile and torsional stresses are determined with information from surface interactions.

### *5.1.4 Asphalt mixtures*

For asphalt mixtures, the used damaging protocol resulted in the most successful campaign. There is a clear trend in ITS, ITSR, |E*| and fatigue resistance for all mixtures as well as the conditioned samples.

The behavior of anti-stripping liquid agent reduces asphalt mixtures ITS values, and |E*|, but increases the admitted strain at fatigue. On the other hand, Hydrated Lime leads to a gain in resistance due to water interactions reducing its environmental susceptibility and increasing its stiffness. Nevertheless, it is necessary to determine whether this behavior is good or not for other distresses as well as the influence of aging coupled to moisture effects.

The 2S2P1D calibration parameters did not diverge significantly after conditioning.

Even considering isolated dry or wet results, most constants could be kept almost the same. The major variations were in the WLF constants as well as $E_0$ and $E_\infty$. While the WLF constants are related to temperature susceptibility, the last two parameters are linked to the aggregates and aggregate-binder interactions, thus they are expected to vary with the anti-stripping agent or conditioning method used.

Another finding considering the reduction in fatigue life (i.e. strain at Nf of 1E+6) is related to the evolution of damage in a real structure from simulation data. Both analysis programs used, FlexPAVE$^{TM}$ and CAP3D-D, showed similar results for mixtures performances.

Although field data involves traffic, temperature, aging, construction mistakes and other variability sources, the use of standard characterization can induce overestimation of material's fatigue-life. Consequently, the use of conditioned data leads to a minimum expected fatigue life, and these data could be used for a weighted calibration of analysis software.

## 5.2 Suggestions for future works

Considering the findings of the research presented, following are suggestions for further works:

- Evaluate the effects of moisture damage in rutting tests such as the Stress Sweep Rutting as rutting is associated with great loading and high temperature. These are the combinations expected to have the worst behavior due to moisture damage, according to the observed results. Rutting tests also make use of models that describe the damage evolution, and further studies could indicate which model parameters are affected the most by moisture.
- Determine whether rheological models such as 2S2P1D are adjustable to the ABS test data in multiple temperature and pull-off rate despite the non-linearity of the test.
- Evaluate only HL modified asphalt mixtures, considering some aging protocol and moisture damage coupled to fatigue damage. This might be an important observation due to stiffness increase with aging that might reduce VEL properties of asphalt mixtures with HL. For this analysis, the reactions between the fine particles of aggregates and HL must be investigated supported by data from X-Ray Fluorescence (X-RF) characterizing HL and aggregates composition.
- Evaluate mixtures using both liquid anti-stripping and HL to observe if this impacts mixtures' results as both additives work on aggregate-binder chemical adhesion.

- Create a database containing RRT and Conditioned Fatigue results with different: aggregates, binders, and additives. With this data a minimum criterion of RRT could be determined for fatigue life results.
- Propose a testing protocol that results in a minimum expected fatigue life, considering the moisture damage possibility as part of the cumulative damage calculations. This proposition could work as the Balanced Mixture design which considers volumetric parameters, but this time it would consider levels of reliability in expected fatigue life.
- Verify the possibility of using accelerometers, moisture, and temperature sensors on pavements to evaluate more accurate conditions of testing as well as obtaining instant field data to calibrate performance models that considers temperature, stress, and moisture at the surface layer.
- Analyze the opportunity of training Machine Learning models to estimate valid ranges of |E*| and fatigue life Nf's considering the moisture-damaged result as the lowest possible probability inside the confidence interval.

# REFERENCES

AASHTO. **Standard Method of Test for Effect of Heat and Air on a Moving Film of Asphalt Binder (Rolling Thin-Film Oven Test) T240.** Washington, DC. American Association of State Highway and Transportation Officials. 2021.

AASHTO. **Standard Method of Test for Resistance of Compacted Asphalt Mixtures to Moisture-Induced Damage T 283.** American Association of State Highway and Transportation Officials, Washington, DC. 2021.

AASHTO. **Determining Asphalt Binder Bond Strength by Means of the Asphalt Bond Strength (ABS) Test T 361.** Washington, DC. American Association of State Highway and Transportation Officials. 2016.

AASHTO. **Standard Method of Test for Estimating Fatigue Resistance of Asphalt Binders Using the Linear Amplitude Sweep T 391**. Washington, DC. American Association of State Highway and Transportation Officials. 2020.

AASHTO. **Determining the damage characteristic curve of asphalt concrete from direct tension cyclic fatigue tests. Provisional standard TP 107**. Washington, DC. American Association of State Highway and Transportation Officials. 2018.

AKENTUNA, M.; LIU, J.; MOHAMMAD, L. N.; SACHDEVA, S.; COOPER III, S. B.; COOPER JR., S. B. Moisture Susceptibility of Asphalt Mixtures: Conditioning and Testing Protocols. **Transportation Research Record.** Washington, DC. p. 1-11, 2023. DOI: 10.1177/03611981221147214.

AKENTUNA, M.; MOHAMMAD, L. N; SACHDEVA, S.; COOPER III, S. B.; COOPER JR., S. B. Effectiveness of Loaded Wheel Tracking Test to Ascertain Moisture Susceptibility of Asphalt Mixtures. **Transportation Research Record.** Washington, DC. v. 2676, n. 1. p. 421-434, 2022. DOI: 10.1177/03611981211036355.

ALKOFAHI, N.; KHEDAYWI, T. Stripping Potential of Asphalt Mixtures: State of the Art. **International Journal of Pavement Research and Technology**. [s. l.]. v. 15, p. 29-43, 2021. DOI: 10.1007/s42947-021-00003-7.

ALMEIDA, A. J.; MOMM, L.; TRICHÊS, G.; SHINOHARA, K. J. Evaluation of the influence of water and temperature on the rheological behavior and resistance to fatigue of asphalt mixtures. **Construction and Building Materials.** [s. l.]. v. 158, p. 401-409, 2018. DOI: 10.1016/j.conbuildmat.2017.10.030.

ANITELLI, A. **Estudo do dano por umidade de misturas densas com ligantes asfálticos convencional e modificado com polímero SBS.** 2013. Dissertação (Mestrado em Infra-Estrutura de Transportes) - Escola de Engenharia de São Carlos, Universidade de São Paulo, São Carlos. 2013.

ARAUJO, A. F. **Avaliação de misturas de solos estabilizados com Cal, em pó e em pasta, para aplicação em rodovias do Estado do Ceará**. 2009. 175 f. Dissertação (Mestrado em

Engenharia de Transportes)-Centro de Tecnologia, Universidade Federal do Ceará, Fortaleza. 2009.

ARAÚJO, C. B. C. **Gestão integrada de infraestrutura civil em ambiente urbano:** água e transportes. 2019. 235 f. Tese (Doutorado em Engenharia Civil) - Centro de Tecnologia, Programa de Pós-Graduação em Engenharia Civil: Recursos Hídricos, Universidade Federal do Ceará, Fortaleza. 2019.

ASTM D7175-15. **Standard Test Method for Determining the Rheological Properties of Asphalt Binder Using a Dynamic Shear Rheometer.** West Conshohocken, PA. American Society for Testing and Materials. 2015.

AZEVEDO, A. M. **Considerações sobre a drenagem subsuperficial na vida útil dos pavimentos rodoviários.** 2007. Dissertação (Mestrado em Engenharia de Transportes) - Escola Politécnica, Universidade de São Paulo, São Paulo, 2007. DOI:10.11606/D.3.2007.tde-14012008-115049.

BABADOPULOS, L. F. A. L. **Phenomena occurring during cyclic loading and fatigue tests on bituminous materials:** Identification and quantification. 2017. 303 f. Tese (Doutorado) – Universidade de Lyon (ENTPE), Lyon, 2017.

BABADOPULOS, L. F. A. L., OROZCO, G., SAUZÉAT, C. AND DI BENEDETTO, H. Reversible phenomena and fatigue damage during cyclic loading and rest periods on bitumen**. International Journal of Fatigue**, [s. l.]. v. 124, p. 303–314, 2019. DOI: 10.1016/j.ijfatigue.2019.03.008.

BABADOPULOS, L. F. A. L.; FERREIRA, J. L. S.; SOARES, J. B.; NASCIMENTO, L. A. H.; CASTELO BRANCO, V. T. F. Aging-Effect Incorporation into the Fatigue-Damage Modeling of Asphalt Mixtures Using the S-VECD Model. **Journal of Materials in Civil Engineering**. [s. l.]. v. 28, n.12, p.1-11, 2016. DOI: 10.1061/(ASCE)MT.1943-5533.0001676.

BABADOPULOS, L. F. A. L.; SAUZÉAT, C.; DI BENEDETTO, H. Softening and local selfheating of bituminous mixtures during cyclic loading. **Road Materials and Pavement Design**. [s. l.]. v. 18, n. 2, p. 164–177, 2017. DOI: 10.1080/14680629.2017.1304260.

BAHIA, H. U.; HANSON, D.; ZENG, M.; ZHAI, H.; KHATRI, M.; ANDERSON, R. Characterization of modified asphalt binders in Superpave mix design. Transportation Research Board. **National Cooperative Highway Research Program – NCHRP Report 459**, Washington, DC. National Academy Press. v. 1, p. 1-53, 2001. ISSN: 00775614.

BARBOZA JUNIOR, V. S. **Efeito deletério da água em misturas asfálticas com adição de ligante modificado com polímero e de cal.** 2018. Dissertação (Mestrado em Engenharia Civil) – Universidade Federal de Santa Maria. Santa Maria. 2018.

BARRA, B.; MOMM, L.; GUERRERO, Y.; BERNUCCI, L. Fatigue behavior of dense asphalt mixes in dry and environmental-conditioning states. **Construction and Building Materials.** [s. l.]. v. 29. p. 128-134. 2012. DOI: 10.1016/j.conbuildmat.2011.10.003.

BASTOS, J. B. S. **Influência da variação da umidade no comportamento de pavimentos da região metropolitana de Fortaleza.** 164 f. Dissertação (Mestrado em Engenharia de Transportes) - Centro de Tecnologia, Universidade Federal do Ceará, Fortaleza. 2013.

BERNUCCI, L. L. B.; MOTTA, L. M. G.; CERATTI, J. A. P.; SOARES, J. B. **Pavimentação Asfáltica – Formação Básica para Engenheiros**. Rio de Janeiro, RJ. 2022.

BEZERRA, A. K. L. **Análise comparativa entre os ensaios BBS e arrancamento de argamassa utilizados na avaliação da adesividade e do dano por umidade na interface ligante agregado.** 2018. 69 f. TCC (Graduação em Engenharia Civil) – Universidade Federal do Cariri, Centro de Ciência e Tecnologia, Curso de Engenharia Civil. Juazeiro do Norte, 2018.

BOCK, A. L.; HARTMANN, D., BUDNY, J.; SPECHT, L. P.; CERATTI, J. A. P. Estudo laboratorial sobre os efeitos de diferentes formas de adição de cal a concreto asfáltico. **Teoria e Prática na Engenharia Civil**. Rio Grande. Dunas. n.14. p.59-69. 2009.

BRINGEL R. M; VELASQUEZ R.; BAHIA H. U. Measuring the Effect of Moisture on Asphalt–Aggregate Bond with the Bitumen Bond Strength Test. **Transportation Research Record: Journal of the Transportation Research Board.** Washington, DC. n. 2209, p. 70-81, 2011. DOI: 10.3141/2209-09

BRONDANI, C. **Estudo do efeito deletério da água em misturas asfálticas a quente produzidas no Rio Grande do Sul. Dissertação de mestrado.** 2019. 202 f. Dissertação (Mestrado em Engenharia Civil) – Programa de Pós-Graduação em Engenharia Civil. Universidade Federal de Santa Maria. 2019.

BRONDANI, C.; VESTENA, P. M.; FACCIN, C.; SCHUSTER, S. L.; SPECHT, L. P; PEREIRA, D. S. Moisture susceptibility of asphalt mixtures: 2S2P1D rheological model approach and new index based on dynamic modulus master curve changes. **Construction and Building Materials.** [s. l.]. v. 331, p. 1-12, 2022. DOI: 10.1016/j.conbuildmat.2022.127316..

BUDNY, J. **Avaliação dos Efeitos de Diferentes Tipos de Cal em Misturas de Concreto Asfáltico.** 2009. 74 f. TCC (Graduação em Engenharia Civil) – Departamento de Tecnologia, Universidade Regional do Noroeste do Estado do Rio Grande de Sul, Ijuí, 2009.

CALA, A.; CARO, S. Predictive quantitative model for assessing the asphalt-aggregate adhesion quality based on aggregate chemistry. **Road Materials and Pavement Design**. v. 23, p. 1523-1543, 2021. DOI:10.1080/14680629.2021.1900896.

CARDONA D. R.; DI BENEDETTO, H.; SAUZÉAT, C.; CALON, N. Fatigue and Moisture Damage Resistance of Bituminous Mixtures for Railway Trackbeds. *In*: DI BENEDETTO H., BAAJ H., CHAILLEUX E., TEBALDI G., SAUZÉAT C., MANGIAFICO, S. (ed) **Proceedings of the RILEM International Symposium on Bituminous Materials.** ISBM 2020. Lyon. Springer, Cham. 2021. v. 27, p. 927–933. RILEM Bookseries. DOI: 10.1007/978-3-030-46455-4_118.

CHRISTENSEN, R. M. **Theory of Viscoelasticity**. Ed. 2. New York: Academic, 1982.

CORTÉ, J. F.; DI BENEDETTO H. **Matériaux routiers bitumineux 1:** Description et propriétés des constituents. Paris: Hermes-Lavoisier. 2005.

CORTÉ, J. F.; DI BENEDETTO H. **Matériaux routiers bitumineux 2:** Constitution et propriétés thermomécaniques des mélanges. Paris: Hermes-Lavoisier. 2005.

CUI, S.; BLACKMAN, B. R. K.; KINLOCH, A. J.; TAYLOR, A. C. Durability of asphalt mixtures: Effect of aggregate type and adhesion promoters. **International Journal of Adhesion and Adhesives.** [s. l.]. v. 54, p. 100-111, 2014. DOI: doi.org/10.1016/j.ijadhadh.2014.05.009.

CURTIS, C. W.; ENSLEY, K; EPPS, J. **Fundamental properties of Asphalt-Aggregate interactions including adhesion and absorption.** Washington, DC. Strategic Highway Research Program, National Research Council. 1993.

DI BENEDETTO, H.; DE LA ROCHE, C.; BAAJ, H.; PRONK, A.; LUNDSTRÖM, R. Fatigue of Bituminous Mixtures. **Materials and Structures**. [s. l.]. v. 37, p. 202–216, 2004. DOI: 10.1007/BF02481620

DI BENEDETTO, H.; GABET, T.; GRENFELL, J.; PERRATON, D.; SAUZÉAT, C.; BODIN, D. Mechanical testing of bituminous mixtures. *In*: PARTL, M. N.; BAHIA, H. U. ; CANESTRARI, F.; DE LA ROCHE, C; DI BENEDETTO, H.; PIBER, H.; SYBILSKI, D. (Ed). **Advances in inter laboratory testing and evaluation of bituminous materials:** State-of-the-Art Report of the RILEM Technical Committee 206. New York. 2013, p. 143-256. ATB-Series. DOI: 10.1007/978-94-007-5104-0

DIAS, Davidson Menezes. **Estimativa de propriedades viscoelásticas lineares de misturas asfálticas completas a partir da caracterização da matriz de agregados finos.** 2016. 77 f. Monografia (Graduação em Engenharia Civil)-Universidade Federal do Ceará, Fortaleza, 2016.DNER 078. Agregado graúdo – adesividade a ligante betuminoso. **Norma Rodoviária. Método de Ensaio.** 1994.

DNER. (Brasil) **Determinação da abrasão "Los Angeles" 035:** Agregados, Rio de Janeiro, 1998.

DNER. (Brasil) **Adesividade a ligante betuminoso 078:** Agregado graúdo, Rio de Janeiro, 1994.

DNIT. (Basil) **Especificação de Serviço 031:** Pavimentos Flexíveis – Concreto asfáltico, Rio de Janeiro, RJ. 2006.

DNIT. (Brasil) **Determinação do dano por umidade induzida 180:** Pavimentação – Misturas Asfálticas – Método de Ensaio, Rio de Janeiro, RJ. 2018.

DNIT. (Brasil) **Determinação do Módulo Dinâmico 416** – ME. Departamento Nacional de Infraestrutura e Transportes. Pavimentação – Misturas asfálticas – Método de ensaio, Rio de Janeiro, RJ. 2019.

DNIT. (Brasil) **Manual de Utilização do MeDiNa.** Departamento Nacional de Infraestrutura e Transportes. Available in: <https://www.gov.br/dnit/pt-br/assuntos/planejamento-e-pesquisa/ipr/medina/medina-1-1.5>. Accessed in: 30/04/2023 at 16:48.

EPPS, J.; BERGER, E.; ANAGNOS, J. N. TOPIC 4: Treatments. *In:* MOISTURE Sensitivity of Asphalt Pavements: A National Seminar. Washington, DC: Transportation Research Board, 2003, p. 117-177.

ESLAMINIA, M.; THIRUNAVUKKARASU, S.; GUDDATI, M. N.; KIM, Y. R. Accelerated Pavement Performance Modeling Using Layered Viscoelastic Analysis. In: Scarpas A., Kringos N., Al-Qadi I., A. L. (eds) **7th RILEM International Conference on Cracking in Pavements.** Delft. Springer, Dordrecht. 2012, v. 4, p. 497-506. RILEM Bookseries. DOI: 10.1007/978-94-007-4566-7_48.

FERREIRA, W. L. G. **Análise do fluxo d'água em revestimentos asfálticos com diferentes permeabilidades.** 131 f. Dissertação (Mestrado em Engenharia de Transportes) – Centro de Tecnologia, Universidade Federal do Ceará, Fortaleza, 2015.

FERREIRA, W. L. G. **Avaliação da permeabilidade de misturas asfálticas com diferentes granulometrias.** 82 f. Monografia (Graduação em Engenharia Civil) - Universidade Federal do Ceará, Fortaleza, 2013.

FERRY, J. D. **Viscoelastic Properties of Polymers**. Ed. 3. New York: John Wiley & Sons, 1980.

FLÜGGE, W. **Viscoelasticity.** Ed. 2. Berlin: Springer-Verlag, 1975.

FROSSARD, R. M.; TEIXEIRA, J. E. S. L.; KIM, Y. R. Effects of Aggregate/Filler Characteristics on Semi-Circular Bend Fracture Parameters of Asphalt Concrete Mixtures Subject to Moisture Damage. **Transportation Research Record.** Washington, DC. v. 2676, n. 11, p. 408–421, 2022. DOI: https://doi.org/10.1177/03611981221093329.

HICKS, R. P. **Moisture Damage in Asphalt Concrete**. National Cooperative Highway Research Program. Synthesis of Highway Practice 175. Washington, DC. Transportation Research Board (TRB). 1991.

HINTZ, C.; BAHIA H. Simplification of Linear Amplitude Sweep Test and Specification Parameter**. Transportation Research Record**. Washington, DC. 2370(1):10-16. 2013. DOI: 10.3141/2370-02.

HINTZ, C.; VELASQUEZ, R.; JOHNSON, C.; BAHIA, H. Modification and Validation of Linear Amplitude Sweep Test for Binder Fatigue Specification. **Transportation Research Record.** Washington, DC. v. 2207, n. 1, p. 99–106, 2011. DOI: https://doi.org/10.3141/2207-13.

HOLANDA, A. S. de et al. Finite element modeling of flexible pavements. *In:* Iberian Latin American Congress on Computational Methods in Engineering, 27., 2006, Belém. **Anais...** Belém: Iberian Latin-American Congress on Computational Methods in Engineering, 2006. p. 1-14.

HOPMAN, P. C.; KUNST, P. A. J.; PRONK, A. C. A renewed interpretation method for fatigue measurements: verification of Miner's rule. *In:* **Proceedings of the 4th Eurobitume Symposium**, Madrid, Spain, p. 557–561. 1989.

HUANG, Y. H. **Pavement analysis and design.** Upper Saddle River, NJ: Pearson/Prentice Hall. 2004.

HUNTER, E.; KSAIBATI, K. **Evaluating moisture susceptibility of asphalt mixes.** Report MPC-02-138. Laramie. University of Wyoming. 2002.

KACHANOV, L. M**. Introduction to continuum damage mechanics.** Dordrecht: Springer Netherlands. 1986, v.10. DOI: 10.1007/978-94-017-1957-5.

KIGGUNDU, B. M.; ROBERTS, F., L. The Success/Failure of Methods Used to Predict the Stripping Potential in the Performance of Bituminous Pavement Mixtures. **NCAT Report 88-03.** Auburn, AL. National Center for Asphalt Technology. p. 1-19. 1988.

KIM, Y. R. **Modeling of Asphalt Concrete**. Reston, VA, New York: ASCE Press: McGraw-Hill Construction: 2009.

KIM, Y. R.; LITTLE, D. N. One-Dimensional Constitutive Modeling of Asphalt Concrete. **Journal of Engineering Mechanics.** [s. l.]. v. 116, n. 4, p. 751–772, 1990. DOI: 10.1061/(asce)0733-9399(1990)116:4(751).

KIM, Y. R.; LITTLE, D. N.; LYTTON, R. L. Fatigue and Healing Characterization of Asphalt Mixtures. **Journal of Materials in Civil Engineering**, [s. l.]. v. 15, n. 1, p. 75–83. 2003. DOI: 10.1061/(ASCE)0899-1561(2003)15:1(75)

KIM, Y. R.; LUTIF, J. S.; BHASIN, A.; LITTLE, D. N. Evaluation of moisture damage mechanisms and effects of hydrated lime in asphalt mixtures through measurements of mixture component properties and performance testing. **Journal of materials in civil engineering.** v. 20, n. 10, p.659-667, 2008. DOI: 10.1061/(ASCE)0899-1561(2008)20:10(659).

LAMOTHE, S.; PERRATON, D.; DI BENEDETTO, H. Fatigue behaviour of dry or partially saturated hot mix asphalt (HMA). **Fatigue & Fracture of Engineering Materials & Structures**. [s. l.]. v. 43, n. 6, p. 1100-1114, 2019. DOI: 10.1111/ffe.13176.

LEMAÎTRE, J.; CHABOCHE, J. L. **Mechanics of solid materials**. Cambridge: Cambridge University Press. 1990.

LITTLE, D. N.; JONES, D. R. TOPIC 2: Chemical and mechanical processes of moisture damage in hot-mix asphalt pavements. *In:* MOISTURE Sensitivity of Asphalt Pavements: A National Seminar. Washington, DC: Transportation Research Board, 2003, p. 37-70.

LOTTMAN, R. P. NCHRP Report 192: Predicting Moisture-Induced Damage to Asphaltic Concrete. **Transportation Research Board, National Research Council**, Washington, DR. p. 1-60, 1978.

LUCAS JÚNIOR, J. L. O. **Influência da adesividade agregado-ligante no trincamento por fadiga de misturas asfálticas.** 2018. 134 f. Dissertação (Mestrado em Engenharia de Transportes)-Centro de Tecnologia, Universidade Federal do Ceará, Fortaleza, 2018.

LUCAS JÚNIOR, J. L. O., BABADOPULOS, L. F. A. L., & SOARES, J. B. Moisture-induced damage resistance, stiffness and fatigue life of asphalt mixtures with different aggregate-binder adhesion properties. **Construction and Building Materials.** [s. l.]. v. 216, p. 166–175, 2019. DOI:10.1016/j.conbuildmat.2019.04.241

LUCAS JÚNIOR, J. L. O.; SILVA, L. S. V.; ROCHA, W. S.; BABADOPULOS, L. F. A. L.; SOARES, J. B. Effects of rheology and adhesiveness of asphalt binders to different substrates on the resistance to moisture conditioning, **The Journal of Adhesion**. [s. l.]. v. 98, n. 13, p. 1937-1956, 2021. DOI: 10.1080/00218464.2021.1942855

LUNDSTRÖM, R.; ISACSSON, U. Characterization of Asphalt Concrete Deterioration Using Monotonic and Cyclic Tests. **International Journal of Pavement Engineering**, [s. l.]. v. 4, n. 3, p. 143–153, 2003. DOI: 10.1080/10298430310001646002

MAIA, M. M. A. S.; DINIS-ALMEIDA, M.; MARTINHO, F. C. G. The influence of the affinity between aggregate and bitumen on the mechanical performance properties of asphalt mixtures. **Materials.** [s. l.]. v. 14, n. 21, p. 1-13, 2021. DOI: 10.3390/ma14216452

MANGIAFICO, S**. Linear viscoelastic properties and fatigue of bituminous mixtures produced with Reclaimed Asphalt Pavement and corresponding binder blend**s. 2014. 336 f. Tese (Doutorado) – Universidade de Lyon (ENTPE), Lyon, 2014.

MANGIAFICO, S.; DI BENEDETTO, H.; SAUZÉAT, C.; OLARD, F.; POUGET, S.; PLANQUE, L. Quantification of biasing effects during fatigue tests on asphalt mixes: non-linearity, self-heating and thixotropy. **Road Materials and Pavement Design**, [s. l.]. v. 16, p. 73–99. 2015. DOI: 10.1080/14680629.2015.1077000.

MEDEIROS, M. M.; FERREIRA, W. L. G.; LESSA, F. L. O. Avaliação da influência da umidade em misturas asfálticas compostas por cal como fíler. *In:* CONGRESSO DE PESQUISA E ENSINO EM TRANSPORTES. XXXI., Recife, 2017. **Anais [...],** Recife: Editora: Associação Nacional de Pesquisa e Ensino em Transportes, 2017, [Recife, PE].

In: CONGRESSO DE PESQUISA E ENSINO EM TRANSPORTES. 34º., 100% Digital, 16 a 21 nov. 2020. Anais [...], [s.l]: Editora: Associação Nacional de Pesquisa e Ensino em Transportes, 2020. p.1410-1421.

MOHAMMAD, L. N.; ABADIE, C.; GOKMEN, R.; PUPPALA, A. J. Mecanistic Evaluation of Hydrated Lime in hot-mix asphalt mixtures. **Transportation Research Record: Journal of the Transportation Research Board.** Washington, DC. v. 1723, n.1, p. 26-36, 2000. DOI: 10.3141/1723-04.

MOURA, Edson de. **Estudo do efeito de aditivos químicos e da cal como melhoradores de adesividade em misturas asfálticas densas.** 2001. Dissertação (Mestrado) – Universidade de São Paulo, São Paulo, 2001.

NASCIMENTO, L. A. H. **Apresentação realizada no Departamento de Engenharia de Transportes na Universidade Federal do Ceará.** Fortaleza, 2016

NASCIMENTO, L. A. H. **Implementation and Validation of the Viscoelastic Continuum Damage Theory for Asphalt Mixture and Pavement Analysis in Brazil.** 2015. 336 f. Tese (Doutorado em Engenharia Civil) – Graduate Faculty of North Carolina State University. Raleigh, North Carolina, 2015.

NAZZAL, M. D.; QTAISH, L. A.; AL-HOSAINAT, A.; TALHA, S. A.; KAYA, S.; ABBAS, A. R. Evaluation of Moisture Damage in Asphalt Mixtures at Macro- and Nanoscales. **Journal of Materials in Civil Engineering.** [s. l.]. v. 33, n. 12, p. 1-9, 2021. DOI: 10.1061/(ASCE)MT.1943-5533.0003993.

NGUYEN, H. M.; POUGET, S.; DI BENEDETTO, H.; SAUZÉAT, C. Time-temperature superposition principle for bituminous mixtures. **European Journal of Environmental and Civil Engineering.** [s. l.]. v. 13, n. 9, p. 1095–1107. 2009. DOI:10.1080/19648189.2009.9693176.

OLARD, F.; DI BENEDETTO, H. General "2S2P1D" model and relation between the linear viscoelastic behaviours of bituminous binders and mixes. **Road Materials and Pavement Design.** [s. l.]. v. 4, p. 185–224. 2003. DOI: https://doi.org/10.1080/14680629.2003.9689946.

OROZCO, G. **Relationship between thermomechanical performances of bituminous binders and mixtures with focus on the binder-aggregate adhesion.** 2021. 242 f. Tese (Doutorado) – Universidade de Lyon (ENTPE), Lyon, 2021.

PAPAZIAN, H. S. The response of linear viscoelastic materials in the frequency domain with emphasis on asphalt concrete. *In:* **Proceedings of international conference on the structural design of asphalt pavements.** Ann Arbor, Michigan, v. 203, n. 1, p. 453–464. Trabalho apresentado na International conference on the structural design of asphalt pavements, 1962 [Ann Arbor, Michigan].

PARK, S. W.; KIM, Y. R.; SCHAPERY, R. A. A viscoelastic continuum damage model and its application to uniaxial behavior of asphalt concrete. **Mechanics of Materials.** [s. l.]. v. 24, n. 4, p. 241–255, 1996. DOI:10.1016/s0167-6636(96)00042-7.

PEREIRA, A. C. O. **Influência da drenagem subsuperficial no desempenho de pavimentos asfálticos.** 2003. Dissertação (Mestrado em Engenharia de Transportes) - Escola Politécnica, Universidade de São Paulo, São Paulo, 2003. doi:10.11606/D.3.2003.tde-27062007-191216.

PETERSEN, J. C.; PLANCHER, H.; HARNSBERGER, P. M. **Lime Treatment of Asphalt—Final Report**. National Lime Association. 1987.

RIBEIRO, E. de A. **O efeito da modificação de ligante asfáltico com o liquido da castanha de caju (LCC) na resistência ao dano por umidade em misturas asfálticas.** 2011. 134 f. Dissertação (Mestrado em Engenharia de Transportes) – Centro de Tecnologia, Universidade Federal do Ceará, Fortaleza, 2011.

SABOURI, M.; KIM, Y. R. Development of a failure criterion for asphalt mixtures under different modes of fatigue loading. **Transportation Research Record.** Washington, DC. v. 2447, n. 1, p. 117-125, 2014. DOI: 10.3141/2447-13.

SAFAEI, F.; CASTORENA, C. Temperature Effects of Linear Amplitude Sweep Testing and Analysis. **Transportation Research Record.** Washington, DC. v. 2574, n. 1, p. 92–100, 2016. DOI: https://doi.org/10.3141/2574-10.

SAFAEI, F.; CASTORENA, C.; KIM, Y. R. Linking asphalt binder fatigue to asphalt mixture fatigue performance using viscoelastic continuum damage modeling. **Mechanics of Time-Dependent Materials.** [s. l.]. v. 20, n. 3, p. 299–323. 2016. DOI: 10.1007/s11043-016-9304-1

SAFAEI, F.; LEE, J.; NASCIMENTO, L. A. H.; HINTZ, C.; KIM, Y. R Implications of warm-mix asphalt on long-term oxidative ageing and fatigue performance of asphalt binders and mixtures. **Road Materials and Pavement Design**. [s. l.]. v. 15, n. 1, p. 45-61, 2014. DOI: 10.1080/14680629.2014.927050.

SANTIAGO, L. S.; BABADOPULOS, L. F. A. L; SOARES, J. B. Desenvolvimento de função de transferência para previsão de área trincada em pavimentos asfálticos por meio da simulação do dano por fadiga utilizando modelo S-VECD e análises elásticas. **Revista Transportes**, Rio de Janeiro. v. 28, n. 3, p. 121-136. 2019.

SANTIAGO, L. S.; TORQUATO E SILVA, S. A.; SOARES, J. B. Determinação do dano em pavimentos asfálticos por meio da combinação do modelo S-VECD com análises elásticas. **Revista Transportes**. Rio de Janeiro. v. 26, n. 2, p. 31-43. 2018.

SCHAPERY, R. A. Simplifications in the behavior of viscoelastic composites with growing damage. **Symposium on Inelastic Deformation of Composite Materials, Mechanics and Materials Center.** Texas A&M University, College Station, TX, 1990.

SILVA, C. E. D. B. **Estudo da permeabilidade de misturas asfalticas de graduação aberta.** 2005. 111p. Dissertação (mestrado) - Universidade Estadual de Campinas, Faculdade de Engenharia Civil, Arquitetura e Urbanismo, Campinas, SP. Disponível em: https://hdl.handle.net/20.500.12733/1602107.

SILVA, L. S. V.; BASTOS, J. B. S.; SOARES, J. B. Efeito do uso de corpos de prova moldados e extraídos na caracterização mecânica de misturas asfálticas. **TRANSPORTES**. Rio de Janeiro. v. 30, n. 1, p. 2620-2635. 2022. DOI: 10.14295/transportes.v30i1.2620.

SUDARSANAN, N.; FONTE, B. R.; KIM, Y. R. Application of time-temperature superposition principle to pull-off tensile strength of asphalt tack coats. **Construction and Building Materials.** [s. l.]. v. 262. 2020. DOI: 10.1016/j.conbuildmat.2020.120798.

TAVARES FILHO, P. P. M; UCHOA, A. F. J.; SOARES, J. B.; **Relatório PIBIC 2022/2023 (em desenvolvimento)**. Fortaleza. Programa Institucional de Bolsas de Iniciação Científica. Universidade Federal do Ceará, Pró-Reitoria de Pesquisa e Pós-Graduação. 2023.

TERREL, R. L.; SHUTE, J. W. **Summary Report on Water Sensitivity. SHRP-A/IR-89-003.** Washington, DC. Strategic Highway Research Program: National Research Council, 1989.

UNDERWOOD, B. H.; HOU, E. T.; KIM, Y. R. Application of Simplified VECD Modeling to the Fatigue Prediction of Asphalt Concrete Mixtures. *In:* INTERNATIONAL RILEM SYMPOSIUM ON ADVANCED TESTING AND CHARACTERIZATION OF BITUMINOUS MATERIALS, 7, 2009, Rodes, **Proceedings […].** Rodes, 2009, [Rodes].

UNDERWOOD, B. S. A continuum damage model for asphalt cement and asphalt mastic fatigue. **International Journal of Fatigue**. [s. l.]. v. 82, p. 387–401, 2016. DOI: 10.1016/j.ijfatigue.2015.08.020.

UNDERWOOD, B. S.; BAEK, C.; KIM, Y. R. Simplified viscoelastic continuum damage model as platform for asphalt concrete fatigue analysis. **Transportation Research Record: Journal of the Transportation Research Board.** Washington, DC. n. 2296, p. 36-45, 2012.

FLEXPAVE 1.1 alpha: Layered ViscoElastic Pavement analysis for critical destresses: (user guide). [North Carolina, US]: Departament of Civil, Construction, and Environmental Engineering North Carolina State University, 2018. Disponível em: http://onlinepubs.trb.org/Onlinepubs/nchrp/docs/FlexPAVE1.1Standalone_UserManual.docx. Accessed in: 30/04/2023 at 19:24

VALE *et al.* ACÚMULO DE DEFORMAÇÃO PERMANENTE EM CAMADAS ASFÁLTICAS NO DIMENSIONAMENTO DE PAVIMENTOS A PARTIR DE MODELO VISCOPLÁSTICO. *In:* ANAIS DO 36º CONGRESSO DE PESQUISA E ENSINO EM TRANSPORTES, 2022, Fortaleza. **Anais eletrônicos...** Campinas, Galoá, 2022, [Fortaleza, CE]. Disponível em: <https://proceedings.science/anpet-2022/trabalhos/acumulo-de-deformacao-permanente-em-camadas-asfalticas-no-dimensionamento-de-pav?lang=pt-br>. Acesso em: 20 abr. 2023 às 21:03.

VASCONCELOS, K. L**. Moisture Diffusion in Asphalt Binders and Fine Aggregate Mixtures.** Doctoral dissertation, Texas A&M University. 2010.

WANG, C.; CASTORENA, C.; ZHANG, J.; KIM, Y. R. Unified failure criterion for asphalt binder under cyclic fatigue loading. **Road Materials and Pavement Design.** [s. l.]. v. 16, n. 2, p. 125-148. 2015. DOI: 10.1080/14680629.2015.1077010.

WANG, Y. D., GHANBARI, A., UNDERWOOD, B. S., KIM, Y. R. Development of preliminary transfer functions for performance predictions in FlexPAVE™. **Construction and Building Materials**. [s. l.]. v. 266, p. 1-8, 2021. DOI: 10.1016/j.conbuildmat.2020.121182.

WANG, Y. D.; KESHAVARZI, B.; KIM, Y. R. Fatigue Performance Prediction of Asphalt Pavements with FlexPAVETM, the S-VECD Model, and DR Failure Criterion. **Transportation Research Record.** Washington, DC. v. 2672, n. 40, p. 217–227, 2018. DOI: 10.1177/0361198118756873.

YUSOFF, N. I. M.; SHAW, M. T.; AIREY, G. D. Modelling the linear viscoelastic rheological properties of bituminous binders. **Construction and Building Materials.** [s. l.]. v. 25, n. 5, p. 2171-2189, 2011. DOI: 10.1016/j.conbuildmat.2010.11.086.